Design and Modeling of Shipwide Navy Integrated Power and Energy Corridor Cooling System

by Avi Chatterjee

B.S., Physics, United States Naval Academy (2015) Submitted to the Department of Mechanical Engineering in partial fulfillment of the requirements for the degrees of Master of Science in Naval Architecture and Marine Engineering

and

Master of Science in Mechanical Engineering at the

MASSACHUSETTS INSTITUTE OF TECHNOLOGY May 2023

©2023 Avi Chatterjee. All rights reserved. The author hereby grants to MIT a nonexclusive, worldwide, irrevocable, royalty-free license to exercise any and all rights under copyright, including to reproduce, preserve, distribute and publicly display copies of the thesis, or release the thesis under an open-access license.

Author
Avi Chatterjee
Department of Mechanical Engineering
May 12, 2023
Certified by
Julie Chalfant
Research Scientist
Thesis Supervisor
Certified by
Chryssostomos Chryssostomidis
Professor of Mechanical and Ocean Engineering
Thesis Supervisor
Accepted by
Nicolas Hadjiconstantinou
Chairman, Department Committee on Graduate Theses

Design and Modeling of Shipwide Navy Integrated Power and Energy Corridor Cooling System

by

Avi Chatterjee

Submitted to the Department of Mechanical Engineering on May 12, 2023, in partial fulfillment of the requirements for the degrees of Master of Science in Naval Architecture and Marine Engineering and Master of Science in Mechanical Engineering

Abstract

Naval ship systems are increasingly requiring more and more electricity to power the myriad advanced offensive and defensive electrically-powered systems. The Zumwalt class destroyer was the Navy's first fully electric ship. The next generation destroyer, DDG(X), is also planned to be an electric ship. The ships of the future can thus be anticipated to employ 100 megawatts or more of electric power. This rise in electrical demand begets the need to transfer that power more efficiently through compact and robust power distribution systems.

As part of an ongoing U.S. Navy research consortium of next-generation all-electric warships, the Design Laboratory of the Massachusetts Institute of Technology (MIT) Sea Grant Program is developing the Navy integrated Power and Energy Corridor (NiPEC) to serve as the vessel's power distribution system. The corridor comprises several modular compartments capable of operating independently or as part of a network to execute energy storage, conversion, protection, control, isolation, and transfer functions [18]. The power conversion process is carried out by the corridor's integrated Power Electronics Building Block (iPEBB). The iPEBB is a comprehensive and self-contained converter configured to provide power-dense solutions to the ship's stochastic and dynamic loads [45]. The thermal management of the iPEBB is a central challenge in being able to fully realize its advanced semiconductor technology, constrained by the provision of indirect liquid cooling methods and sailor-friendly accommodations vis-à-vis handling, user interface, and operation.

Padilla et al. [36] conducted a preliminary analysis of Power Electronics Building Block (PEBB) heat dissipation strategies utilizing liquid-cooled cold plates across the dry interface of the PEBB's external surface. Reyes [39] extended this analysis in proposing a first-pass design of a NiPEC liquid cooling system capable of servicing a single nominal compartment within the larger corridor architecture. However, this most recent design presents infeasible operational and maintenance aspects given the number of cooling components required to adequately cool all envisioned NiPEC

corridors, compartments, and PEBB stacks.

This thesis used a combination of first-principles thermodynamic analysis and multi-physics-based modeling to design a NiPEC liquid cooling system and architecture suitable for shipwide deployment. Using Reyes' first-pass cooling system design as a starting point, additional design iterations of the computer-modeled system were conducted and analyzed for thermal management robustness, success against key performance benchmarks, and adherence to relevant military standards. Additional modeling and analysis were conducted to determine how the cooling system could be scaled to accommodate an entire future all-electric Navy destroyer warship. This analysis examined key architectural system design considerations such as the level of component redundancy, utilization of different loop and zonal cooling schemes, and system survivability and control.

Thesis Supervisor: Julie Chalfant

Title: Research Scientist

Thesis Supervisor: Chryssostomos Chryssostomidis Title: Professor of Mechanical and Ocean Engineering

Acknowledgments

I would like to show my deepest gratitude to my thesis supervisors, Dr. Julie Chalfant and Professor Chryssostomos Chryssostomidis, for their guidance throughout this year-long endeavor. They provided me with the support and resources I needed, and the confidence to navigate through the difficult portions of the process.

I am deeply grateful for the resources provided and groundwork laid by LT Ivan Reyes, a fellow 2N graduate who pursued this research topic in earnest last year. I could not have completed this work without his insight and willingness to answer any and all questions I had.

I wish to acknowledge the contributions and sponsorship of Kelly Cooper and L.J. Petersen from the U.S. Office of Naval Research (ONR). This material is based upon research supported by, or in part by, the ONR under award number ONR N00014-21-1-2124.

Finally, I would like to thank my family and friends for their unconditional support and encouragement not only during my two years here in Cambridge but throughout my entire life.

Contents

1	Intr	roduction	17
	1.1	Background	17
	1.2	Power Electronics Power Distribution System	19
		1.2.1 Navy integrated Power Electronics Building Block (iPEBB) .	20
		1.2.2 Navy integrated Power and Energy Corridor (NiPEC)	21
	1.3	Problem Statement	22
	1.4	Previous Research	23
	1.5	Thesis Outline	26
2	Sing	gle Compartment Thermal Analysis	29
	2.1	Governing Equation	30
	2.2	Demineralized Water Temperature Basis	30
	2.3	Heat Exchanger Redesign	32
		2.3.1 Heat Exchanger Characteristics	33
		2.3.2 Completing Heat Exchanger Redesign	36
		2.3.3 Modeling and Simulation	40
		2.3.4 Heat Exchanger Redesign Conclusions	45
3	Full	l Ship Analysis	47
	3.1	Nominal Ship Electrical Load	47
		3.1.1 Electric Power Load Analysis	48
		3.1.2 PEBB Conversion Requirements and Functionality	50
		3.1.3 iPEBB-only Deployment	52

		3.1.4	iPEBB and PEBB 6000 Joint Deployment	54
	3.2	Spatia	al Analysis	55
	3.3	Thern	nal Analysis	57
		3.3.1	Heat Loss Reassessment	57
		3.3.2	Chilled Water Flow Reassessment	58
		3.3.3	Demineralized Water Flow Reassessment	59
		3.3.4	Corridor Heat Exchanger Design	61
4	Hea	at Excl	hanger Evaluation for One Corridor	65
	4.1	First 1	Design	65
	4.2	Second	d Design	68
		4.2.1	Design Approach	68
		4.2.2	Simulation Results and Analysis	69
	4.3	Final	Design	72
		4.3.1	Design Approach	72
		4.3.2	Simulation Results and Analysis	73
	4.4	Heat 1	Exchanger Redesign Conclusions	75
	4.5	Altern	native Heat Exchanger Solutions	76
		4.5.1	Plate Heat Exchangers	76
		4.5.2	Printed Circuit Heat Exchangers	79
		4.5.3	Spiral Heat Exchangers	81
5	Ove	erall C	ooling System Architecture	85
	5.1	Separa	ation and Redundancy	85
		5.1.1	Improved Redundancy	87
	5.2	Zonal	Strategy and Arrangement	88
		5.2.1	First Design: One System Per Corridor	88
		5.2.2	Second Design: Forward and Aft Quadrants	89
		5.2.3	Inadequate Mass Flow Rate at Cold Plates	91
	5.3	Final	Design: Six Cooling Zones	91
		531	Heat Loss Dependency on Operational Load	02

		5.3.2	Heat Loss Distribution Across Cooling Zones	93
		5.3.3	Final System Design Decisions	95
		5.3.4	System Parameter Summary and Concept of Operations	102
6	Oth	er Sys	tem Component Evaluation	103
	6.1	Pump		103
		6.1.1	Flow Rate	103
		6.1.2	Total Differential Head	104
		6.1.3	Piping Frictional Pressure Losses	105
		6.1.4	Equipment Frictional Pressure Losses	106
		6.1.5	Fitting Frictional Pressure Losses	106
		6.1.6	Total Losses and Pumping Power Determination	108
	6.2	Expan	sion Tank	109
		6.2.1	Volume and Pressure Requirements	109
7	Dyr	namic]	Modeling	113
	7.1	Use C	ases	115
		7.1.1	Nominal Destroyer Corridor Arrangement	115
		7.1.2	Single Power Train Arrangements	116
8	Fut	ure Wo	ork and Conclusions	119
	8.1	Future	e Work	119
		8.1.1	Detailed Electrical Plant Operational Analysis	120
		8.1.2	Heat Exchanger Pressure Drop Mitigation	120
		8.1.3	PEBB Arrangement Solution in PMM Compartments	121
		8.1.4	Expansion of Dynamic Modeler Capabilities	122
	8.2	Conclu	asions	122
A	List	of Ac	ronyms	129
В	Loa	d Fact	or Analysis and Values	133
\mathbf{C}	PEI	BB All	ocation Breakdown	143

D	Cooling Zone Heat Load Breakdown	147
\mathbf{E}	Air Conditioning Plant and Chilled Water System Impacts	149

List of Figures

1-1	Increasing, complex demands require new power systems [28]	18
1-2	Topdown and isometric views of a Navy iPEBB model [21]	21
1-3	Four-corridor NiPEC incorporated into destroyer-type vessel model [20]. 22	
1-4	Nominal power corridor section for one compartment [18]	23
1-5	One-line diagram of the single compartment NiPEC cooling system [39].	25
1-6	Detailed view of NiPEC cooling system arrangements at the PEBB	
	stack [39]	26
2-1	Required baffle thickness given shell inner diameter and unsupported	
	tube length between central baffles [43]	38
2-2	Maximum unsupported straight tube spans [43]	38
2-3	Maximum allowable pressure drops [30]	41
2-4	Maximum cooling water velocities [30]	41
2-5	Maximum cooling water inlet temperature [30]	42
2-6	Demineralized water velocity flow	42
2-7	Demineralized water pressure gradient	43
2-8	Demineralized water pressure drop	43
2-9	Chilled water velocity flow	44
2-10	Chilled water pressure gradient	44
2-11	Chilled water pressure drop	45
3-1	Load Factor calculation example [19]	49
3-2	Proposed half-zone layout of the Power Electronics Power Distribution	
	System (PEPDS) bus	51

3-3	Industry example of shipboard power conversion cabinet [9]	56
3-4	Navy iPEBB heat loss characteristics [21]	
4-1	Design 1 chilled water velocity flow	66
4-2	Design 1 chilled water pressure gradient	66
4-3	Design 1 demineralized water velocity flow	67
4-4	Design 1 demineralized water pressure gradient	67
4-5	Design 2 chilled water velocity flow	69
4-6	Design 2 chilled water pressure gradient	69
4-7	Design 2 demineralized water velocity flow	71
4-8	Design 2 demineralized water pressure gradient	71
4-9	Final design chilled water velocity flow profile	74
4-10	Final design chilled water pressure gradient	74
4-11	Final design demineralized water velocity profile	75
4-12	Final design demineralized water pressure gradient	75
4-13	Flat Plate Heat Exchangers (PHE) for Electronic Cooling Water Sys-	
	tems (ECWS) [33]	77
4-14	Illustration of counter-current flow path in a PHE using chevron-corrugate	ed
	plates [3]	78
4-15	Space savings incurred by using PHEs [7]	78
4-16	Printed Circuit Heat Exchanger (PCHE) model developed by MIT's	
	Atomistic Simulation and Energy Research Group [4]	80
4-17	Exploded view of Heatric PCHE internals [44]	80
4-18	Illustration of the hot and cold fluid flow paths within a Spiral Heat	
	Exchangers (SHE) [5]	82
4-19	Alfa Laval SHE external view [5]	82
5-1	Main header piping of NiPEC cooling system. The basic architecture	
	is adaptable to a variety of cooling zone strategies and layouts	90

5-2	Topdown view of cooling skid locations. The white heat exchanger fig-	
	ures are representative of a singular cooling skid, $i.e.$ a non-redundant	
	source of cooling.	90
5-3	Cold plate conditions for a fully loaded PEBB, assuming an inlet tem-	
	perature of 22°C and \dot{m}_{plate} of 0.115 kg/s. Metal-Oxide-Semiconductor	
	$\label{eq:field-Effect Transistor} \ (\text{MOSFET}) \ \text{temperature limits are exceeded.} \ .$	97
5-4	Cold plate conditions for a fully loaded PEBB, assuming an inlet tem-	
	perature of 22°C and \dot{m}_{plate} of 0.370 kg/s	98
5-5	Cold plate conditions for a low-loaded PEBB, assuming an inlet tem-	
	perature of 22°C and \dot{m}_{plate} of 0.008 kg/s	99
5-6	Cold plate conditions for a low-loaded PEBB, assuming an inlet tem-	
	perature of 22°C and \dot{m}_{plate} of 0.030 kg/s	100
7-1	Modeler user interface allows direct input of stack needs for each com-	
	partment, which are then automatically generated	114
7-2	Model of six-zone NiPEC cooling system with PEBB arrangements	
	specified by compartment, corridor, and deck	116
7-3	NiPEC power train footprint to enable Medium Voltage Alternating	
	Current (MVAC)-Medium Voltage Direct Current (MVDC)-Low Volt-	
	age Direct Current (LVDC) conversion	117
7-4	Power train stack array displaying internal arrangement and spacing	
	of PEBBs	118
B-1	Inter-relationship of DDS 310-1 tasks [19]	133
B-2	Ship Work Breakdown Structure (SWBS) Group 2 Load Factors [19].	134
B-3	SWBS Group 3 Load Factors [19]	135
B-4	SWBS Group 4 Load Factors [19]	136
B-5	SWBS Group 5 Load Factors [19]	137
B-6	SWBS Group 5 Load Factors (cont'd) [19]	138
B-7	SWBS Group 5 Load Factors (cont'd) [19]	139
B-8	SWBS Group 5 and 6 Load Factors [19]	140

B-9	SWBS Group 6 Load Factors (cont'd) [19]	141
B-10	SWBS Group 7 Load Factors [19]	142
E-1	The higher capacity High Efficiency Super Capacity (HES-C) units are	
	slated to replace the 200-ton units for Flight III DDGs and other future $$	
	U.S. Navy platforms [2]	150
E-2	York YZ Magnetic Bearing Centrifugal Chiller, Style A [6]	151

List of Tables

2.1	Allowable tube outside diameter and required thickness [30]	33
2.2	Chilled Water and Heat Exchanger Properties	33
2.3	Comparison of Previous vs. Corrected Mass Flux Values	34
2.4	Demineralized Water and Heat Exchanger Properties	35
2.5	Initial Heat Exchanger Characteristics	36
2.6	Minimum Tube Spacing [30]	37
2.7	Minimum Depth of Tube Expansion [30]	37
2.8	Flare of Tube End Holes [30]	37
2.9	Two-pass heat exchanger model geometries and arrangement	40
3.1	Minimum Number of PEBBs Required By Conversion Type	52
3.2	Load Type by Rated Voltage	52
3.3	Number of iPEBBs Required Per Compartment	53
3.4	Bulkhead Locations and Compartment Lengths	56
3.5	Naval Ship's Technical Manual (NSTM) 505 Fluid Velocity Limits	59
3.6	Demineralized Water Flow Sensitivity Analysis	61
3.7	Shell Outer Diameter Sensitivity Analysis	62
3.8	Initial one corridor heat exchanger thermal-hydraulic parameters	63
3.9	Initial one corridor heat exchanger model geometries and arrangement	63
4.1	Second corridor heat exchanger model geometries and arrangement .	68
4.2	Final Heat Exchanger Characteristics	72
4.3	Final heat exchanger model geometries and arrangement	73

5.1	Quadrant Cooling PEBB Allocation and Heat Load	91
5.2	Cooling Skid Locations (all are located on 3rd Deck)	92
5.3	Six-Zone Cooling: Normal Operating Conditions	93
5.4	ΔT Effect on Predicted Flow Rates and Velocities	96
5.5	Final System Operational Parameters	102
6.1	System Coolant Properties	104
6.2	Suction & Discharge Piping Frictional Losses	106
6.3	System Pressure Losses	108
C.1	iPEBB-only: Breakdown Per Compartment (Port)	143
C.2	iPEBB-only: Breakdown Per Compartment (Starboard)	144
C.3	Joint Deployment: Breakdown Per Compartment (Port)	144
C.4	Joint Deployment: Breakdown Per Compartment (Starboard)	145
D.1	Six-Zone Cooling: Compartment Assignments and Heat Loads By Type	147
D.2	Six-Zone Cooling: Heat Loads Following Loss of Corridor	147
D.3	Six Zone Cooling: Heat Loads Following Loss of Cooling Zone (Port)	148
D.4	Six Zone Cooling: Heat Loads Following Loss of Cooling Zone (Star-	
	board)	148

Chapter 1

Introduction

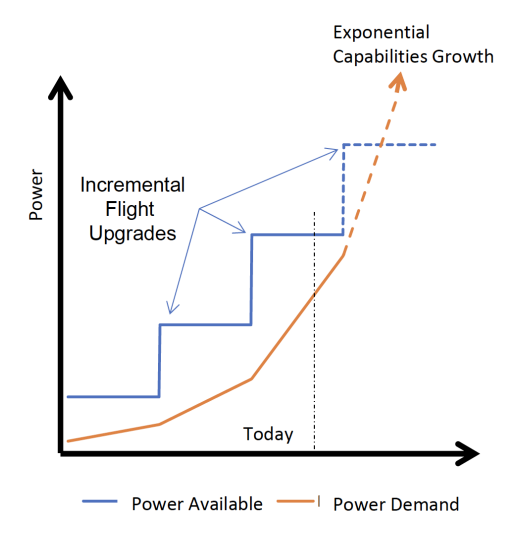
1.1 Background

Naval ship systems are increasingly requiring more and more electricity to power the myriad advanced offensive and defensive electrically-powered systems providing combat capability and lethality. These systems will prove essential for the United States Navy in pacing technological growth, outpacing adversarial threat, and maintaining maritime dominance for the decades to come [28]. Some of the key driving technologies include high-powered directed energy weapons such as lasers, stochastic Electronic Warfare (EW) systems, and radiated energy systems such as the Air and Missile Defense Radar (AMDR). These increased power levels and novel load profiles, as provided in Figures 1-1a and 1-1b, introduce challenging types of evolving power demand that current power systems cannot support.

Future warships must also be equipped with the flexibility and capacity to handle capability upgrades. The ships of the future can be anticipated to employ 100 MW or more of electric power. At the Directed Energy Summit in 2017, then Chief of Naval Operations Admiral John M. Richardson remarked that he would buy, "..as much power as I can afford because I know by the time I retire the ship, I'll use it all." [16]. This current and anticipated rise in electrical demand and complexity begets the need to transfer and store that energy more efficiently through compact and robust power distribution systems.

MORE POWER

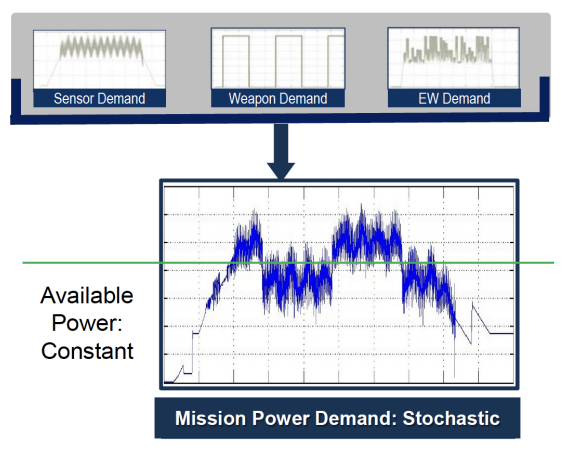
STEP CHANGE INCREMENTAL DEVELOPMENT OF POWER GENERATION VS. INCREASE IN POWER REQUIREMENT OVER TIME



(a) Exponential increase in anticipated power demand.

DIFFERENT DEMAND

NEW CAPABILITIES DEMAND PULSE AND STOCHASTIC POWER



CURRENT AVAILABLE POWER ABOARD SHIPS
CANNOT SUPPORT DYNAMIC LOADS

(b) Pulse and stochastic loads will exceed current capacity.

Figure 1-1: Increasing, complex demands require new power systems [28].

As such, the United States Navy has invested heavily in the development of new energy distribution systems capable of supporting these emerging power requirements onboard the nation's capital warships. The Zumwalt class destroyer (DDG 1000) was the Navy's first fully electric ship. Through its Integrated Power System (IPS), the main generators, which are considerably larger than those previously employed in legacy systems, provide electric power to a MVAC distribution bus in order to provide power to both the ship's propulsion and electrical distribution systems. While this architecture proved successful in responding to an increased overall base load, it is ill-equipped to manage the stochastic and high-energy pulse demands previously described. In these scenarios, the gas turbine or diesel engines driving the generator lack the electrical "inertia" to withstand the ramping and rippling effects of these complex profiles and the unpredictability underpinning their stochastic nature. The generators' capacities may be exceeded, and the engines may experience excessive thermal and mechanical stresses, causing equipment malfunction and unacceptable loss of capability [16].

To this end, Vice Admiral Thomas J. Moore, then Commander of the Naval Sea Systems Command (NAVSEA 00) established the Naval Power and Energy Systems (NPES) Technology Development Roadmap (TDR) in 2019. This document emphasized that fundamental to fleet capability is the electric power behind the fleet, and it outlined the Navy's strategy for the continued evolution of "naval electrification", identified as a critical part of the kill chain (a military term used to describe the structure of a wartime attack)[16]. Some examples of the ongoing progress towards this goal of electrification are the Energy Storage Module (ESM) installed on the USS Portland (LPD 27) and the AMDR Power Conversion Module (PCM) installation on the next-generation DDG 51 Flight III destroyer class [40].

One of the major advancements proposed was the Integrated Power and Energy System (IPES), which uses the IPS framework but also provides integrated energy storage and power, and utilizes an advanced system controls suite known as Tactical Energy Management (TEM) [40]. These advances would address the principal short-comings identified with IPS, namely its inability to respond to on-demand and highly stochastic loads, by enabling full utilization of the shipboard power and energy systems. However, IPES development is currently focused on using either a MVDC or MVAC architecture and thus does not offer the system-wide flexibility coveted in the next-generation power and energy system.

1.2 Power Electronics Power Distribution System

The PEPDS is a new power, energy, and control distribution and management concept to deliver on the vision of the NPES TDR and Navy's electrification goals writ large. Leveraging recent advances in ONR-developed technology – to include high-power density, high-efficiency power electronics, Silicon-Carbide (SiC) power semiconductors, and various modeling, simulation design, and analysis tools – PEPDS represents an entirely new class of system. Unlike the aforementioned IPES, which uses either Alternating Current (AC) or Direct Current (DC) electrical power distribution, PEPDS will enable the conversion, storage, and distribution of either AC, DC, or

both, providing a "universal solution" to the power and energy management problem [37]. PEPDS will be able to recognize the load or source type once connected to the system, and thus tailor the energy and power delivered based on that component's specific needs. By soliciting the storage capabilities of all components within the network, PEPDS will be able to deliver point and distributed storage, transient control, and active filtering to power and quality of service to all loads [37].

Ultimately, the goal of PEPDS is to revolutionize electrical distribution system design and operation for future naval shipboard application [37]. Within this framework, there are five major lines of effort where science and technology development are needed: the Navy iPEBB, the Power Corridor, Model is the Specification, Control, and System Simulation. The focus of this thesis primarily concerned the first two areas, which are addressed in greater detail in the following sections.

1.2.1 Navy integrated Power Electronics Building Block (iPEBB)

The Navy iPEBB is a modular, repeatable, programmable, sailor-carryable universal converter whose topology offers a flexible, power-dense solution to meet the various requirements of the ship's electrical loads. Multiple identical iPEBB units are used together and configured through specifically tailored software to provide the necessary conversion solution. The advances in the SiC-based technology over the last two decades have provided significantly improved dynamic behavior and speed performance compared to existing options, specifically enabled by higher switching speeds, higher breakdown voltages, and higher operating temperatures [37] [38].

Within the overall PEPDS architecture, the iPEBB is the most essential component, responsible for the conversion processes and control of the flow of the power. Thus, it is considered the Least Replaceable Unit (LRU). The current Navy iPEBB, a model of which is depicted in Figure 1-2, weighs approximately 35 *lbs* and is designed such that any sailor can easily remove the unit at its plug-in connection port, handle and transport it throughout the ship, and then install it elsewhere in the power corridor wherever it is needed [37]. In this way, there will be hundreds of these identical components distributed throughout the ship rather than a variety of bespoke units,

thereby reducing costs in production, installation, testing, and training [18].

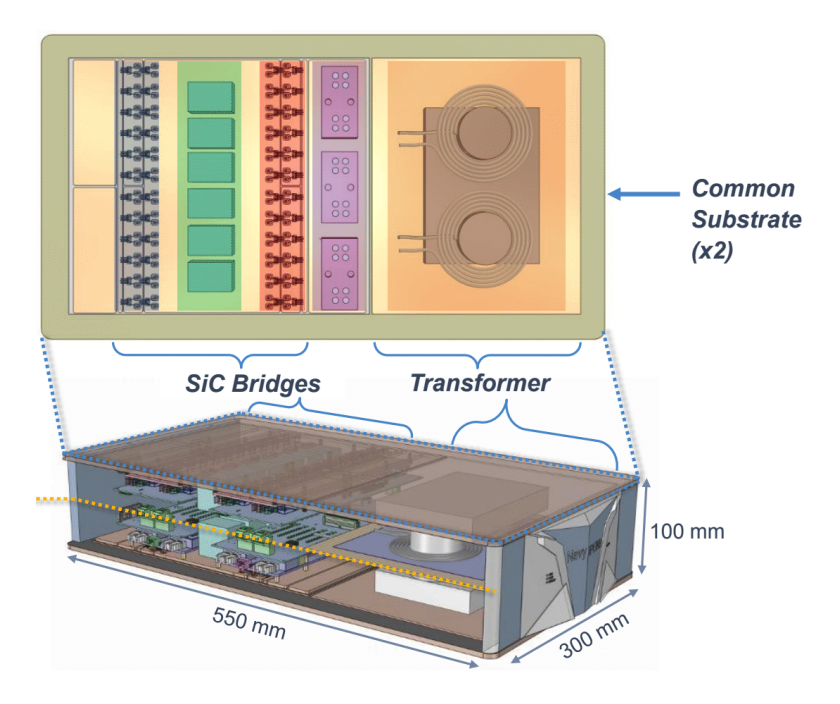


Figure 1-2: Topdown and isometric views of a Navy iPEBB model [21]

.

1.2.2 Navy integrated Power and Energy Corridor (NiPEC)

The NiPEC represents a revolutionary approach as a power distribution platform in executing all the functions of a ship's electrical distribution system. As a single modular entity, it incorporates all the necessary components for energy and power handling throughout the ship: main bus cables, conversion, protection, isolation, control systems, and energy storage. Unlike legacy IPES systems, the NiPEC can execute conversion and power delivery functions across the entire spectrum of conversion pathways: AC-AC, AC-DC, DC-AC, and DC-DC.

The power corridor is treated as reserved space in the early stages of the ship design process [37]. Given the particular importance of electrical power generation and distribution for the all-electric ship, this design philosophy prioritizes sufficient space allocation for the corridor. While the corridor concept in general exploits modularity by utilizing the same converters, controls, components, and cabling throughout all sections of the ship, it is intended to be customized to specific watertight subdivisions,

or compartments, within the ship. In this way, co-located sources and loads dictate how much corridor is required in that section, while also ensuring reliability through redundant power sources for all vital loads.

Energy storage is also incorporated in the power corridor design, not only through the inherent storage capacity of the individual iPEBBs but also through proposed energy banks or magazines that would be directly incorporated into the main bus. These energy banks would provide the necessary power reservoir for current and future pulse-load weapons which present temporary large demand signals, a feature that current electrical distribution systems are hard-pressed to handle. This energy storage capacity would also provide the flexibility to operate in a variety of efficient electrical plant lineups, including single-generator and in-port battery operations [37].

Previous research and studies have assumed a four-corridor layout, occupying the second and fourth decks along the port and starboard sides of the ship. A rendering of this NiPEC architecture is provided in Figure 1-3, and a schematic drawing of a given compartment's power corridor section is provided in Figure 1-4. The layouts and dimensions provided therein served as the initial starting points for certain assumptions used in this thesis.

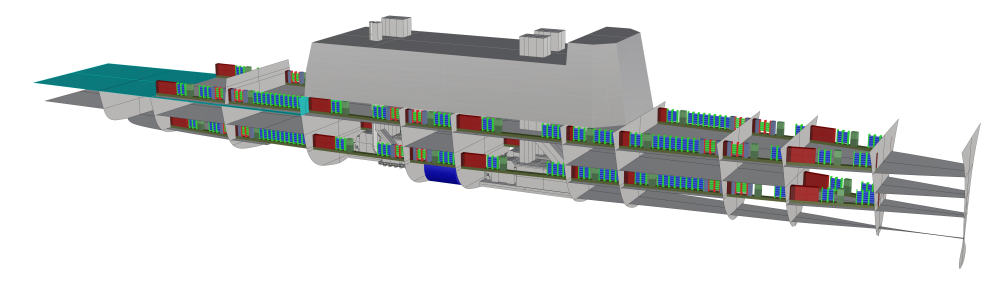


Figure 1-3: Four-corridor NiPEC incorporated into destroyer-type vessel model [20].

1.3 Problem Statement

Although the PEBB promises high-power efficiency in delivering its robust power conversion and storage functions, it still dissipates heat from electrical losses which pose thermal management challenges and which must be adeptly addressed [45]. Ad-

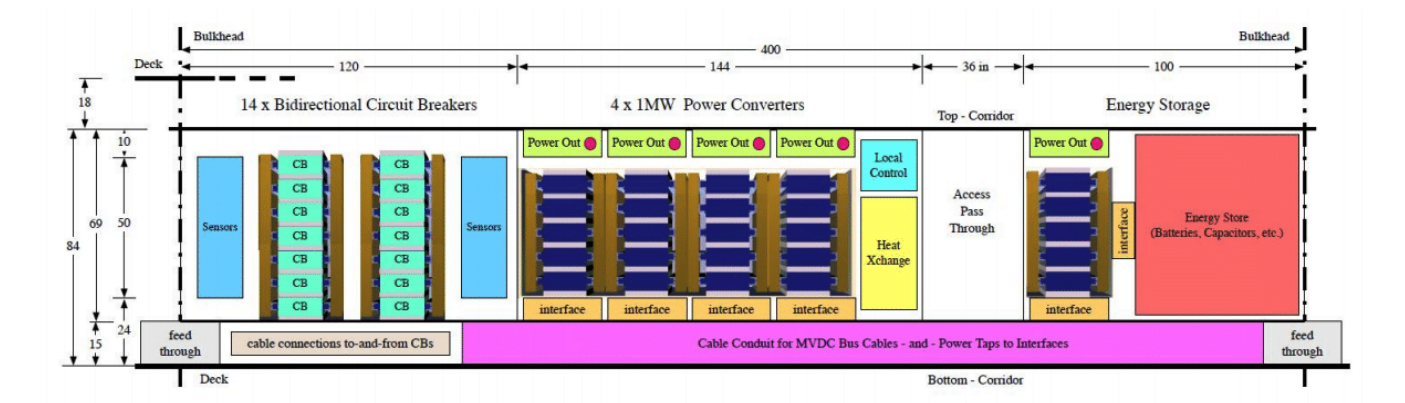


Figure 1-4: Nominal power corridor section for one compartment [18].

ditional constraints levied by the envisioned PEPDS and NiPEC system design make the challenge even more imposing and preclude the pursuit of conventional cooling methods. These constraints include: the compactness of the power corridor which limits space and sizing for cooling equipment; the desire for modularity and "sailor-carryable" units to allow insertion and removal of PEBB units into the power corridor as necessary; and the undesirability of placing any cooling water connections in close proximity to any electrical components. This last restriction effectively eliminates any direct liquid cooling options.

1.4 Previous Research

In light of these restrictions, previous research has explored alternative cooling methods to address the thermal management problem at hand. Yang et al. [45] determined that while air cooling alone was likely sufficient for the PEBB 1000, this method may prove insufficient or infeasible for the larger, more power-dense, and higher-loss Navy iPEBB and PEBB 6000 variants. Different water cooling strategies were discussed and identified as potentially viable strategies for meeting the expected cooling demand [45]. Among the more promising candidates was an external liquid cooling approach utilizing a dry interface. In this method, a cooling fluid is passed through inlaid copper piping within the cold plate, which is placed in contact with the top and bottom solid surfaces of the PEBB, facilitating heat transfer via conduction. This approach

offers advantages particularly suited for power corridor use, such as the elimination of manual external connections, the absence of any liquid entering the PEBB, and the promise of electrical isolation. However, the contact resistance between the cold plate and PEBB surface can greatly inhibit the heat transfer process, especially when grit or dirt may be present as is common in a shipboard environment.

To this end, Padilla et al. [36] conducted a preliminary thermal analysis of PEBB heat dissipation strategies utilizing liquid-cooled cold plates across the dry interface of the PEBB's external surface. To address the contact resistance concerns, a Thermal Interface Material (TIM) was incorporated into the design. This material lowers the contact resistance by filling in the small gaps between the PEBB and cooling surfaces, when placed under a compressive load [35] [36]. This work demonstrated that the proposed method of incorporating a counter-flow heat exchanger in conjunction with a TIM is a viable solution for removing up to 10 kW of heat from the PEBB.

Reyes [39] extended Padilla's findings in proposing a first-pass design of a closed-loop, pressurized, demineralized water cooling system. In this design, a main heat exchanger serviced by the ship's chilled water system was used to cool the demineralized water servicing the counter-flow heat exchanger at the cold plates. A one-line schematic diagram of this proposed system is provided in Figures 1-5 and 1-6. This design proved capable of dissipating up to 240~kW of system heat generated by 20~kW iPEBB units – which includes a 20% conservative safety margin – assigned to a "notional" single compartment in the aforementioned "notional" destroyer.

While this design provided an excellent starting point in proposing a potential water-cooled approach to the NiPEC thermal management problem, it likely cannot be feasibly scaled for shipwide employment. The notional destroyer has portions of the power corridor across two decks on both sides of the ship, running throughout the majority of the length of the vessel. As such, there could be upwards of 50 of these smaller compartment sections which served as the basis of analysis and design for the first-pass system. This alone suggests that efforts to simply replicate the current design across all the compartments would result in roughly 50 separate cooling systems, and hundreds of heat exchangers and pumps, given the need for component

redundancy. It is untenable across construction, operational, maintenance, and cost considerations. Beyond that, each corridor may have disparate power demand conditions, and thus the base assumption of sizing cooling system components to meet the demand of 20 PEBBs is insufficient.

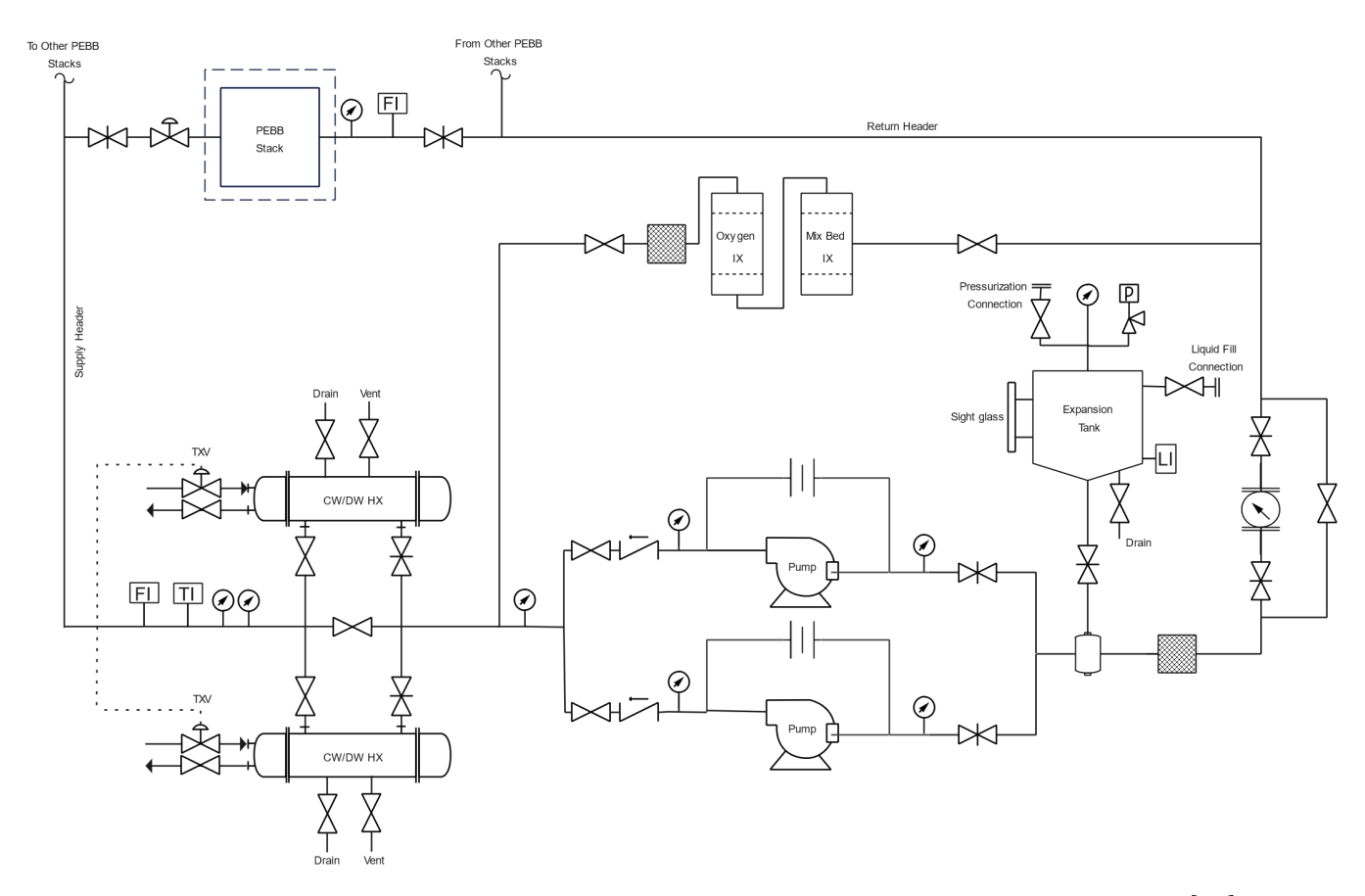


Figure 1-5: One-line diagram of the single compartment NiPEC cooling system [39].

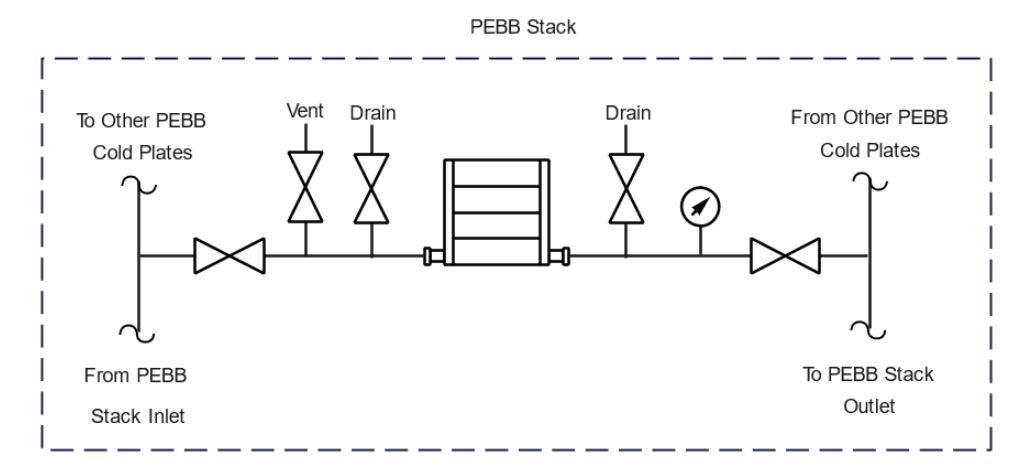


Figure 1-6: Detailed view of NiPEC cooling system arrangements at the PEBB stack [39].

1.5 Thesis Outline

The goal of this thesis was to design and model a NiPEC liquid cooling system and architecture suitable for shipwide deployment. The system must operate in conjunction with ongoing PEBB and support system research, and bear the constraints levied by the non-intrusive interface requirements and complexities inherent in shipboard application. Additionally, the cooling system must meet the requirements set forth by the U.S. Navy, shipping classification societies, and engineering industry standards.

In Chapter 2, using the first-pass cooling system design proposed by Reyes [39] as an initial starting point, additional design iterations of the computer-modeled system were performed and analyzed until all key performance benchmarks and military standards were satisfied for the single-compartment scenario. This provided important insight and design strategies in order to adequately scale up the system for the entire ship.

In an effort to scale the system for shipwide deployment, a more detailed Electric Power Load Analysis (EPLA) was conducted in Chapter 3, which used a predicted total ship electrical load list to determine the relevant power demand scenarios and PEBB allocation requirements. A methodology that employs both the Navy iPEBB and the larger, higher power output PEBB 6000 was explored and recommended for

system implementation.

Chapter 4 documents the heat exchanger redesign process in consideration of the updated heat load assumptions, specified to the most limiting corridor heat load. Various design iterations were modeled and simulated to improve the component's performance against key metrics, particularly maximum velocity and pressure drop across the component for both the tube-side and shell-side flow.

Additional analyses were then conducted in Chapter 5 to determine an overall cooling system architecture that could be feasibly incorporated in the nominal destroyer-type electric warship. This again built off the preliminary results of Reyes [39], but further interrogated crucial aspects of the system design with respect to the level of component redundancy, loop and zonal cooling schemes, and system survivability. A 3D model of the shipwide cooling system was concurrently developed in the computer modeling software Rhino3D to analyze the viability of various arrangements and distribution strategies. Additional cold plate Computational Fluid Dynamics (CFD) analysis improved and augmented the design process in order to determine major system parameters such as cold plate inlet temperature, normal operating temperature range, and required flow rates both at the cold plate and cooling zone levels. A final shipwide cooling system consisting of six separate cooling zones, each capable of being aligned to the other two zones on that side of the ship in casualty scenarios, is ultimately recommended.

Based on the cooling zone layout and major system parameter decisions finalized in Chapter 5, pumping power requirements and expansion tank sizing for the design basis heat load were derived in Chapter 6.

Chapter 7 details the concurrent work performed in developing a dynamic NiPEC cooling system model responsive to changes in various component sizes and dimensions, such as the PEBBs, PEBB stacks, the number of PEBBs accommodated by each stack, branch and inlet/outlet piping leading to the stacks, component spacing within the corridor, and more. Two use cases are discussed to illustrate the utility of this model for power corridor spatial and arrangement analysis given the current uncertainty of various components' sizing.

Chapter 8 provides conclusions of the work conducted in this research and recommendations for future work to pursue in the development of the shipwide NiPEC cooling system.

Chapter 2

Single Compartment Thermal

Analysis

The first-pass NiPEC cooling system proposed by Reyes [39] assumed a four-corridor architecture, each comprised of 12 watertight "nominal" compartments. Each of these compartments contained 20 iPEBBs: 4 iPEBBs in vertical alignment, which constituted a single "stack", and five stacks allocated the compartment in total. The cooling system developed in that research serviced just one of these 48 compartments, and thus likely proves infeasible to implement given construction, operational, and maintenance considerations. The proposed system nonetheless provides an excellent starting point for subsequent design iterations and the ultimate development of a viable shipwide NiPEC cooling system architecture.

To that end, additional design iterations had to be implemented to ensure that the proposed system was, in fact, suitable for single-compartment employment. Of note, not all flow requirements within the heat exchanger met requisite military standards. Specifically, the chilled water pressure drop exceeded the $6 lbf/in^2$ (psi) limit imposed by MIL-DTL-15730N [30]. Addressing this non-conformance served as the initial motivation for modifying the reference heat exchanger. In that process, other assumptions, calculations, and design decisions were revisited and changed as necessary, and are also outlined below.

2.1 Governing Equation

The fundamental equation governing the heat exchanger design is given by a derivation of Fourier's Equation provided below:

$$\dot{Q} = UA\Delta T \tag{2.1}$$

where \dot{Q} is the rate of heat transfer (W), U is the overall heat transfer coefficient $(\frac{W}{m^2-K})$, A is the total required heat transfer surface area (m^2) , and ΔT is the Logarithmic Mean Temperature Difference (LMTD) (K). This equation can be rearranged to determine the required total heat transfer surface area, which will directly drive the tube bundle arrangement and overall heat exchanger design.

Following the assumptions and conservative safety margins of previous heat load estimates, each iPEBB was initially assumed to dissipate 10 kW of heat. As the nominal compartment houses 20 total iPEBBs, and after applying an additional 20% design safety margin, it is assumed that \dot{Q} is 240 kW.

Additional calculations, assumptions, and design decisions must be made in order to determine U and ΔT in order to find A, and are described below.

2.2 Demineralized Water Temperature Basis

The iPEBB's limiting thermal condition assumes that half of the 96 SiC MOSFET switches in the iPEBB produce 80% of the heat loss, and the other half produce the remaining 20% (hereafter known as the 80/20 load condition). Following the baseline assumption that each iPEBB is capable of producing 10~kW of heat, the maximum heat load per switch is 167~W.

Padilla et al. [36] determined the total thermal resistance between the heatproducing semiconductor switches and the cooling water to be .6064 K/W. The thermal resistance equation can then be used to determine the temperature difference from the semiconductor to the cooling water:

$$\dot{Q} = \Delta T_{Net} / R_{Tot} \tag{2.2}$$

where \dot{Q} is the rate of heat transfer (W), ΔT_{Net} is the temperature difference between the semi-conductor switch and cooling water (K), and R_{Tot} is the total thermal resistance between the semiconductor switch and the cooling water (K/W).

The net temperature difference is $101.3^{\circ}(K \text{ or } C)$. The absolute maximum allowable temperature for the iPEBB semi-conductors is 180°C in order to preclude component damage and the possibility of thermal runaway. In keeping with assumptions and analysis established by Padilla et al. [36], an additional 30°C safety margin is applied to this upper bound, so that the maximum allowable semiconductor temperature is 150°C . Given the above calculated net temperature difference, the theoretical maximum allowable cooling water temperature at the cold plate is 48.7°C . MIL-STD-1399 [31] adjudicates flow and cooling requirements based on a maximum 2°C rise across the cooling medium to the given electronic component. Therefore, the theoretical maximum cooling water inlet temperature is 46.7°C .

However, MIL-STD-1399 [31] stipulates that the cooling water temperature provided to the electronic equipment inlet connections shall not be greater than 40°C on surface ships. Reyes [39] ultimately recommended a demineralized water normal operating temperature band of 23.9-29.4°C (75-85°F) which provides sufficient margin to the 46.7°C limit calculated above. Nevertheless, the 40°C inlet temperature restriction should be considered a strict requirement early in the heat exchanger design and optimization process to ensure conformance with applicable standards. Therefore, a maximum cold plate coolant inlet temperature of 40°C was initially assumed and served as the heat exchanger's demineralized water outlet temperature. This new assumption influenced various follow-on calculations which ultimately determined the necessary sizing of the heat exchanger.

2.3 Heat Exchanger Redesign

The final proposal by Reyes [39] featured a four-pass heat exchanger, wherein chilled water from the Air Conditioning system supplied cooling to the demineralized water servicing the iPEBB stacks in the nominal compartment. The chilled water flowed through the tubes (tube-side flow) and the demineralized water flowed over the tubes (shell-side flow). These flow paths, and the corresponding flow rates and pressures, were carried forward in this initial stage of the redesign. A detailed treatment of these design decisions can be found in [39]. As such, the following inlet conditions at the heat exchanger were assumed:

- Chilled water inlet pressure of 100 psi, at a mass flow rate of 2.893 kg/s at 7°C.
- Demineralized water inlet pressure of 100 psi, at a mass flow rate of 21.017 kg/s at 42°C.

The four-pass design yielded a chilled water pressure drop of 27.39 psi, which greatly exceeded the aforementioned 6 psi limit. This pressure drop represented a greater than twofold pressure drop increase from a previous design iteration featuring only two passes (11.74 psi). In that two-pass design, the demineralized water pressure drop also exceeded the 6 psi limit. This second limit violation was decreased to within the acceptable range in the four-pass design primarily by increasing the tube and baffle spacing. Importantly, increasing the number of passes did not itself have a significant effect on the demineralized water pressure drop. Thus, consideration was given to incorporating the increased spacing back into the two-pass design to address the demineralized water pressure drop, while modifying other parameters in order to address the excessive chilled water pressure drop.

The first parameter addressed was the tubes' outside diameter. MIL-DTL-15730N [30] specifies the allowable tube diameters and corresponding tube thicknesses for coolers with freshwater coolant, summarized in Table 2.1.

The tubes' outside diameter and corresponding thickness were increased to 1/2 in and 0.049 in, respectively. This change was implemented specifically to address

Table 2.1: Allowable tube outside diameter and required thickness [30]

Outside Diameter (in)	Minimum Tube Wall Thickness (in)
5/8	0.049
1/2	0.049
3/8	0.035

the significant pressure drop occurring between the chilled water inlet piping and the chilled water tubes at the heat exchanger waterbox. Initially, the shell diameter was maintained at $8\ in$.

2.3.1 Heat Exchanger Characteristics

This design change directly influenced a variety of dimensional and non-dimensional parameters which govern the convective chilled water heat transfer coefficient, and subsequently, the overall heat transfer coefficient. The results of these parameter changes are shown in Table 2.2.

Table 2.2: Chilled Water and Heat Exchanger Properties

Density	ρ	kg/m^3	999.86
Fluid Velocity	v	m/s	2.5
Hydraulic Diameter	D_{ID}	in	0.402
Dynamic Viscosity	μ	$N - s/m^2$	1.43-3
Reynolds number	Re	non-dim	17848.55
Specific Heat Capacity	c_p	J/kg - K	4200
Thermal Conductivity	k	W/m-K	0.574
Prandtl number	Pr	non-dim	10.46
Darcy Friction Factor	f_D	non-dim	0.027
Nusselt number	Nu	non-dim	156.65
Chilled Water Heat Transfer Coefficient	h_{CW}	$W/m^2 - K$	8806.32

The Bell-Delaware method was utilized in order to determine the convective heat transfer of the shell-side demineralized water. This method is widely used for the design and development of shell-and-tube heat exchangers (STHE). It employs a set of empirical correlations which accounts for tube pitch, baffle arrangement, flow differences in the baffles' tip and window regions, and the presence of leakage and

bypass streams in the shell [41]. A full treatment and explanation of all calculations are presented in [1], [13], and Serth [41], and specified to the reference heat exchanger by Reyes [39].

Increasing the tube outer diameter and thickness did not have a direct effect on any of these calculations, but during a review of the previous design calculations, it was determined that certain incorrect values were used which significantly affected the resulting demineralized water heat transfer coefficient, and consequently, the overall heat transfer coefficient and required total heat transfer surface area. Specifically, determining the mass flux of the shell-side fluid is required to calculate the shell-side heat transfer coefficient:

$$G = \frac{\dot{m}}{Sm} \tag{2.3}$$

where G is the mass flux of the shell-side fluid $(\frac{kg}{m^2-s})$, \dot{m} is the mass flow rate of the shell-side fluid (kg/s) and Sm is the cross-flow area at the shell centerline (m^2) . All previous calculations incorrectly used the mass flow rate of the tube-side fluid (2.893 kg/s) instead of the mass flow rate of the shell-side fluid (21.017 kg/s). Table 2.3 illustrates the significant difference between the previously calculated values of G and the corrected values, both for the previous 3/8 in tube outer diameter design and the updated 1/2 in design.

Table 2.3: Comparison of Previous vs. Corrected Mass Flux Values

Tube Outer Diameter (in)	Previous $G(kg/m^2 - s)$	Corrected $G(kg/m^2 - s)$
3/8	137.50	1018.03
1/2	52.38	678.68

All other relevant parameters and thermal properties of the demineralized water (DI) at the new reference inlet condition of 42°C were updated and are listed in Table 2.4.

Table 2.4: Demineralized Water and Heat Exchanger Properties

Dynamic Viscosity	μ	$N-s/m^2$	6.290E-4
Specific Heat Capacity	c_p	J/kg - K	4180
Thermal Conductivity	k	W/m-K	0.6319
Prandtl number	Pr	non-dim	4.16
Mass Flow	\dot{m}	kg/s	21.02
Cross-Flow Area	Sm	m^2	0.0310
Mass Flux	G	$kg/m^2 - s$	678.68
Colburn Factor	j	non-dim	0.0086
Heat Transfer Coefficient	h_{DI}	$W/m^2 - K$	9449.38
Corrected Heat Transfer Coefficient	h_{DIcorr}	$W/m^2 - K$	4167.18

Having determined the convective heat transfer coefficients for both the tube-side and shell-side fluids, Eqn 2.1 can be recast using the definition of U provided in [27]:

$$U = \frac{\dot{Q}}{A\Delta T} = \frac{1}{\frac{1}{h_{CW}} + \frac{L}{k} + \frac{1}{h_{DI_{corr}}}}$$
(2.4)

where L is the tube thickness (m) and k is the thermal conductivity of the tube material $(\frac{W}{m-K})$, which is assumed to be Copper-Nickel (CuNi) alloy 90-10, as proposed in the first-pass system design and in conformance with MIL-DTL-15730N [30], for Type 1, Class 5 coolers. All values on the right-hand side were subsequently calculated, and the overall heat transfer coefficient was determined to be 2115.26 $(\frac{W}{m^2-K})$.

The last value calculated prior to determining A was ΔT , the LMTD, defined as:

$$\Delta T = \frac{(T_{hin} - T_{cout}) - (T_{hout} - T_{cin})}{ln(\frac{T_{hin} - T_{cout}}{T_{hout} - T_{cin}})}$$
(2.5)

where T_{hin} is the demineralized water inlet temperature, T_{hout} is the demineralized water outlet temperature, T_{cin} is the chilled water inlet temperature, and T_{cout} is the chilled water outlet temperature. All values were previously calculated with the exception of T_{cout} , which was calculated using the heat transfer equation cast in terms

of mass flow rate:

$$\dot{Q} = \dot{m_{cw}} c_p \Delta T_{cw} = \dot{m_{cw}} c_p (T_{cin} - T_{cout})$$
(2.6)

where \dot{Q} is the previously calculated total compartment heat load of 240 kW (240000 W or J/s), \dot{m}_{cw} is the previously calculated chilled water mass flow rate of 2.839 kg/s, and c_p is the specific heat capacity of water (4184 $\frac{J}{kg-K}$). Rearranging this equation yielded a T_{cout} value of 300.36°K, or 27.21°C.

The LMTD was then calculated, and after substituting all now known values into Eqn 2.4 and rearranging to solve for A, the total required heat transfer surface area of the tube bundle was determined to be 5.00 m^2 . A summary of the major heat exchanger parameters and characteristics is provided in Table 2.5.

QHeat Transfer kW240 Logarithmic Mean Temperature Difference ΔT K22.69 Tube Outer Diameter D_{OD} 1/2in0.049Tube Thickness LinW/m-KThermal Conductivity of Tube k40 $W/m^2 - K$ Chilled Water Heat Transfer Coefficient h_{CW} 8806.32 $\overline{W/m^2-K}$ Corrected DI Water Heat Transfer Coefficient 4167.18 h_{DIcorr} $W/m^2 - K$ Overall Heat Transfer Coefficient U2115.26 m^2 Tube Surface Area A5.00

Table 2.5: Initial Heat Exchanger Characteristics

2.3.2 Completing Heat Exchanger Redesign

By increasing the tube outer diameter and driving a change in the required heat transfer surface area, other features of the heat exchanger also had to be redesigned to conform to a new set of standards or geometric constraints.

Tables 2.6, 2.7, and 2.8 provide the relevant tube specifications governing spacing, depth of expansion, and depth of flare dictated by MIL-DTL-15730N [30].

The minimum tubesheet thickness for joints with inlet-end flared holes must equal the depth of expansion plus the depth of flare plus 1/8 in. Thus, the tubesheet thickness of this design iteration increased from 0.9375 in to 1.125 in.

Table 2.6: Minimum Tube Spacing [30]

Tube Outer Diameter (in)	Tube Spacing, Center-to-Center (in)
3/8	1/2
1/2	21/32
5/8	13/16

Table 2.7: Minimum Depth of Tube Expansion [30]

Tube Outer Diameter (in)	Minimum Depth of Expansion (in)
3/8	1/2
1/2	5/8
5/8	5/8

Transverse baffles must be installed to provide multiple passes of the shell-side fluid for optimum heat transfer and to provide support for the tube bundles. Baffle thickness and spacing must be in accordance with the standards set forth for Class C heat exchangers as defined by the Tubular Exchangers' Manufacturers Association (TEMA), and provided in Figures 2-1 and 2-2, respectively.

Prior to the discovery of the erroneously calculated shell-side fluid mass flux, it was assumed that the shell's inner diameter would have to increase considerably in order to accommodate the bigger, thicker, and more widely spaced tubes in this design change. However, the required heat transfer surface area for this design iteration was nearly 33% less than that determined by Reyes [39] (5.00 m^2 compared to 7.42 m^2). This new surface area could have been accommodated in an 8 in inner diameter shell with 100, 50 in tubes in an optimal arrangement. However, to ensure that all tube spacing requirements were met in accordance with MIL-DTL-15730N [30], it was preferable to employ a square pitch tube arrangement, which reduced the number of

Table 2.8: Flare of Tube End Holes [30]

Tube Outer Diameter (in)	Radius of Flare (in)
3/8	5/16
1/2	3/8
5/8	1/2

TABLE CB-4.41 BAFFLE OR SUPPORT PLATE THICKNESS Dimensions in Inches (mm)

							1101100 (1111	•••					
				Plate Thickness									
Nominal Shell ID U		Unsupported tube length between central baffles. End spaces between tubesheets and baffles are not a consideration.											
		(305) Under	Over 12 (305) to 24 (610) Inclusive Over 24 (610) to 36 (914) Inclusive		36 (914)	Over 36 (914) to 48 (1219) Inclusive		Over 48 (1219) to 60 (1524) Inclusive		Over 60 (1524)			
6-14	(152-356)	1/16	(1.6)	1/8	(3.2)	3/16	(4.8)	1/4	(6.4)	3/8	(9.5)	3/8	(9.5)
15-28	(381-711)	1/8	(3.2)	3/16	(4.8)	1/4	(6.4)	3/8	(9.5)	3/8	(9.5)	1/2	(12.7)
29-38	(737-965)	3/16	(4.8)	1/4	(6.4)	5/16	(7.5)	3/8	(9.5)	1/2	(12.7)	5/8	(15.9)
39-60	(991-1524)	1/4	(6.4)	1/4	(6.4)	3/8	(9.5)	1/2	(12.7)	5/8	(15.9)	5/8	(15.9)
61-100	(1549-2540)	1/4	(6.4)	3/8	(9.5)	1/2	(12.7)	5/8	(12.7)	3/4	(19.1)	3/4	(19.1)

Figure 2-1: Required baffle thickness given shell inner diameter and unsupported tube length between central baffles [43].

TABLE RCB-4.52 MAXIMUM UNSUPPORTED STRAIGHT TUBE SPANS Dimensions in Inches (mm)

		יווט טווי	nensions in Inches (m	m)		
		F (° C)				
Tube	e OD	Carbon Steel & High	Alloy Steel, 750	Aluminum & Aluminum Alloys, Copper &		
		(399)		Copper Alloys, Titani	ium Alloys At Code	
		Low Alloy Steel, 850	(454)	Maximum Allowable	Temperature	
		Nickel-Copper, 600 ((316)			
		Nickel, 850 (454)				
		Nickel-Chromium-Iro	n, 1000 (538)			
1/4	(6.4)	26	(660)	22	(559)	
3/8	(9.5)	35	(889)	30	(762)	
1/2	(12.7)	44	(1118)	38	(965)	
5/8	(15.9)	52	(1321)	45	(1143)	
3/4	(19.1)	60	(1524)	52	(1321)	
7/8	(22.2)	69	(1753)	60	(1524)	
1	(25.4)	74	(1880)	64	(1626)	
1-1/4	(31.8)	88	(2235)	76	(1930)	
1-1/2	(38.1)	100	(2540)	87	(2210)	
2	(50.8)	125	(3175)	110	(2794)	
2-1/2	(63.5)	125	(3175)	. 110	(2794)	
3	(76.2)	125	(3175)	110	(2794)	

Figure 2-2: Maximum unsupported straight tube spans [43].

tubes that could fit on the tubesheet face to 85. This corresponded to a $0.76~m^2$ reduction in the available heat transfer surface area, which had to be accounted for to ensure the required heat exchanger performance.

Increasing the length of the exposed tube bundle region could have made up for this lost surface area, but would have had deleterious effects on the already limiting pressure drop conditions. Instead, increasing the shell's inner diameter to allow for more tubes and more spacing was pursued. This arrangement accounted for the required heat transfer surface area while promoting amenable pressure drop conditions not only on the chilled water side (due primarily to the increased tube diameter) but also on the demineralized water side by increasing tube spacing and maintaining the original tube bundle length.

Accordingly, the shell inner diameter was increased to 10~in, which allowed for the placement of 107 tubes at 0.75~in center-to-center spacing. The additional tubes made up for the previously lost heat transfer surface area, but the resizing of the shell diameter and respacing of the tubes also directly affected the heat transfer coefficients, and ultimately the required surface area. Therefore, another iteration through the preceding equations was required to reevaluate the required heat transfer surface area. This yielded a new required surface area of $5.37~m^2$ which could be provided by 106, 50~in tubes.

A 10 in shell diameter heat exchanger still falls within the smaller grouping of exchanger designs as delineated by TEMA, and so the first row in Figure 2-1 was used to determine the required baffle thickness, which itself is dependent on the unsupported tube span.

Per Figure 2-2, the maximum unsupported tube span for a 1/2 in copper alloy tube is 38 in. In this design, that translates to a maximum spacing between baffles of 19 in, given that the baffles are of a semi-hemispherical, half-span arrangement, i.e. half of the baffles support the upper tubes and the other half support the lower tubes. Baffles should not be spaced closer than 1/5 of the shell's inner diameter or 2 in, whichever is greater [43]. In this design, those values are equivalent, and so the 2 in threshold served as the lower bound for the baffle spacing. In keeping

with the previous design iterations which demonstrated improved demineralized water pressure drop performance with more widely spaced baffles, baffle spacing was set at 6 in, comfortably within the allowable range. Based on a baffle spacing of 6 in, baffle thickness is determined to be 1/16 in, as delineated in Figure 2-1.

Finally, to ensure adequate distribution of coolant to the tubes, the waterbox head depth must be sized appropriately. For a given shell inner diameter (D), the waterbox head depth shall be not less than 0.5D for single-pass coolers, 0.345D for two-pass coolers, or 0.25D for four-pass coolers. Thus, for this two-pass, 10 in diameter design, the minimum waterbox head depth is 3.45 in, and was initially set at 7 in.

All major prescribed parameters influencing the size and arrangement of the heat exchanger are summarized in Table 2.9.

Table 2.9: Two-pass heat exchanger model geometries and arrangement

	Value	Unit
Waterbox head depth	7	in each
Exposed tube length	50	in
Tube sheet thickness	1.125	in each
Overall heat exchanger length	66.25	in
Heat exchanger internal shell diameter	10	in
Tube spacing (centerline-to-centerline)	0.750	in
Total number of tubes	107	non-dim
Number of inlet tubes	54	non-dim
Baffle thickness	0.0625	in
Baffle spacing	6	in

2.3.3 Modeling and Simulation

The redesigned heat exchanger was modeled in the 3D solid modeling Computer Aided Design (CAD) software SOLIDWORKS and analyzed using its CFD Flow Simulation add-on feature. Allowable pressure drop and maximum velocity limits exist for both the shell-side and tube-side fluids as dictated by MIL-DTL-15730N [30] and are provided in Figures 2-3 and 2-4. Regarding maximum velocity limits, MIL-DTL-15730N [30] stipulates that the shell-side velocities shall not exceed the "Velocity through tubes" limit listed in Figure 2-4, and thus this 9 ft/s limit was

also applied to the demineralized water flow. These values served as the primary fluid flow performance criteria to determine if a given heat exchanger design performed adequately. Additionally, there are limits associated with the cooling water inlet temperature, as provided in Figure 2-5. For freshwater-cooled systems on surface ships, the upper limit is 95°F, far above the assumed 7°C (44.6°F) value assumed for the chilled water inlet temperature.

Cooler type	Fluid side	Allowable pressure drop (lb/in²)
Main propulsion turbine lubricating oil coolers that use scoop injection of	Tube (seawater) side	4
circulating water	Shell (oil) side	15
Other lubricating oil coolers and	Coolant side	6
freshwater coolers	Cooler fluid side (oil)	12
	Cooled fluid side (freshwater)	6
Hydraulic oil coolers	Tube (coolant) side	6
	Shell (oil) side	25

Figure 2-3: Maximum allowable pressure drops [30].

Coolant and method of supply	Velocity through inlet flange (feet per second)	Velocity through tubes (feet per second)
Seawater, supplied by scoop injection	11.0	9.0
Seawater, otherwise supplied	9.0	7.5
Fresh water, however supplied	11.0	9.0

Figure 2-4: Maximum cooling water velocities [30].

The shell-side demineralized water flow was simulated using the previously derived initial conditions: inlet flow at 100 psi, inlet temperature at 42°C, and a mass flow rate of 21.017 kg/s. The mass flow rate is replicated at the outlet nozzle owing to the continuity of mass in a steady flow condition and was used as the primary outlet boundary condition. The velocity and pressure profiles are provided in Figures 2-6 and 2-7.

The demineralized water flow maintains a velocity over the tubes less than the aforementioned 9 ft/s limit. Moreover, Figure 2-8 shows that the global pressure

Ship or craft	Coolant	Temperature (°F)
Submarines	Seawater	85
	Fresh water	95
Large surface ships	Seawater (electronic system)	95
	Seawater (other systems)	90
	Fresh water	95
Patrol boats and small craft	Seawater	95
	Fresh water	100

Figure 2-5: Maximum cooling water inlet temperature [30].

drop from the inlet nozzle to outlet nozzle is approximately 5.50 *psi*, below the 6 *psi* limit. Thus, this design iteration proved viable from a shell-side, demineralized water perspective.

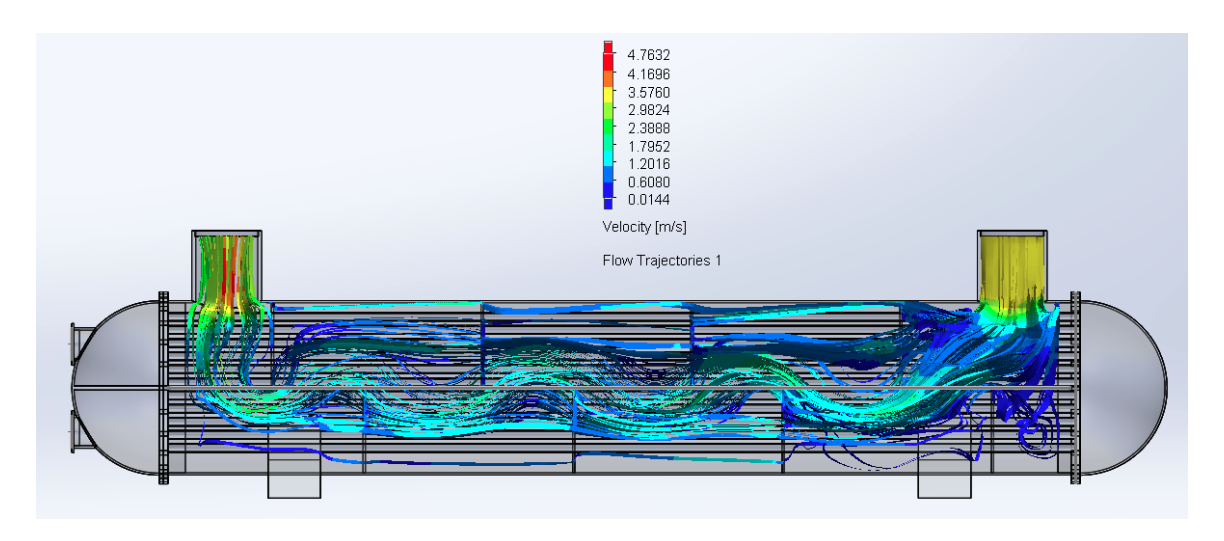


Figure 2-6: Demineralized water velocity flow.

The same model was used to simulate the tube-side chilled water flow, again using the previously derived initial conditions: inlet flow at 100 psi, inlet temperature at 7°C, and a mass flow rate of 2.84 kg/s. The velocity and pressure profiles are provided in Figures 2-9 and 2-10. The chilled water flows through the inlet flange and nozzle at approximately 2.8 m/s (9.2 ft/s), safely below the upper 11 ft/s velocity limit. The chilled water flow through the tubes never exceeds 2 m/s (6.56 ft/s), safely below the corresponding 9 ft/s velocity limit for tube-side cooling flow. Moreover, Figure 2-11 shows that the average pressure drop from the inlet nozzle to outlet nozzle is

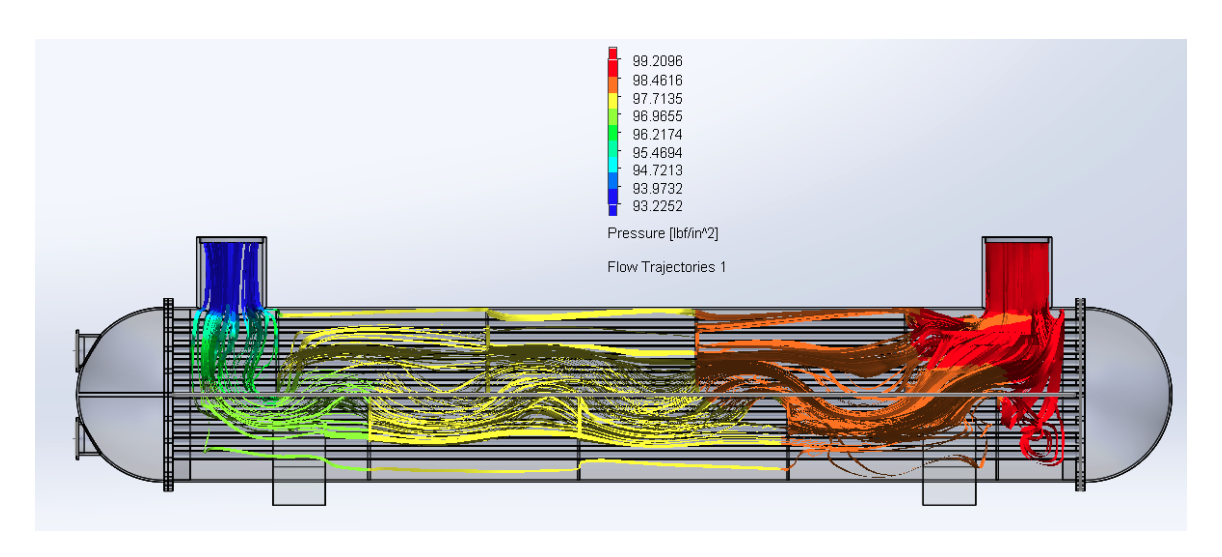


Figure 2-7: Demineralized water pressure gradient.

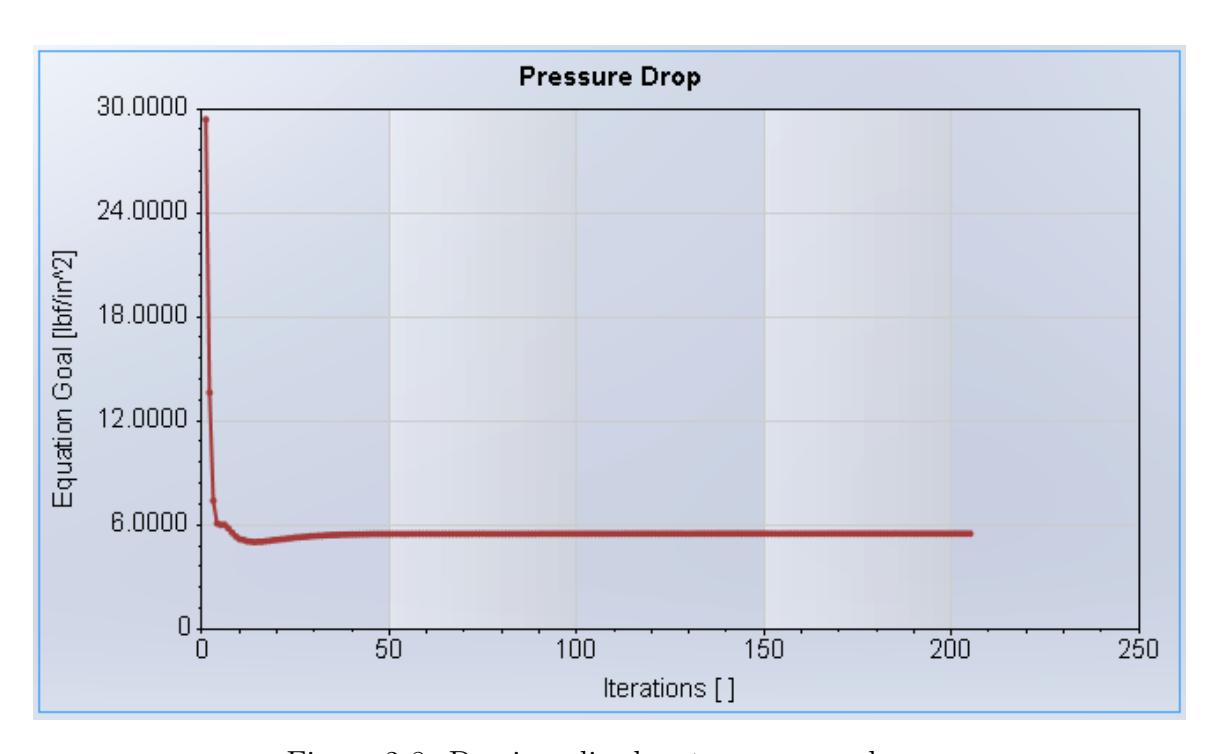


Figure 2-8: Demineralized water pressure drop.

approximately $1.58\ psi$, and the global maximum pressure drop observed is $2.28\ psi$, both of which are below the $6\ psi$ limit. Thus, this design iteration also proved viable from a tube-side, chilled water perspective.

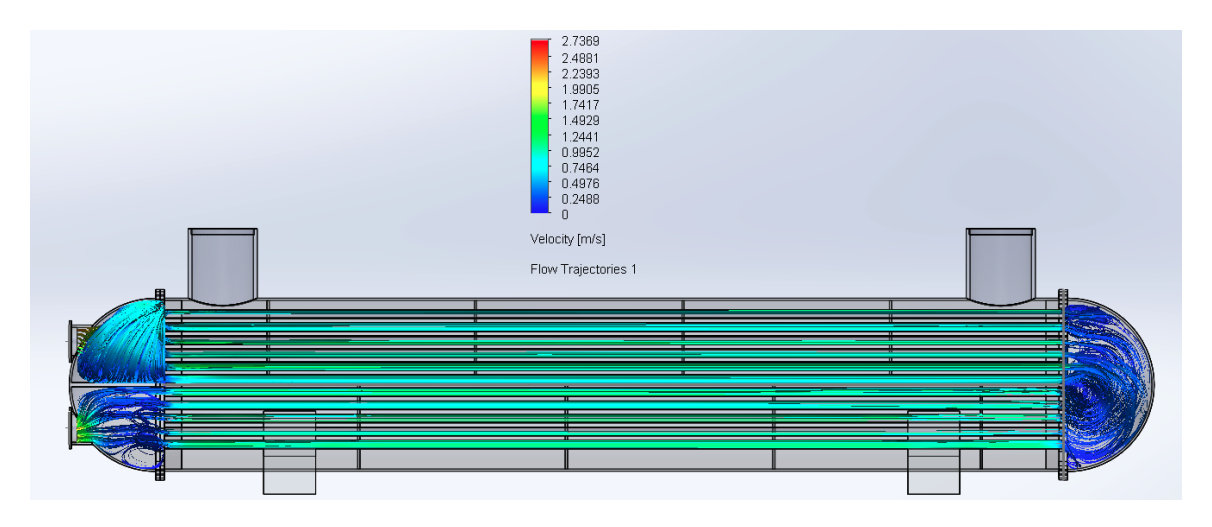


Figure 2-9: Chilled water velocity flow.

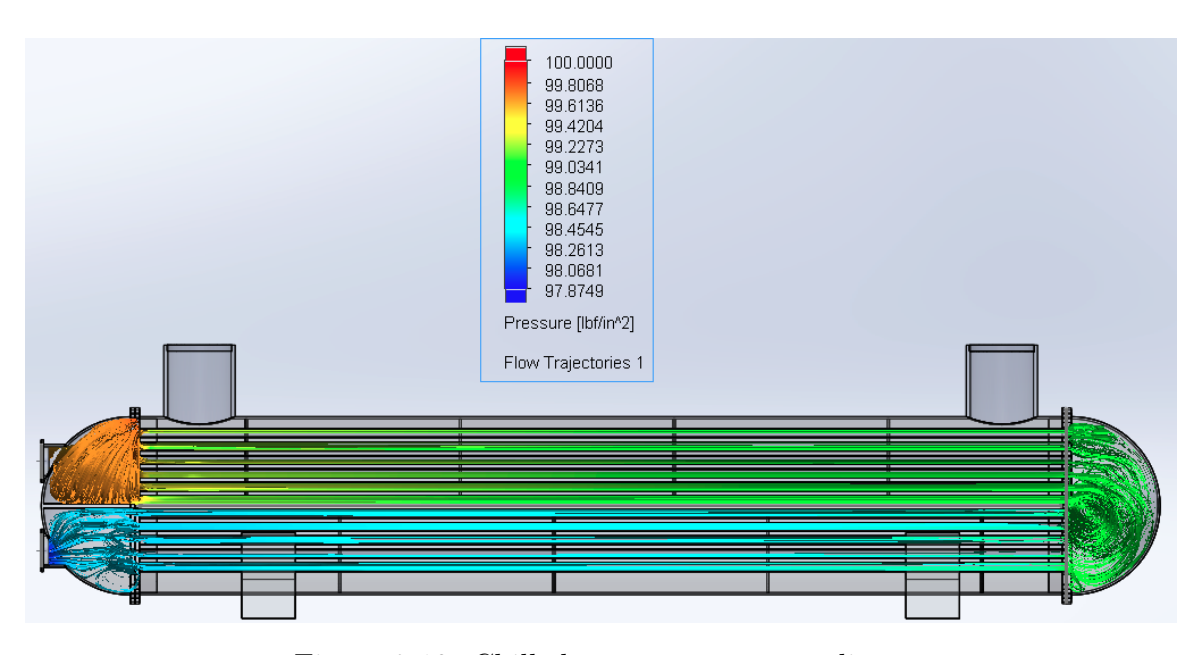


Figure 2-10: Chilled water pressure gradient.

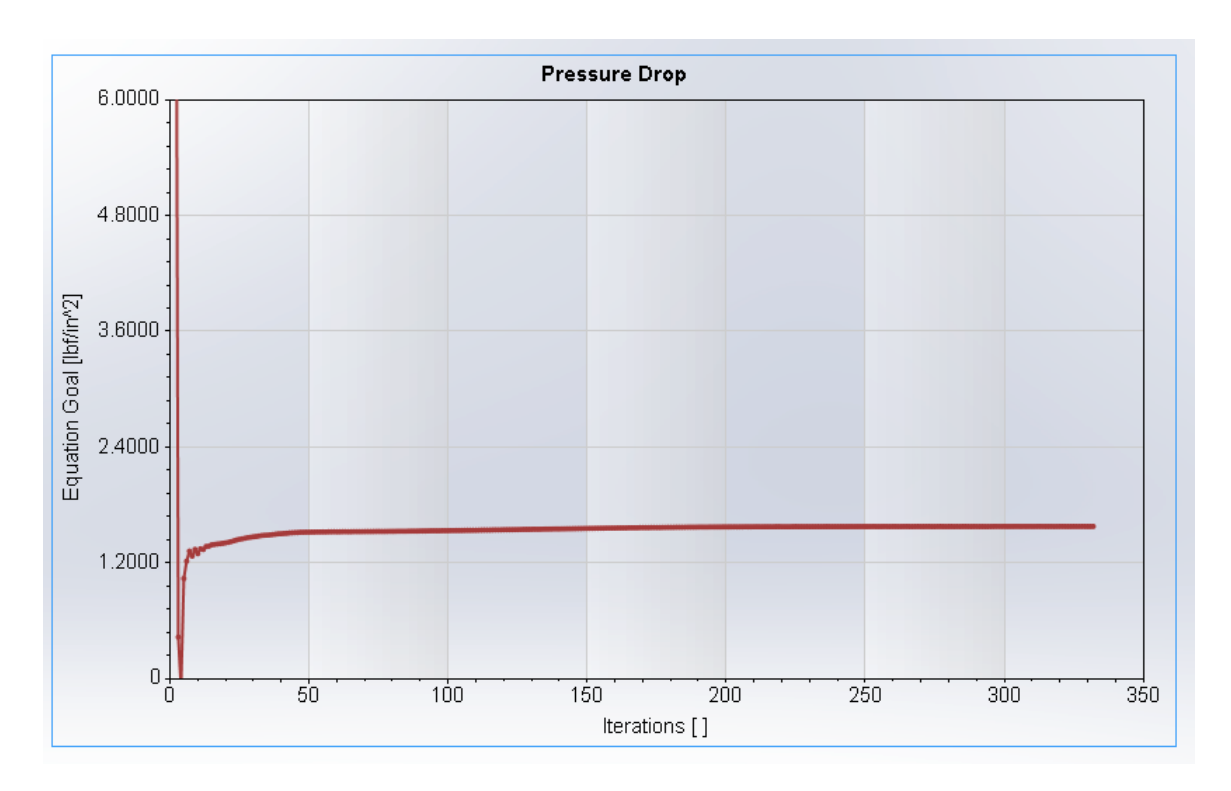


Figure 2-11: Chilled water pressure drop.

2.3.4 Heat Exchanger Redesign Conclusions

This modified heat exchanger design fulfilled all heat transfer and design requirements. Previous chilled water pressure drop issues were addressed primarily by increasing the tube outer diameter from 3/8 in to 1/2 in. Demineralized water pressure drop issues were addressed by maintaining favorable baffle spacing and increasing the shell inner diameter from 8 in to 10 in, which directly increased the flow area, reduced the cross-flow velocity, and consequently reduced the pressure drop. Increasing the shell diameter also enabled increasing the tube spacing from the previous 1/2 in and 0.656 in iterations to the current 0.75 in proposal, which also increased the flow area. Additionally, a reassessment of the temperature and flow conditions determined that the actual required heat transfer surface area was considerably lower than what was previously proposed. This allowed the heat exchanger's length to remain essentially unchanged from the four-pass design developed by Reyes [39] and thus maintained a relatively consistent spatial and volumetric footprint.

As such, this heat exchanger design represents a viable thermal management solution for a nominal portion of a single compartment within the overall NiPEC architecture and an improved starting point from which to scale up the cooling system to meet the full ship's demand.

Chapter 3

Full Ship Analysis

The single-compartment NiPEC cooling system developed by Reyes [39] is an excellent starting point in finding a potential thermal management solution, but it likely cannot be feasibly scaled for shipwide employment given the burdensome construction, operation, maintenance, and cost considerations. Indeed, it was not intended for replication within every compartment on the ship and instead provided a compelling proof-of-concept case that this cooling approach was a viable one. The lessons learned from this previous exploration were used as the basis for expanding to a full ship application. In order to properly expand the scope, the entire ship and its electrical load had to be taken into account to better understand the potential total power demand, how the NiPEC architecture could be configured to accommodate that demand, and how a larger-scale cooling system could be designed to accommodate the heat load across multiple compartments and multiple corridors.

3.1 Nominal Ship Electrical Load

The previous single-compartment analysis assumed an overall four-corridor NiPEC layout, wherein each corridor consisted of twelve of these nominal compartments. The choice to fit four PEBBs per stack was based primarily on vertical clearance restrictions within the compartment, whereas the decision to incorporate five stacks per compartment was chosen for initial analysis based on reasonable yet general thermal

load assumptions. In reality, there is no one "nominal" compartment which can suitably represent the power and thermal load conditions of all the ship's compartments. Given the variability in load size, type, and location, individual compartment power requirements may vary greatly. A more thorough analysis of an entire ship's expected load, and the distribution of this load, was therefore required before determining how to best scale up the proposed single-compartment cooling system into one suitable for shipwide employment.

3.1.1 Electric Power Load Analysis

Building off previous research and estimates, a notional all-electric destroyer-type warship was modeled to provide the framework for subsequent analysis. Anticipated electrical loads were reviewed, assessed, and accounted for in order to construct an allocation and breakdown strategy for the ship's power demand. These loads included major combat weapons systems (i.e. dual-band radars, sonar suite equipment, Vertical Launch System (VLS), laser, railgun), major propulsion and engineering equipment (i.e. Permanent Magnet Motors (PMM), all required generator sets, chillers), and various allowances for miscellaneous AC and DC loads.

Of note, the ship was assumed to be outfitted with one railgun, one port and one starboard PMM, three LM2500 gas turbine generator sets (two port, one starboard), and two LM500 gas turbine generator sets (one port, one starboard). Nearly all loads were initially considered "vital" and were given at least two sources of power, *i.e.* accounted for by twice the number of PEBBs than what the power rating would otherwise dictate. Assuming this level of redundancy provides improved system reliability, and also aligns with previous work done by del Águila Ferrandis et al. [20] which assumed that N-1 corridors must supply the total load, where N is the total number of corridors.

Each load or source was initially assigned a three-dimensional spatial location, a watertight compartment based on that location, rated electrical power (kW), current type, and rated voltage (V). Although one could conservatively design for the total connected load (all loads operating at all times at 100% rated capacity), this approach

would overdesign the system and dictate unnecessary demands on other system components. Instead, a more detailed treatment of the electrical load list was required in order to get a more accurate model of the resulting demand profile.

To this end, every listed load was assigned a load factor, which refers to the ratio of the operating load to the connected load, and provides a representation of how often (i.e. duty cycle) and to what extent a load is actually operating and drawing power [19]. The NAVSEA Design Data Sheet 310, EPLA for Surface Ships (DDS-310) provides load factors for various ship platforms, as depicted in Figure 3-1, and was consulted in order to establish valid values for the model all-electric destroyer warship. Load factors vary based on the ship's operating condition, the most demanding of which is its functional condition, i.e. the condition in which it is performing its design function. For a destroyer, the primary functional condition is battle during wartime, and was chosen as the condition for load factor assignment. In choosing this operating condition, it ensured that subsequent cooling system design decisions would be scaled to meet the most limiting scenario available.

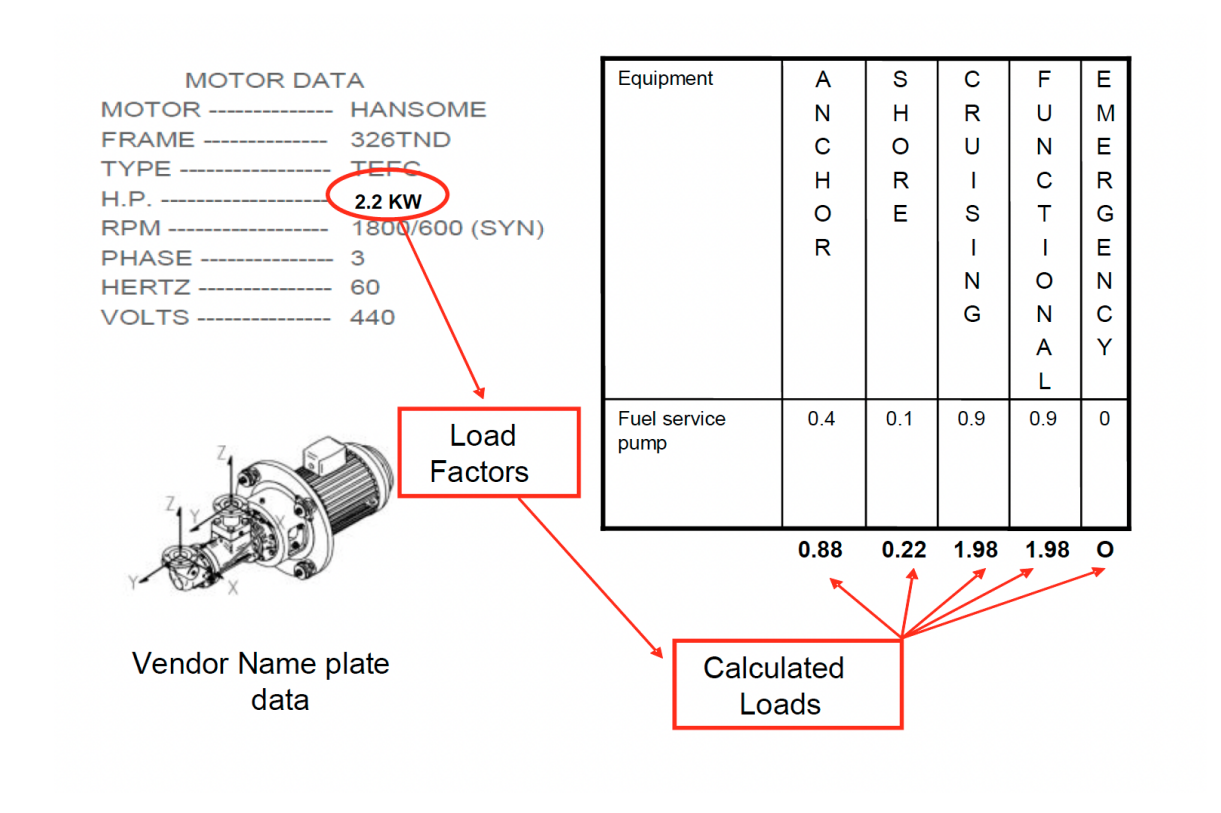


Figure 3-1: Load Factor calculation example [19].

The complete load factor lists are provided in Appendix B. In the cases where no data existed, sound engineering judgment was used to predict reasonable duty cycle times, power demand profiles, and the resulting load factor assignment. For example, a traditional gun mount is assigned a 0.6 load factor, but the model destroyer is assumed to be outfitted with a railgun instead, which is not included in DDS-310 [19]. Given the pulse-type characteristics and attendant short duty cycle of the imagined rail gun, a lower but still conservative load factor of 0.4 was considered reasonable.

Additionally, DDS-310 [19] provides specificity with regard to the number and types of electrical loads included, but the model nominal destroyer did not possess that same level of granularity. Many loads were bundled into the "Miscellaneous AC/DC" categories, whose constituents' individual load factors could vary considerably. A comparison was made between the loads expected to fall in these categories and those specified in DDS-310 [19]. Average load factors were determined across SWBS groups, and modified as necessary in order to account for mutually exclusive loads, i.e. redundant components such as an operational pump and its standby unit. In order to ameliorate the uncertainty underlying these calculations, an additional 15% safety margin was applied, resulting in a 0.7 load factor assigned to all miscellaneous AC and DC loads.

3.1.2 PEBB Conversion Requirements and Functionality

Figure 3-2 represents a generic half-zone layout of the proposed PEPDS bus with a sampling of the expected conversion requirements, which are described below.

The power train and electrical distribution processes begin at the installed LM2500 and LM500 generator sets, which produce 29~MW and 3.7~MW of power, respectively, at an output voltage of $6900~V_{AC}$. This output is converted to $12000~V_{DC}$ for transmission and distribution across the main MVDC bus. Certain large mission loads tap directly off the MVDC bus, such as Integrated Topside (InTop), a multi-functional system of electronic warfare, radar, and communications capabilities, depicted in the bottom right corner of Figure 3-2. The propulsion PMMs require conversion to a 15-phase MVAC operating voltage but also tap off the MVDC bus.

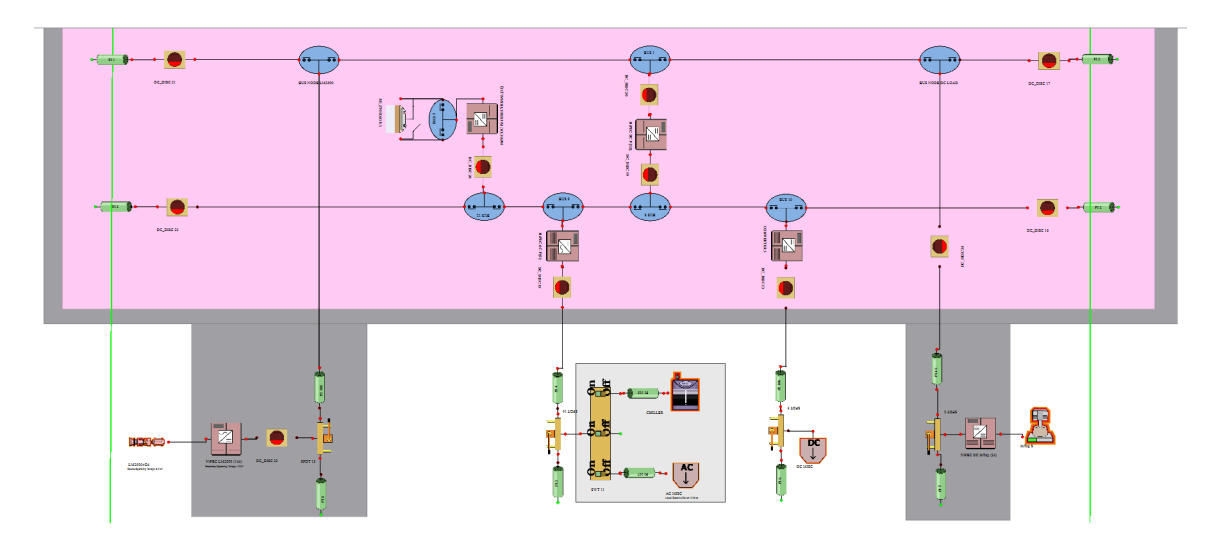


Figure 3-2: Proposed half-zone layout of the PEPDS bus.

Power from the MVDC bus is transferred to the LVDC bus via power conversion "stations" which perform a step-down transformation process to convert the 12000 V_{DC} main bus voltage to 1000 V_{DC} . This specific conversion capacity is required throughout the ship, and so these stations are strategically located within offset port and starboard compartments, envisioned to be evenly distributed between the second-deck and fourth-deck corridors. Power carried through the LVDC bus can then be conveyed to an in-zone DC or Low Voltage Alternating Current (LVAC) load center, the latter of which requires conversion from 1000 V_{DC} to 450 V_{AC} .

Each of these conversion or distribution processes requires a minimum number of PEBBs, which is dependent on the type of PEBB being employed. These values are summarized in Table 3.1. Thus, the total amount of required PEBBs for a given compartment is jointly dependent on these minimum thresholds and the actual power demand from the compartment loads.

Each component's rated voltage corresponded to one of four load types, described in Table 3.2. This categorization of load type informed which conversion process would be required to convey power to that load, and was necessary in order to correctly allocate PEBBs at the compartment level. It also proved useful in order to ascertain which load types were driving power demand, and where that demand was being generated within the ship. Loads were then grouped according to voltage requirements

Table 3.1: Minimum Number of PEBBs Required By Conversion Type

Conversion Type	nversion Type iPEBBs Required		PEBB 6000s	Power Converted
Conversion Type	iredds Required	(kW)	Required	(kW)
LVDC-LVAC	3	750	3	3000
LVDC-LVDC	1	250	1	1000
MVDC-LVDC	12	3000	2	2000
MVAC-MVDC	36	9000	12	12000
MVDC-MVAC	180	45000	30	30000

and summed to determine the total power by rated voltage within the compartment. Finally, this power requirement was correlated to the associated number of required PEBBs to meet that demand within each compartment.

Table 3.2: Load Type by Rated Voltage

Rated Voltage (V)	Load Type
450 (AC)	LVAC
1000 (DC)	LVDC
12000 (DC)	MVDC
6900(AC)	MVAC

3.1.3 iPEBB-only Deployment

In the first iteration, only the 250~kW-rated Navy iPEBBs were utilized within the NiPEC. In keeping with the previous assumptions made by del Águila Ferrandis et al. [20], partially-filled stacks were not permitted in the design and allocation scheme. For example, if a compartment's power demand necessitated six iPEBBs, this would, in turn, necessitate the dedication of two stacks and eight iPEBBs to this compartment since the model assumed each stack contains four iPEBBs. The excess iPEBB capacity is envisioned to be utilized for energy storage.

Table 3.3 provides the number of iPEBBs required per compartment for each side of the ship, as well as the total allocation requirements. A more thorough allocation breakdown specified by load type is provided in Appendix C.

These initial estimations made clear that a "nominal" compartment cannot ac-

Table 3.3: Number of iPEBBs Required Per Compartment

Compartment	Port	Starboard	Total
1	4	4	8
2	4	16	20
3	16	4	20
4	8	8	16
5	32	20	52
6	36	24	60
7	164	164	328
8	12	148	160
9	156	60	216
10	144	8	152
11	20	8	28
12	4	16	20
13	20	44	64
14	4	4	8
Total	624	528	1152

curately capture the load demand and distribution of an entire ship. Only three of the proposed compartment sections exactly required the 20 iPEBBs which were assumed in all previous single-compartment analyses. There also exists high variability in the number of iPEBBs required for each compartment. Overall, there is a standard deviation of approximately 55 iPEBB units per compartment. Power demand and corresponding iPEBB allocation are comparatively very low in the forward-most and aft-most compartments and increase significantly in a few mid-ship compartments, which makes sense given the major equipment location but again weakens the utility of the "nominal" compartment approach. Some of the major pieces of equipment driving power demand are listed below:

- 27 iPEBBs designated for MVDC usage due to the 16600 kW-rated (6640 kW operating load) railgun in Compartment 4.
- 144 iPEBBs designated for generator usage due to the 29000 kW-rated LM2500 generator sets, one for each side of Compartment 6, and one additional set in Compartment 8.

• 135 iPEBBs designated for MVDC usage due to the 37500 kW-rated (33750 kW operating load) PMMs, one in Compartment 7 (starboard) and one in Compartment 9 (port).

Rendering a more accurate depiction of the power demand and load distribution also illustrated the capacity challenges at hand. These figures estimate that 1152 iPEBBs would be required to meet the functional operating condition scenario, compared to the 960 iPEBB total resulting from taking the load assumptions used by Reyes [39] and extrapolating to a shipwide configuration. This represents a 19.6% increase in predicted iPEBB allocation, which not only exacerbates the thermal management situation but could also pose significant arrangement challenges to incorporate the required number of iPEBBs into the overall NiPEC and PEPDS system architecture.

3.1.4 iPEBB and PEBB 6000 Joint Deployment

In an effort to reduce the overall PEBB footprint, a second model was constructed which utilized a combination of iPEBBs and the PEBB 6000, the latter of which is assumed to convert up to $1000 \ kW$ at $6000 \ V$. The higher capacity PEBB 6000 was targeted to handle the largest loads, such as the aforementioned railgun, generators, and PMMs.

The same process as before was followed to determine the total power demand in each watertight compartment within the ship, and the corresponding number of PEBBs and stacks required in each compartment to fulfill said demand. The full results are provided in Appendix C.

Incorporating the higher-capacity PEBB 6000 into the NiPEC infrastructure significantly reduced the total number of PEBBs from 1152 to 604, a 47.4% unit reduction. It is also significantly limited the variation in number of PEBBs required per watertight division, lowering the standard deviation of units per compartment to approximately 20. Importantly, however, the current PEBB 6000 design is considerably bigger than the iPEBB and requires the addition of support drawers and components

which will contribute to each unit's spatial and weight footprint. Therefore, the benefits of eliminating approximately 660 iPEBBs will not be fully realized due to these added constraints imposed by PEBB 6000 installation.

Nonetheless, the joint iPEBB-PEBB 6000 deployment offers a more reasonable total PEBB allotment, while also providing flexibility for additional PEBB installment to address energy storage needs.

3.2 Spatial Analysis

One of the major design philosophies of the NiPEC is its customization at the water-tight subdivision level, that it is tailored to the sources and loads in that section [10]. In other words, all the power inputs and outputs ideally occur within each section individually; every load physically located in a watertight division is fully supplied from the corridors within that division [20]. What this practically means is that all the PEBB stacks assigned to a given compartment must actually fit within that compartment.

To assess the initial viability of the proposed PEBB allocations, bulkhead locations and compartment lengths were taken from the nominal destroyer model and are provided in Table 3.4. Cabinet sizing for the iPEBB stacks was determined using the dimensions proposed by Reyes [39] for the idealized iPEBB cabinet but also included an additional 6 in on each side of the stack to account for structural support components and cooling piping. This estimate was based on a comparison to similar commercial equipment, such as ABB's OMD880LC Onboard Microdrive cabinet pictured in Figure 3-3 [9]. The dimensions of the PEBB 6000 and its stack were unknown at the time of analysis and were assumed to be 1.5 times that of the Navy iPEBB. It was assumed that three PEBB 6000s could fit in a stack.

Given these assumptions and the above PEBB arrangements, the total stack length for each portion of each corridor was determined on a compartment-by-compartment basis. The initial results were promising, as only two corridor sections featured a stack length that exceeded its compartment length. Compartment 9, port side, required a

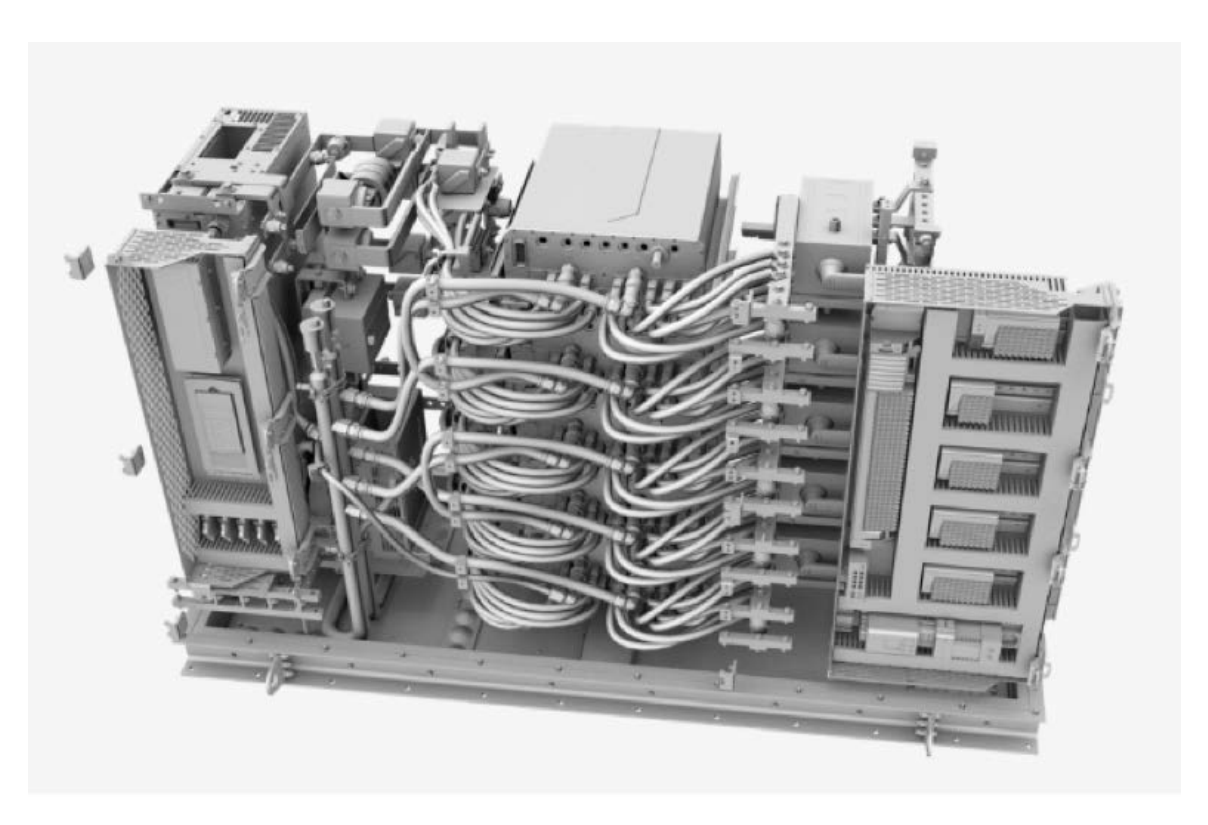


Figure 3-3: Industry example of shipboard power conversion cabinet [9].

Table 3.4: Bulkhead Locations and Compartment Lengths

Bulkhead	Distance from FP (m)	Compartment	Length (m)
1	8.41	1	8.41
2	19.31	2	10.90
3	35.06	3	15.75
4	42.05	4	6.99
5	52.18	5	10.13
6	60.12	6	7.94
7	76.63	7	16.51
8	84.57	8	7.94
9	101.02	9	16.45
10	109.02	10	8.00
11	120.77	11	11.75
12	132.39	12	11.62
13	144.07	13	11.68
_	-	14	9.93

stack length of 10.13 m on each deck; Compartment 9 is only 8.00 m long. Similarly, Compartment 7, starboard side, also required a stack length of 10.13 m on each deck; Compartment 7 is only 7.94 m long. The principal driver of these mismatches is the presence of the PMMs, each of which requires 60 PEBB 6000 units, and thus 20 PEBB 6000 stacks. All other required corridor lengths are shorter than their respective compartment lengths, which indicates that the remaining NiPEC equipment and infrastructure required for each compartment could comfortably fit within the remaining space.

3.3 Thermal Analysis

Given the encouraging ongoing progress of the PEBB 6000 development, and the spatial and power distribution advantages it offers within the larger NiPEC system architecture, the subsequent thermal analysis assumed a joint Navy iPEBB-PEBB 6000 deployment approach. Tables C.3 and C.4 provide the total PEBB footprint for an entire side of the ship, so each corridor was initially allocated half of the total PEBB units listed.

3.3.1 Heat Loss Reassessment

All previous calculations had assumed that each Navy iPEBB dissipates $10 \ kW$ of heat when operating at maximum capacity, but this was an overly conservative estimate, made more onerous by the additional 20% safety margin applied to the overall heat load. As such, the iPEBB heat loss term was reassessed to determine a more accurate, and less demanding, value. Based on research conducted at the Virginia Tech Center for Power Electronics System (CPES), where the Navy iPEBB is being built, the inner half of the iPEBB and its transformer exhibit the loss characteristics provided in Figure 3-4. These losses sum to 5.91 kW, and the full iPEBB is not expected to double these losses. As such, the maximum heat loss term was reduced to 8 kW (corresponding to a 96.8% operating efficiency at full capacity). The PEBB 6000 was assumed to dissipate $10 \ kW$ of heat at full load, in light of its assumed $1 \ MWe$

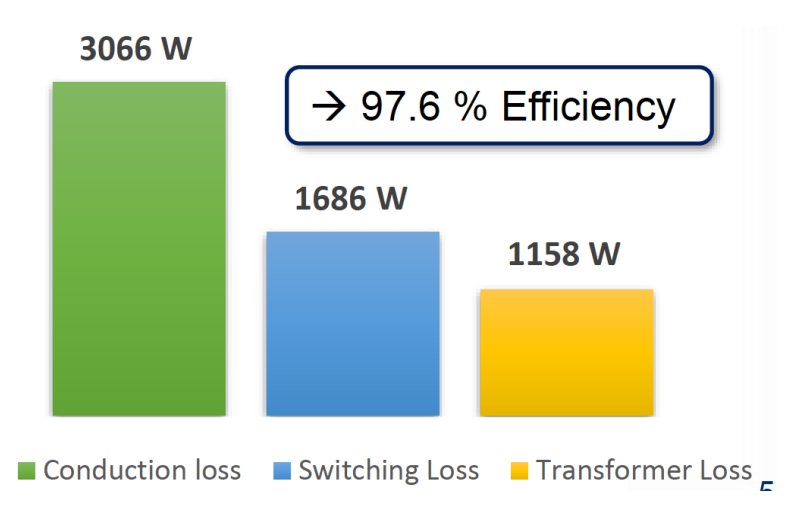


Figure 3-4: Navy iPEBB heat loss characteristics [21].

maximum capacity and 99% operating efficiency.

Given these updated heat loss terms, the worst-case corridor heat load, based on the PEBBs' maximum capacities, was determined to be $1515.8 \ kW$.

3.3.2 Chilled Water Flow Reassessment

Reyes [39] assumed that the nominal ship's Air Conditioning system would provide chilled water to each of the four power corridors via four chilled water pumps. Each pump, which was assumed rated at 600 gpm, would be assigned to one of the four corridors, and after apportioning 60 gpm to non-NiPEC loads, would provide 540 gpm to service all the corridor's compartments. The chilled water flow rate to the system's heat exchanger was thus initially assumed at 540 gpm, since the intent was to dissipate many compartments' heat loads at a single heat sink. This increased flow rate required increasing the size of the chilled water inlet and outlet piping, previously assumed to both have a 1.5 in outer diameter, in order to ensure conformance to relevant military standards.

NSTM 505, which governs piping systems onboard U.S. Navy vessels, places limitations on the allowable pipe velocities in order to minimize excessive pipe wear and promote system longevity. In the case of seawater systems, erosion corrosion is of particular concern, and the manual provides specific limits which are provided in

Table 3.5: NSTM 505 Fluid Velocity Limits

Nominal Pipe Size	Pipe OD (in)	Velocity (fps)	Flow (gpm)
1/2	0.840	4.2	5.2
3/4	1.050	4.8	9.9
1	1.315	5.4	18.6
1-1/4	1.660	6.2	34.9
1-1/2	1.900	6.6	49.8
2	2.375	7.4	88.4
2-1/2	2.875	8.2	147
3	3.500	9.1	244
3-1/2	4.000	9.8	348
4	4.500	10.3	462
5	5.563	11.5	794
6 and larger	6.625	12.0	1187

Table 3.5. Although the proposed NiPEC cooling system utilizes chilled water and demineralized water, the NSTM 505 limits provide conservative upper bounds and served to orient follow-on design decisions concerning pipe sizing and fluid velocity.

As Table 3.5 indicates, a chilled water flow rate of 540 gpm requires a considerably larger piping diameter than the currently assumed 1.5 in piping. This flow rate falls between the limits of the Nominal Pipe Size (NPS) 4 and 5 systems, and so NPS 5, Schedule 80 piping was assumed for the chilled water inlet and outlet piping, corresponding to a pipe outer diameter of 5.563 in, and a pipe wall thickness of 0.375 in.

3.3.3 Demineralized Water Flow Reassessment

The proposed demineralized water flow was initially modified in accordance with MIL-STD-1399 [31], which stipulates that cooling flow shall be adjusted to a maximum of 1.4 gpm for every additional kW of load in order to maintain a maximum 2°C temperature rise in the water. In previous analyses, the assumed heat load of 240 kW correlated to a demineralized water flow of 336 gpm when servicing just a portion of a single compartment. By following this same process to account for an entire corridor's heat load based on the EPLA, the required cooling flow values increased to 2990 gpm

and 2554 gpm for each of the port and starboard corridors, respectively. These values are not only unreasonably large in terms of required pump sizing they invoke but would also violate the velocity limits listed in Table 3.5 and recommendations governing shell-side fluid dynamics.

Section RCB-4.62 of the TEMA manual states that "in no case shall the shell or bundle entrance or exit area produce a value of ρV^2 in excess of 5953 where V is the linear velocity of the fluid (m/s) and ρ is its density (kg/m^3) " [43]. The exit area of the tube bundle represents the more limiting region since the demineralized water is assumed to be at 40°C there versus 42°C at the entrance area, resulting in a slightly higher water density and slightly lower allowable velocity. Given a density of 992.22 kg/m^3 at 40°C, this results in an allowable entrance and exit velocity of 2.45 m/s(8.04 fps). Prior to considering additional changes to the system heat exchanger, the shell-side inlet and outlet piping diameter of 2 in from the original model was assumed. This pipe sizing, in conjunction with the limiting 2990 gpm volumetric flow rate derived from the MIL-STD-1399 [31] heuristic, resulted in an entrance and exit velocity of 93.1 m/s, far exceeding the upper limit. Although the inlet and outlet piping was not constrained to the diameter assumed in these calculations, the results illustrate how far beyond the allowable limits this calculated flow rate would bring the current design. As such, further interrogation of acceptable and feasible shell-side flow rate was required.

To this end, consideration was given to reducing the demineralized water inlet temperature in order to permit a reduced flow rate. However, doing so would result in a lower LMTD between the demineralized water and chilled water, which would directly result in a larger required heat transfer surface area as given by Equation 2.1. Alternatively, the LMTD could be increased, and the required demineralized water mass flow rate thereby decreased, by lowering the chilled water inlet temperature, but this was deemed infeasible given that the chilled water system was already assumed to be operating very near its minimum header temperature.

Instead, a sensitivity analysis was conducted by adjusting demineralized water flow across a range of values spanning from the originally proposed 336 gpm to the

2290 gpm derived from MIL-STD-1399 [31] in order to determine values for the following key parameters: minimum allowable inlet and outlet piping diameter (to meet the prescribed velocity limits), required heat exchanger tube area, and overall heat exchanger length. In this analysis, the shell diameter was fixed at 36 in, which was chosen as a reasonable initial estimate given the single compartment heat exchanger's 10 in diameter, and the need to appropriately scale up the design to manage the much larger heat load of an entire corridor. The results of this analysis are provided in Table 3.6.

Table 3.6: Demineralized Water Flow Sensitivity Analysis

Flow Rate (gpm)	Pipe Diameter (in)	Required Tube Area (m^2)	Overall Length (ft)
336	4.20	57.07	6.32
500	5.10	46.13	5.72
750	6.20	37.81	5.26
1000	7.20	32.02	4.94
2000	10.15	25.78	4.60
2990	11.40	23.19	4.46

In light of these results, and in correlating them with the NSTM 505 velocity limits, NPS 5 size pipe was chosen as a reasonable redesign starting point for the demineralized water inlet and outlet piping. This permitted a flow rate up to 794 gpm, but a lower target flow rate of 460 gpm was initially selected to provide margin to the relevant limits and mitigate anticipated increases in pressure drop with increased flow rates.

3.3.4 Corridor Heat Exchanger Design

Following the reassessment of the iPEBB heat loss term and flow rate parameters, the heat exchanger redesign tradespace was reevaluated. As before, priority was placed on minimizing the overall length of the exchanger, both for spatial considerations and pressure drop concerns. A sensitivity analysis was conducted, iterated on the shell's outer diameter. By adequately increasing the shell diameter, a sufficient number of additional tubes could be included such that each tube's length, and thus the overall

heat exchanger length, would not become prohibitively long. The results of this sensitivity analysis are presented for the limiting heat load scenario in Table 3.7.

Table 3.7: Shell Outer Diameter Sensitivity Analysis

Shell Diameter (in)	Required Tube Area (m^2)	Number of Tubes	Overall Length (ft)
10	27.23	111	21.19
18	34.47	377	9.21
26	40.87	805	6.53
34	46.76	1369	5.83
36	48.17	1500	5.83
40	50.93	1739	5.93

There are diminishing returns and eventual trend reversal with respect to overall heat exchanger length as shell diameter increases. This is because, as shell diameter increases above 36 in, the mass flux of the shell side fluid is lowered so much that despite the increased number of tubes available, they must still be lengthened in order to achieve the new required tube heat transfer area. This was a valuable finding in that it effectively established an upper limit on viable shell diameters.

Competing against the intended course of action was that the number of tubes accommodated by a larger shell diameter scales more rapidly than the shell diameter itself, such that the shell-side pressure drop could worsen due to the sheer number of tubes that the demineralized water has to flow over and past. To address this possible outcome, the model was fine-tuned by increasing the shell diameter but only increasing the tube surface area necessary to overcome the shell-side fluid mass flux reduction. In this way, the number of tubes was not necessarily maximized for the given tubesheet surface area, but the increased tube spacing would improve the shell-side fluid flow environment. These concessions resulted in a slightly longer heat exchanger than what could otherwise be optimized, a potentially necessary tradeoff to address all aspects of heat exchanger performance.

It was determined that all corridors would have identical heat exchangers, parameterized by the most limiting heat load. This decision will improve the manufacturability and maintainability of the heat exchangers since they will all be constructed identically and have identical maintenance schedules. As such, the 26 in shell diame-

ter variant, resulting in an overall length of approximately $6.53 \ ft$, was the first option chosen for modeling, simulation, and analysis. All relevant heat transfer parameters and heat exchanger geometry characteristics are summarized in Tables $3.8 \ and \ 3.9$.

Table 3.8: Initial one corridor heat exchanger thermal-hydraulic parameters

Heat Transfer	\dot{Q}	kW	1515.8
Logarithmic Mean Temperature Difference	ΔT	K	28.46
Tube Outer Diameter	D_{OD}	in	1/2
Tube Thickness	L	in	0.049
Thermal Conductivity of Tube	k	W/m-K	40
Chilled Water Heat Transfer Coefficient	h_{CW}	$W/m^2 - K$	8806.32
Corrected DI Water Heat Transfer Coefficient	h_{DIcorr}	$W/m^2 - K$	2214.75
Overall Heat Transfer Coefficient	U	$W/m^2 - K$	1461.34
Tube Surface Area	A	m^2	36.44

Table 3.9: Initial one corridor heat exchanger model geometries and arrangement

	Value	Unit
Waterbox head depth	13	in each
Exposed tube length	50	in
Tube sheet thickness	1.125	in each
Overall heat exchanger length	$78.25 \; / \; 6.52$	in / ft
Heat exchanger internal shell diameter	26	in
Tube spacing (centerline-to-centerline)	0.656	in
Total number of tubes	805	non-dim
Number of inlet tubes	403	non-dim
Baffle thickness	0.0625	in
Baffle spacing	6	in

Chapter 4

Heat Exchanger Evaluation for One Corridor

4.1 First Design

The heat exchanger developed in Chapter 3 was modeled and simulated using the SOLIDWORKS Flow Simulation CFD package. The tube-side, chilled water flow was analyzed first. The predicted velocities were within the prescribed limit, and are illustrated in Figure 4-1. The maximum entrance and exit velocity of $4.2 \ ft/s$ was observed near the outlet nozzle and is well below the $11 \ ft/s$ limit. Moreover, none of the observed velocities through any of the tubes exceeded the $9 \ ft/s$ limit. However, the global pressure drop was calculated at $80.15 \ psi$, which grossly exceeded the $6 \ psi$ limit, as seen in Figure 4-2. Moreover, the flow and pressure profiles did not indicate fully developed flow from the inlet region through the tubes to the outlet nozzle. It is unclear whether there was some underlying discrepancy with the CFD solver itself, or whether there existed such turbulent buildup in the inlet region that the flow could not develop and distribute evenly as expected, especially throughout the second pass tube as Figures 4-1 and 4-2 seem to indicate.

The shell-side, demineralized water flow was then analyzed. The highest velocity of 9.65 ft/s was observed at the outlet nozzle, within the allowable 11 ft/s limit. The global pressure drop was 10.22 psi, which exceeded the 6 psi limit but was at

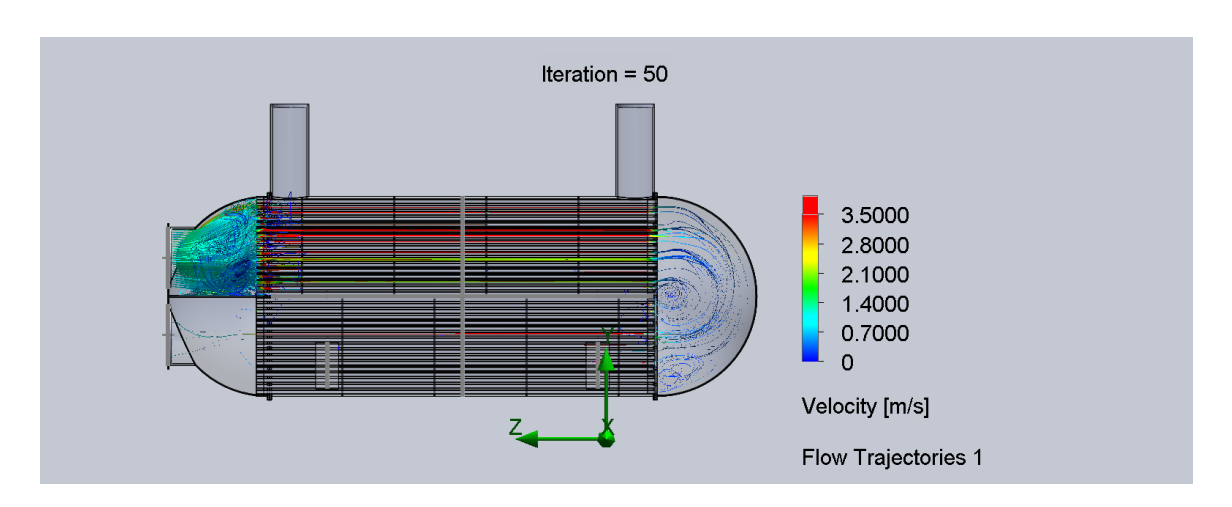


Figure 4-1: Design 1 chilled water velocity flow.

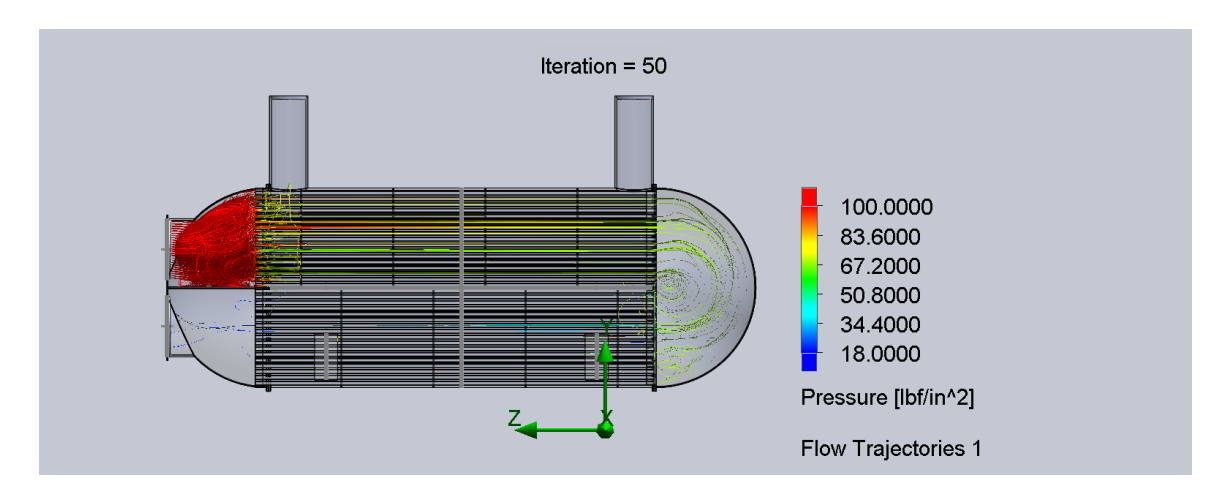


Figure 4-2: Design 1 chilled water pressure gradient.

least within a reasonable range of the desired goal, unlike the chilled water result.

However, the observed flow profile suggested inadequate flow of the demineralized water over and across the tubes. There appeared to be a ducting effect wherein a majority of the flow only traveled near the cross-sectional openings between baffles, rather than traveling fully throughout the heat exchanger. It was assessed that this was likely a combined result of too closely spaced baffles and too large of a shell diameter given the relatively short overall length. Figures 4-3 and 4-4 illustrate the described flow and pressure discrepancies.

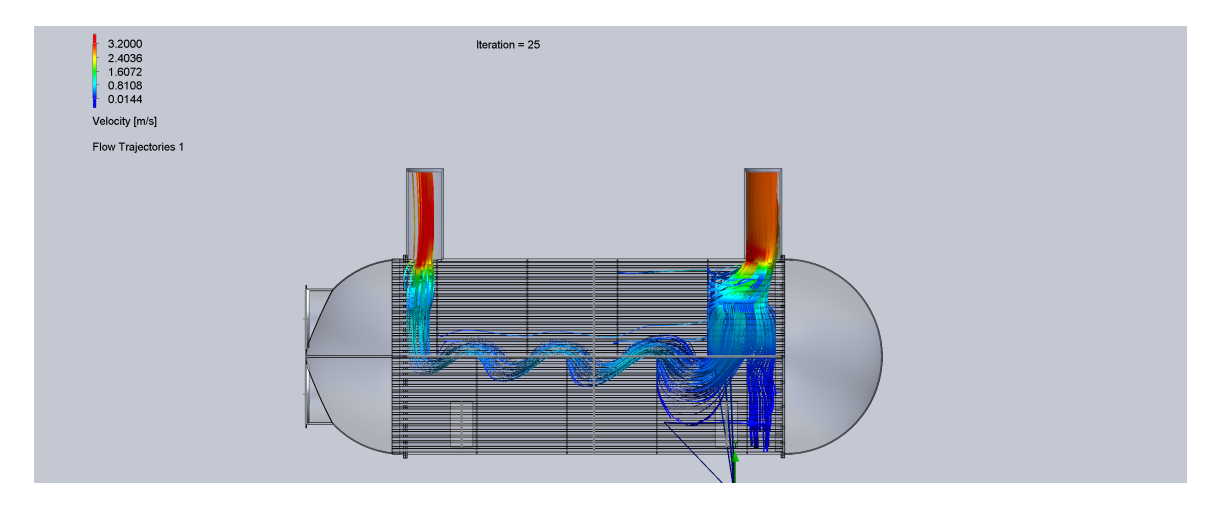


Figure 4-3: Design 1 demineralized water velocity flow.

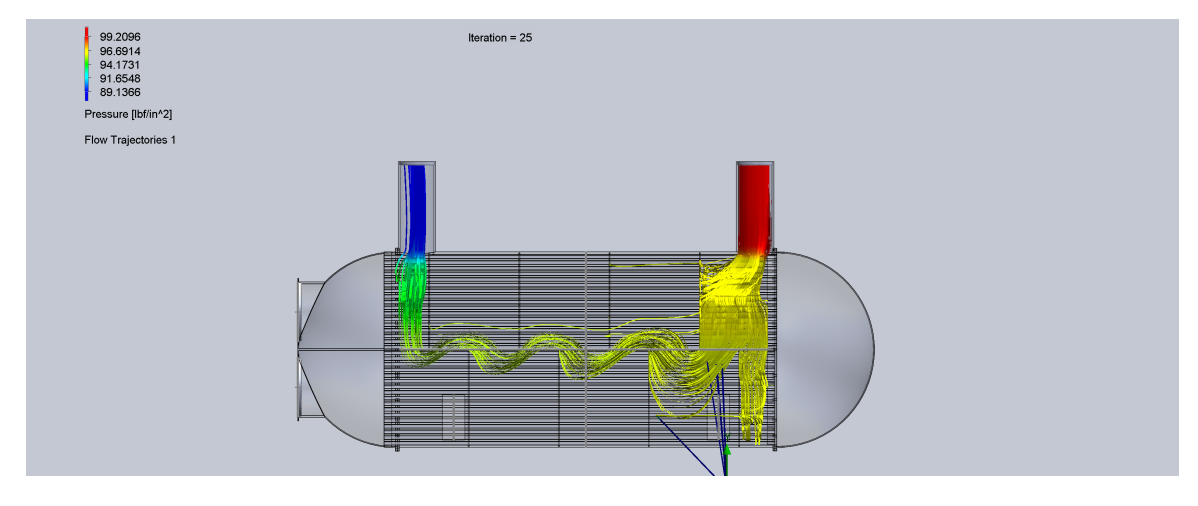


Figure 4-4: Design 1 demineralized water pressure gradient.

4.2 Second Design

4.2.1 Design Approach

A second design iteration was modeled which incorporated the same 5:1 length-todiameter aspect ratio of the single-compartment heat exchanger. Despite newfound concerns for additional pressure drop across a longer body, the intention was to achieve a more uniform and developed flow across the entire heat exchanger, especially on the shell side. The relevant heat transfer equations were revisited in order to determine that a 16 in shell diameter coupled with 80 in length tubes would simultaneously provide the necessary heat transfer surface area (with approximately 3 m^2 excess area to serve as future cooling margin) and the desired aspect ratio.

In order to mitigate the corresponding expected rise in pressure drop due to the lengthened body, the number of baffles was reduced to nearly the minimum permissible as dictated by TEMA [43], which stipulates that the maximum span of unsupported 1/2 in tubes is 38 in.

All relevant heat exchanger geometry characteristics for this second iteration design are summarized in Table 4.1.

Table 4.1: Second corridor heat exchanger model geometries and arrangement

	Value	Unit
Waterbox head depth	8	in each
Exposed tube length	80	in
Tube sheet thickness	1.125	in each
Overall heat exchanger length	102.25 / 8.52	in / ft
Heat exchanger internal shell diameter	16	in
Tube spacing (centerline-to-centerline)	0.656	in
Total number of tubes	410	non-dim
Number of inlet tubes	205	non-dim
Baffle thickness	0.0625	in
Baffle spacing	14	in

4.2.2 Simulation Results and Analysis

The tube-side, chilled water flow was analyzed first. Despite the improved flow profiles demonstrated by this model, the key performance metrics were not met. Under the originally assumed volumetric flow rate of 540 gpm (34.0 kg/s mass flow rate), the outlet velocity limit was slightly exceeded (11.54 ft/s) and the pressure drop limit across the tubes was grossly exceeded. The full velocity and pressure profiles are provided in Figures 4-5 and 4-6, respectively.

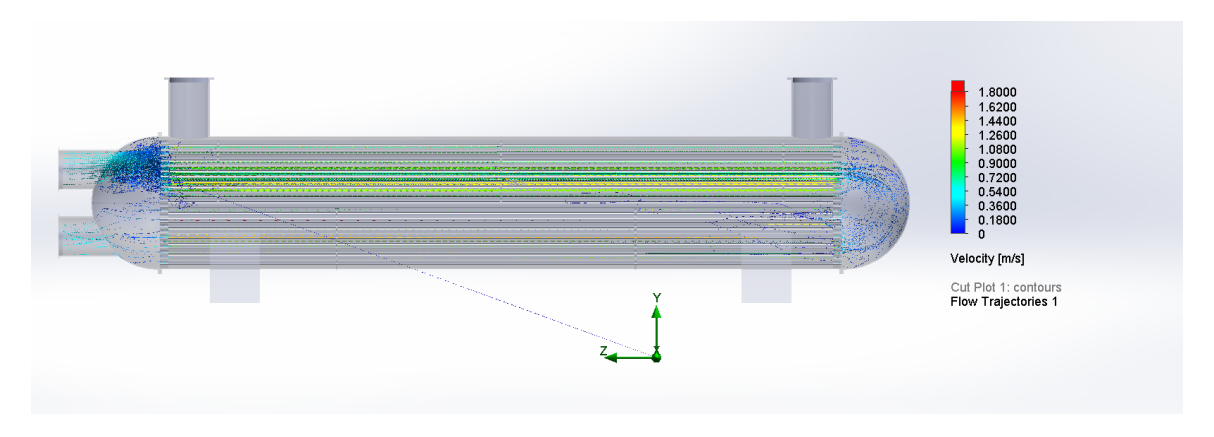


Figure 4-5: Design 2 chilled water velocity flow.

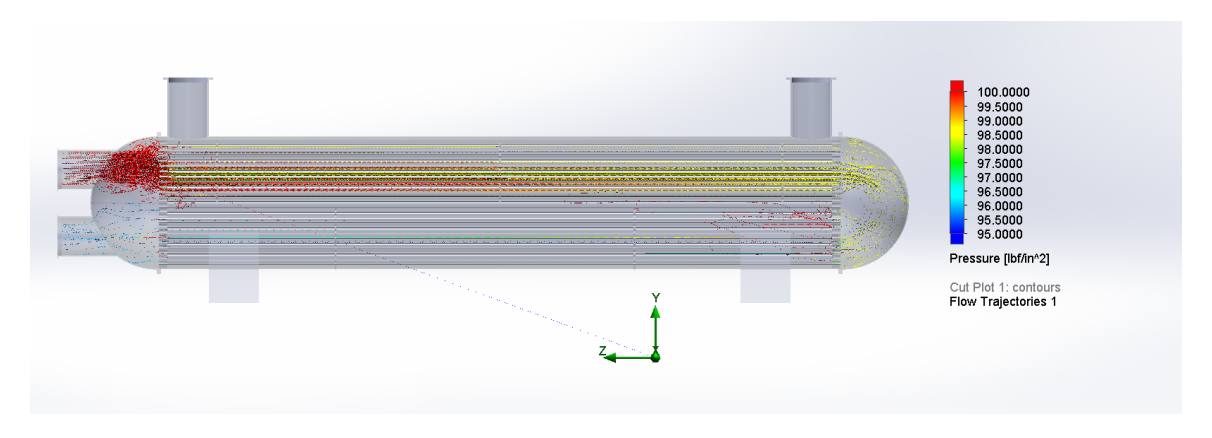


Figure 4-6: Design 2 chilled water pressure gradient.

A set of simulations was conducted in order to better assess the impact of mass flow rate on the pressure drop. Lowering the mass flow rate during these trials effectively invalidated the heat exchanger from a thermal management performance perspective, since the reduced mass flow rate would require additional heat transfer surface area which was not accommodated during this analysis. Nevertheless, the simulations demonstrated that the mass flow rate was driving the global pressure drop. As an example, reducing the mass flow rate from $17 \ kg/s$ to the single-compartment value of $2.83 \ kg/s$ reduced the global pressure drop from over $45 \ psi$ to $2.76 \ psi$.

Although this iteration of the heat exchanger was ultimately inadequate, it provided crucial insight as to the viable range of chilled water mass flow rates given the constraints of the design, particularly the allowable tube diameter size. [30] only allows for three sizes of tube diameters (3/8, 1/2, and 5/8 in) in heat exchanger designs, so there is limited latitude for pressure drop mitigation within that design parameter. It must be addressed by other key parameters such as the mass flow rate.

The simulation environment was reestablished to analyze the demineralized water flow. The same boundary conditions were imposed as in the previous two models, setting an inlet temperature of 42°C, an inlet pressure of 100 psi, and a volumetric flow rate of 460 gpm (corresponding to a mass flow rate of 28.8 kg/s). As previously discussed, this design iteration featured relatively widely spaced baffles in order to offset pressure drop concerns, yet the pressure drop remained excessive. Although the maximum inlet and outlet velocities were predicted to be within the relevant limits at 9.35 ft/s (2.85 m/s), the global pressure drop across the heat exchanger was calculated at 28.13 psi, exceeding the 6 psi threshold. Full velocity and pressure profiles are provided in Figures 4-7 and 4-8, respectively.

Multiple simulations were run to better understand the competing effects of baffle arrangement and mass flow rate on the resultant pressure drop. The general trend was that reducing the number of baffles reduced the pressure drop somewhat, but that the driving factor was the mass flow rate, as was the case for the chilled water flow.

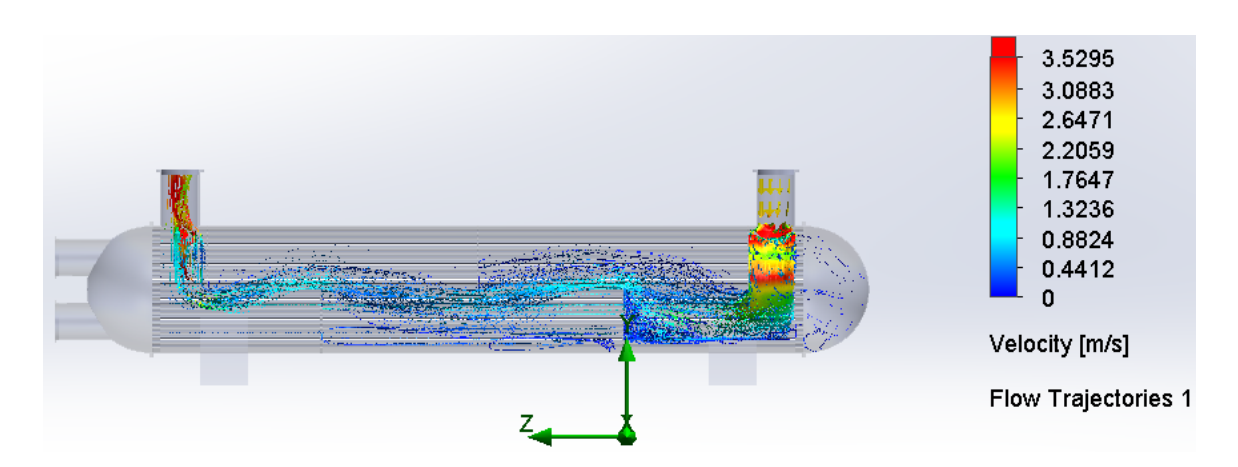


Figure 4-7: Design 2 demineralized water velocity flow.

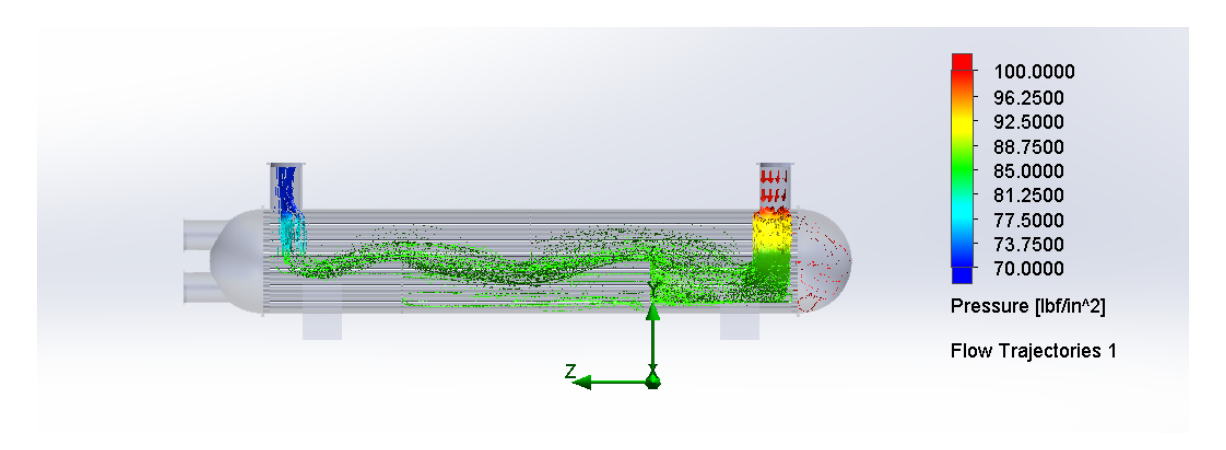


Figure 4-8: Design 2 demineralized water pressure gradient.

4.3 Final Design

4.3.1 Design Approach

The final design required a detailed iterative approach to balance the ensuing, competing constraints: (1) reducing the pressure drop, (2) addressing the emergent additional required heat transfer surface area by creating a larger heat exchanger, (3) mitigating potential new pressure drop sources from a larger heat exchanger, and (4) ensuring that the final design size was not infeasibly large to preclude installation into a compartment or engine room space onboard the ship. Based on the previous results, it was clear that both fluids' flow rates would have to be considerably reduced in order to achieve or get close to achieving the pressure drop goals. It was ultimately determined to re-baseline the chilled water volumetric flow rate at 260 gpm (corresponding to a mass flow rate of 16.40 kg/s) and the demineralized water volumetric flow rate at 275 gpm (corresponding to a mass flow rate of 17.21 kg/s.) This re-characterized a number of the key heat transfer parameters governing the heat exchanger's thermal performance, which are provided below.

Table 4.2: Final Heat Exchanger Characteristics

Heat Transfer	\dot{Q}	kW	1515.8
LMTD	ΔT	K	21.41
Tube Outer Diameter	D_{OD}	in	1/2
Tube Thickness	L	in	0.049
Thermal Conductivity of Tube	k	W/m-K	40
Chilled Water Heat Transfer Coefficient	h_{CW}	$W/m^2 - K$	8806.32
Corrected DI Water Heat Transfer Coefficient	h_{DIcorr}	$W/m^2 - K$	1270.05
Overall Heat Transfer Coefficient	U	$W/m^2 - K$	980.24
Tube Surface Area	A	m^2	72.24

In order to provide all the newly required heat transfer surface area, the shell diameter was increased to 20 in and the tubes were lengthened to 100 in, again retaining the desired 5:1 length-to-diameter aspect ratio in order to promote more favorable flow conditions. A full description of the major heat exchanger geometry characteristics is provided in Table 4.3.

Table 4.3: Final heat exchanger model geometries and arrangement

	Value	Unit
Waterbox head depth	20	in each
Exposed tube length	100	in
Tube sheet thickness	1.125	in each
Overall heat exchanger length	122.25 /10.18	in / ft
Heat exchanger internal shell diameter	20	in
Tube spacing (centerline-to-centerline)	0.656	in
Total number of tubes	710	non-dim
Number of inlet tubes	355	non-dim
Baffle thickness	0.0625	in
Baffle spacing	12.85	in

4.3.2 Simulation Results and Analysis

The chilled water flow was assessed first. By considerably reducing the mass flow rate while maintaining the previous inlet and outlet piping sizes, the resulting velocities were projected to be comfortably within the allowable limits. Specifically, the maximum velocity at the inlet and outlet regions was 5.51 ft/s, well below the 11 ft/s limit, while the tube velocities did not exceed 6.10 ft/s. The full velocity profile is provided in Figure 4-9.

Additionally, the pressure drop results showed marked improvement from the previous designs, as seen in Figure 4-10. The final calculated pressure drop was 7.36 psi. Although this is still technically above the 6 psi limit, minor future design changes could reduce the pressure drop below the prescribed threshold. The most effective and direct means to reach the pressure drop goal of 6 psi would be to slightly increase the heat exchanger size, providing excess heat transfer capacity which could be offset by again lowering the mass flow rate.

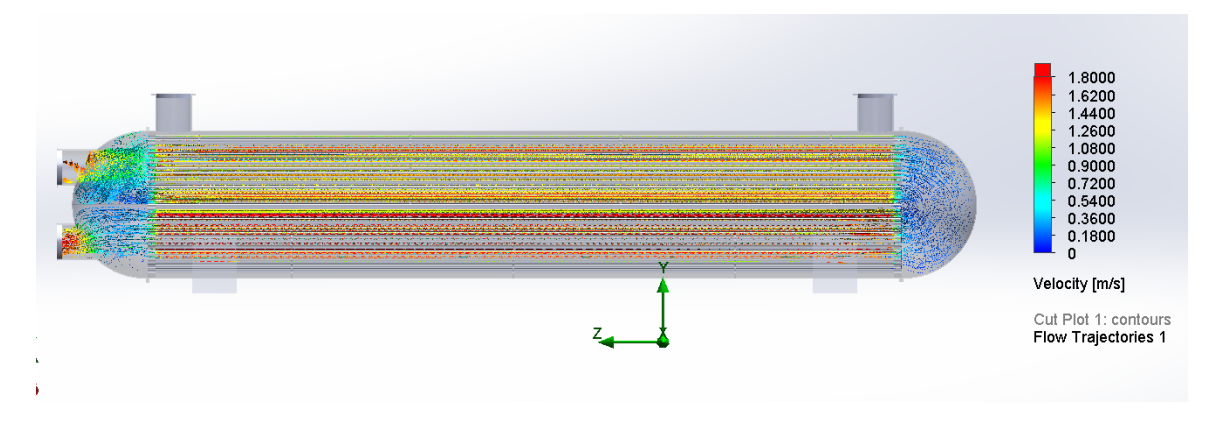


Figure 4-9: Final design chilled water velocity flow profile.

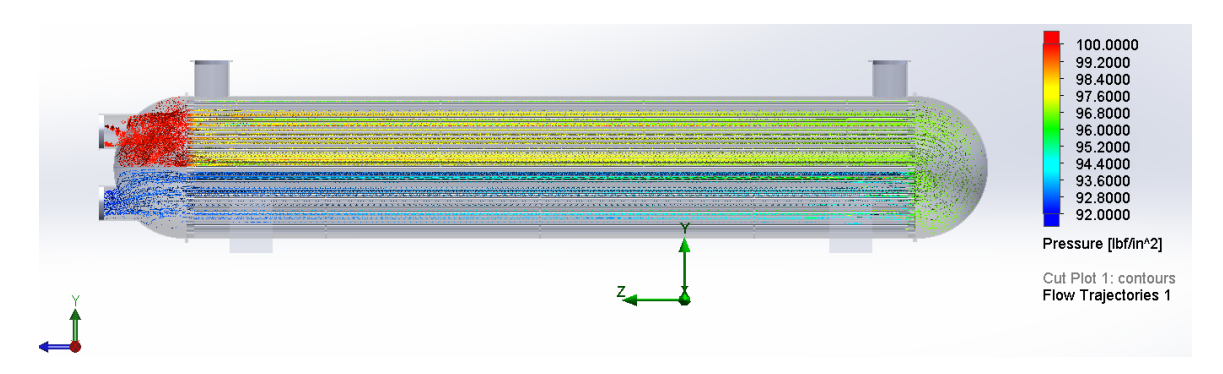


Figure 4-10: Final design chilled water pressure gradient.

Next, the shell-side flow was reanalyzed. All velocities were expected to be within their respective limits; the maximum inlet and outlet velocity was $5.68 \ ft/s$, and all flow throughout the shell was predicted to be below the $9 \ ft/s$ limit. The full velocity profile is provided in Figure 4-11. The pressure drop across the shell was reduced by nearly half from the previous design iteration but still exceeded the $6 \ psi$ limit at $16.16 \ psi$. The full pressure profile is depicted in Figure 4-12.

Although this design offers the flexibility to slightly increase the baffle spacing (by approximately 2 inches) to possibly reduce the pressure drop, that increased spacing would also increase the shell-side cross-sectional flow area and thus increase the required heat transfer surface area. Absent changing any other parameters, the only direct method of subsequently decreasing the heat transfer area would be to increase one or both of the mass flow rates, thereby negating the improvements yielded by establishing lower flow rates initially. As with the chilled water pressure drop

mitigation recommendation, the most effective method to lower the pressure drop is to increase the heat transfer surface area to enable lower mass flow rates.

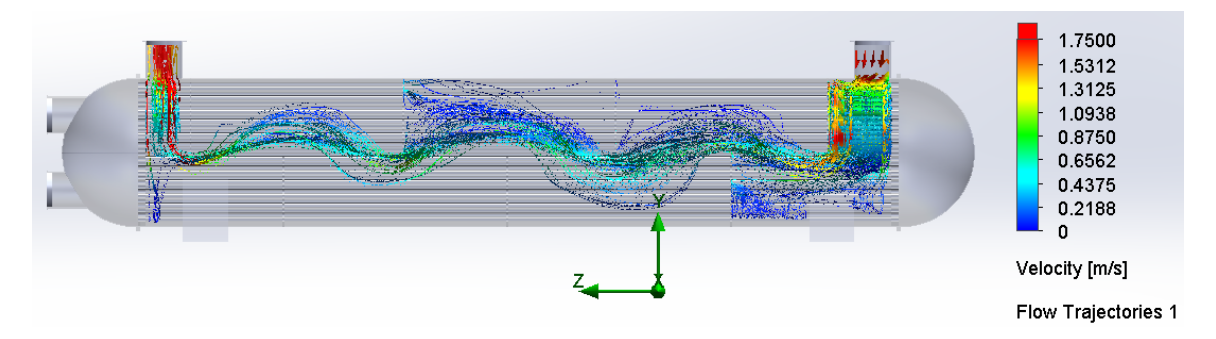


Figure 4-11: Final design demineralized water velocity profile.

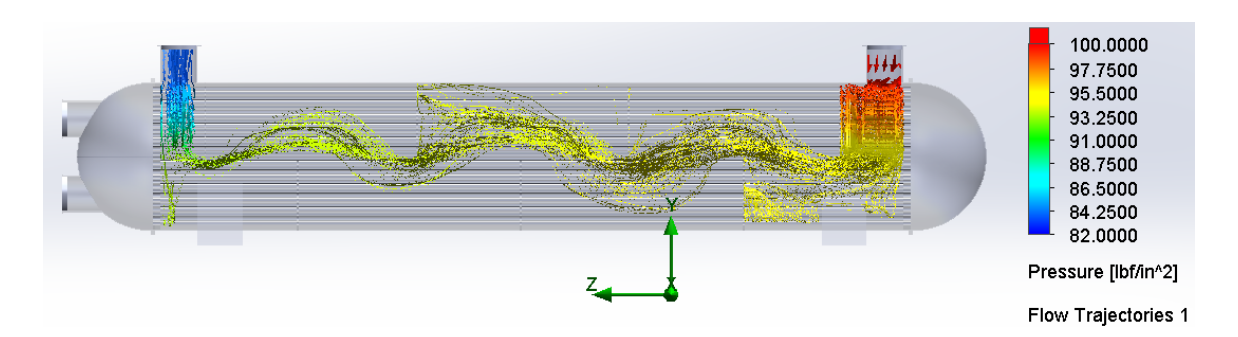


Figure 4-12: Final design demineralized water pressure gradient.

4.4 Heat Exchanger Redesign Conclusions

The initial design philosophy which sought to minimize the lengthening of the corridor heat exchanger did not produce a viable model. The first-pass models predicted substandard hydraulic performance and did not lend confidence that adequate flow would fully develop. Subsequent simulations illustrated the dominant influence of the fluids' mass flow rates on the key performance metrics (velocity and pressure drop). This insight drove subsequent design choices. The iterative design process progressed from an initial model which technically met the thermal management requirements but performed poorly against key operating parameters, to an improved design which met the heat transfer requirements but still requires some design changes to achieve all performance standards. Beyond that, given its projected dimensions—2'x 10.18' x

3'- it presents a feasible size and volume footprint to accommodate multiple units spaced smartly throughout the ship.

4.5 Alternative Heat Exchanger Solutions

Although the STHE has been assumed for the purposes of this study, it is just one among many heat exchanger designs. The remainder of this chapter provides an overview of other thermal management solutions which could be incorporated into the NiPEC cooling system, presenting both the benefits and challenges associated with each approach.

4.5.1 Plate Heat Exchangers

Along with STHE, PHE are the most common design for marine applications. Figure 4-13 provides a representative schematic used in naval systems. Flanged nozzles connect to passages through tightly-arranged plates, each of which is fitted with a gasket arrangement to enable separate flow streams for the cooling and cooled fluids. This prevents the internal mixing of the two liquids, which are directed to alternate sides of the plates in a counter-current flow strategy in order to optimally provide the required heat transfer, as depicted in Figure 4-14. The plates are corrugated to ensure turbulent flow throughout the entire process, which improves the effective heat transfer coefficient but also requires greater pumping power compared to other heat exchanger designs.

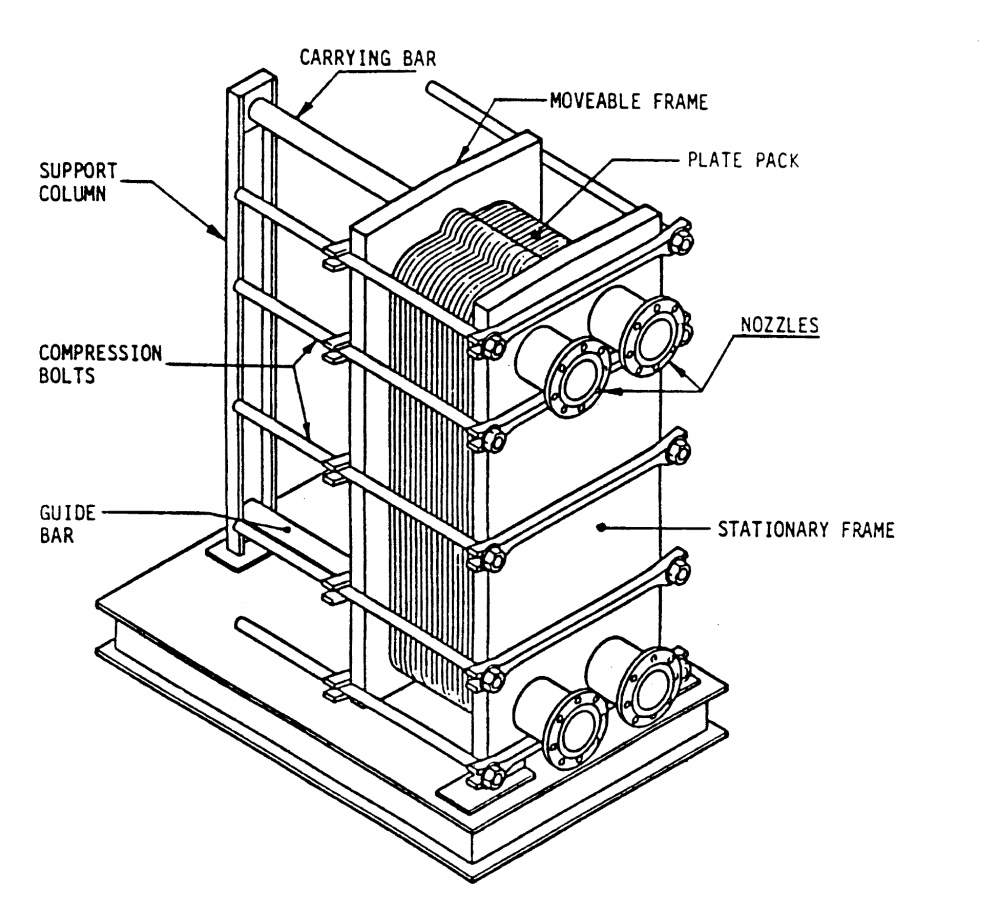


Figure 4-13: Flat PHE for ECWS [33].

One of the biggest advantages PHEs offer is the much larger surface area to which the fluids are exposed, which facilitates faster heat transfer. The temperature approach (*i.e.* the smallest temperature difference between the cooling and cooled fluids) in a PHE can be as low as 1°C, which allows for a smaller heat exchanger for the same amount of heat exchanged, as illustrated in Figure 4-15 [15]. Moreover, PHEs can be adjusted to increase capacity by adding more plates while retaining the existing frame, offering the ability to scale against future system demands and needs. This represents a distinct advantage over STHEs, whose capacity is fixed at the time of installation [7]. In a shipboard environment where space is limited and scale flexibility is coveted, PHEs provide benefits on both fronts which outperform comparable STHEs designs.

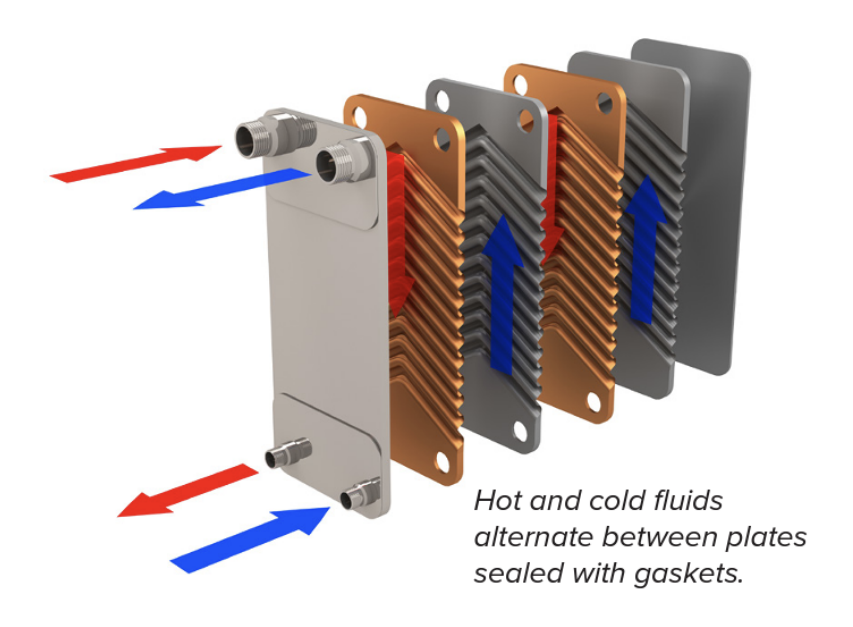


Figure 4-14: Illustration of counter-current flow path in a PHE using chevron-corrugated plates [3].

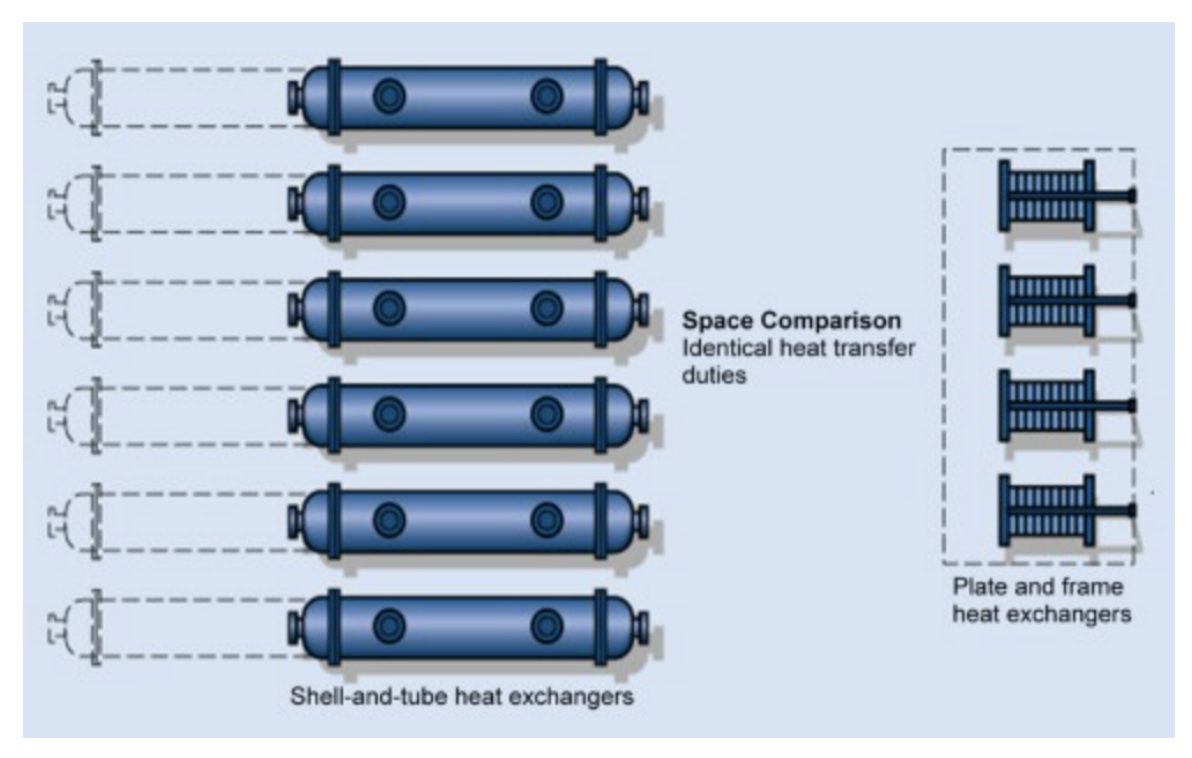


Figure 4-15: Space savings incurred by using PHEs [7].

PHEs are more prone to fouling than other types of heat exchangers due to the exposed flat plates creating stagnant areas for particulates to accumulate and the narrow gaps between plates reducing the space for particulates to move freely. This can lead to reduced heat transfer efficiency and more frequent maintenance requirements, though the overall maintenance costs are generally still lower than other heat exchanger types of similar capacity due to the relative ease of maintenance and less complex system design [3].

4.5.2 Printed Circuit Heat Exchangers

A PCHE at type of compact heat exchanger that consists of a stack of thin metal plates that are either brazed or diffusion-bonded together to form a single unit. The plates are typically made of materials such as stainless steel or titanium and are arranged in a way that creates a network of small, chemically etched channels through which the fluid flows, as illustrated in Figure 4-16. The fluid flows through these channels in a highly turbulent manner, which increases the rate of heat transfer between the two fluids. Figure 4-17 shows all the principal components of a commercial PCHE design produced by Heatric, a UK-based manufacturer that is considered the world leader in diffusion-bonded heat exchangers.

PCHEs are highly efficient heat exchangers due to their compact design, which provides a large surface area for heat transfer in a relatively small volume. This makes them particularly useful in applications where space and weight are at a premium, such as the future all-electric destroyer warship. Additionally, PCHEs offer other benefits such as high thermal performance and reliability, low fouling, and the ability to withstand pressures up to 15,000 psi and temperatures up to 600°C.

However, PCHEs can be more expensive to manufacture than traditional heat exchangers due to generally requiring all stainless steel construction [17]. Additionally, pressure drop development is a significant known limitation in PCHE designs, specifically for high volumetric flow rate and moderate pressure applications, such as the NiPEC cooling system. The small flow channels are often arranged in a zigzag formation, each of which acts as a relatively very small pipe with numerous bends and

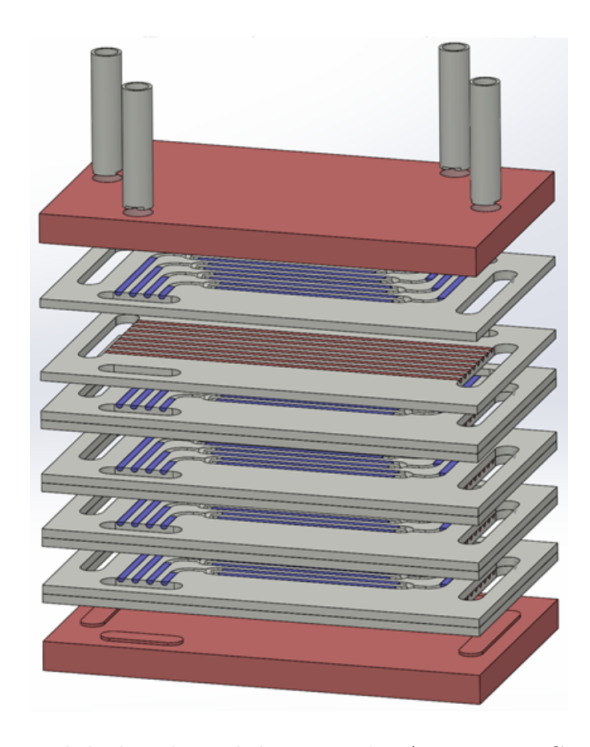


Figure 4-16: PCHE model developed by MIT's Atomistic Simulation and Energy Research Group [4].

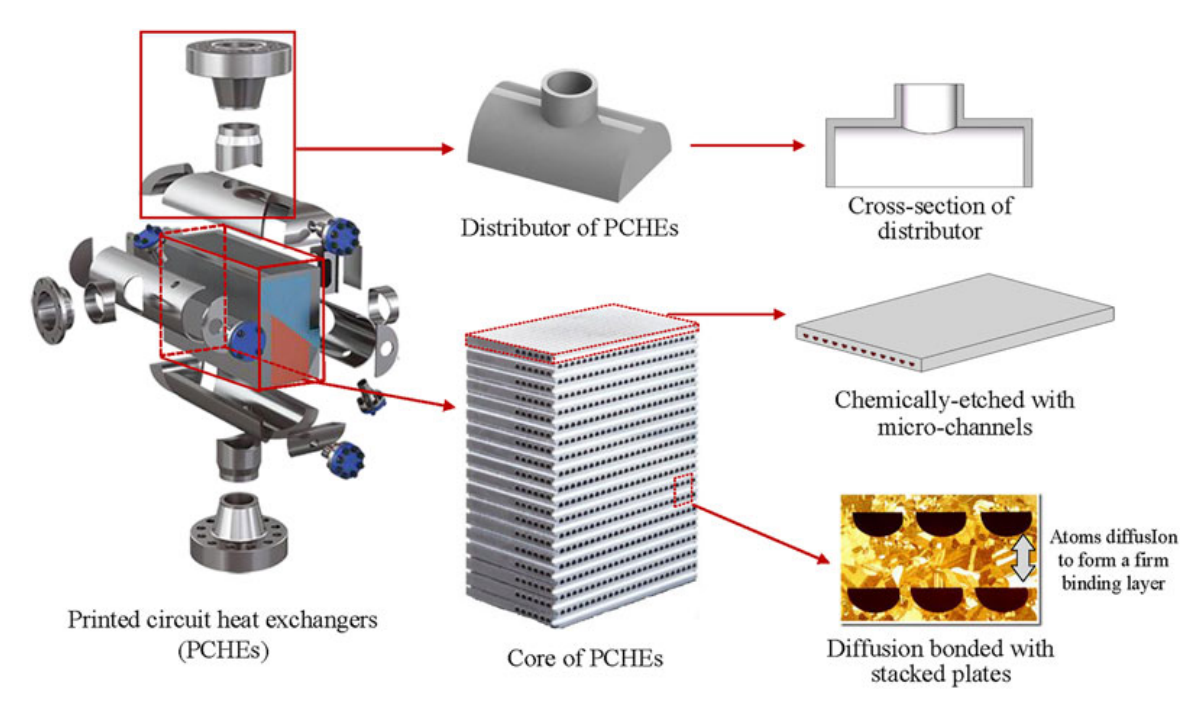


Figure 4-17: Exploded view of Heatric PCHE internals [44].

resulting swirl and eddy flows. These features can collectively introduce unacceptably high pressure drop conditions which would not conform to the standards set forth in [30] and [31]. PCHEs can alternatively be manufactured with S-shaped flow patterns in lieu of the zigzag formation to decrease expected pressure drops by 25-35%, but this requires a much more expensive etching process and introduces challenges in the diffusion bonding process [17]. Additionally, PCHEs are highly susceptible to blockage due to very small flow channels, necessitating the installation of extremely fine filters and strainers which require frequent and thorough cleaning, which in turn increases operating and maintenance costs.

Despite their commercial deployment dating back to the 1980s, PCHE usage still dwarfs in comparison to the more traditional STHE and PHE designs. PCHEs were explored as potential replacements for the U.S. Navy's Littoral Combat Ships (LCS), but still represent a significant risk for the Navy to invest in for future warships. The naval and military standards governing cooler design and performance, specifically for electronic cooling purposes, do not address PCHEs as a potential thermal management solution. Thus, there would need to be a considerable investment on the organization's part to better understand the technology and codify requirements for warship use.

4.5.3 Spiral Heat Exchangers

SHE transfer heat from one fluid to another through a large surface area provided by the spiral channels. Figure 4-18 depicts the flow and heat transfer processes: two fluids are separated by the spiral walls, and heat is transferred from the warmer fluid to the cooler fluid through the walls. The counter-flow configuration ensures efficient heat transfer, with the maximum temperature difference between the two fluids occurring at the start of the channels. Like the other alternative heat exchangers discussed thus far, SHEs offer a more compact and flexible design for similar capacity compared to an STHE. Fouling is drastically reduced due to the single-channel design and self-cleaning effect promoted by the spiral flow path [5]. Although most SHEs cannot handle as wide a range of fluid types and operating conditions as STHEs in general,

the most popular current commercial options offer solutions well within the expected temperatures and pressures of the NiPEC cooling system. Figure 4-19 depicts a commercial SHE model manufactured by Alfa Laval.

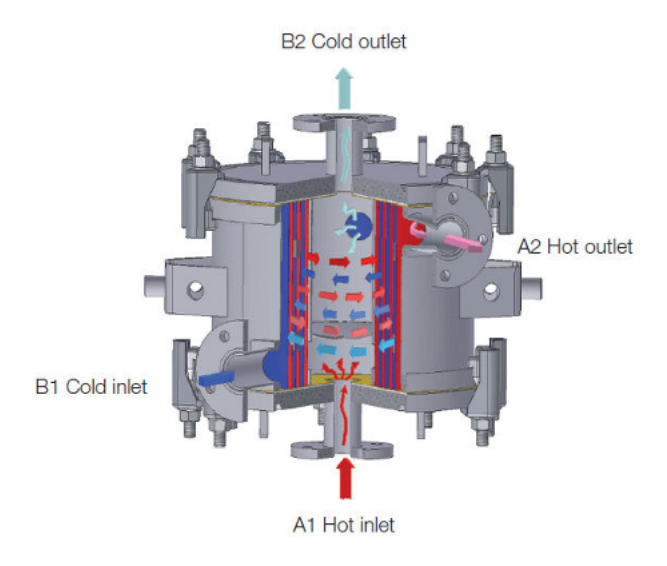


Figure 4-18: Illustration of the hot and cold fluid flow paths within a SHE [5].



Figure 4-19: Alfa Laval SHE external view [5].

Although their installation and operational costs are cost-competitive, SHEs are usually much more expensive to manufacture than STHEs. The spiral shape is more difficult to produce than a straight tube, and its intricate welding procedures and quality control requirements are particularly demanding.

Similar to PCHEs, SHEs are a relatively newer technology with which the U.S. Navy has very little familiarity, as opposed to the multiple decades-long operation and proven track record of STHEs in the fleet. Although SHEs have been a viable and high-performing option commercially, there are currently no industry standards for SHEs that the Navy could adopt or adapt to establish its own standards. Pivoting to this technology would introduce greater uncertainty and higher initial investment for the organization that may ultimately not prove worthy of the cost or technical risk.

Chapter 5

Overall Cooling System Architecture

5.1 Separation and Redundancy

Among the key design considerations governing system survivability and vulnerability are the coupled concepts of redundancy and separation. Achieving these concepts in design normally involves a three-pronged approach: (1) provide vital functions redundantly, (2), separate redundant instances of each vital function, and (3), colocate components of one instance of a redundant function. Broadly speaking, the first objective ensures that no single failure will render the system inoperative, the second objective aims to preclude a common cause event from causing multiple failures which could then render the system inoperative, and the last objective attempts to mitigate the possibility of unrelated events eliminating system redundancy.

The first objective will be achieved in the NiPEC cooling system by ensuring that any section of the NiPEC has access to at least two sources of cooling. A "source of cooling" describes the availability and proper operation of the minimum number of components required to get cooling water to the header piping of a given portion of the corridor. This wording specifically accounts for the case where an initiating event such as significant battle damage incapacitates a given section of the system piping itself. The piping damage is assumed such that the cooling water cannot physically reach the associated PEBB stacks and cold plates, up to and including an entire corridor. In this limiting casualty scenario, redundancy is achieved by considering the entire

affected corridor in an offline status, and relying on the corridor N-1 condition, which stipulates that all loads can be carried with one corridor unavailable.

Within a given corridor, redundancy will also be provided by having two pumps installed in parallel, such that only one pump is online at any given time, but that the offline pump remains in a standby condition in case the other pump fails. Specifically, the pumps shall be electrically interlocked such that if the pump in use stops, the standby pump will start automatically [33]. Pump failure is anticipated to be a likelier occurrence than other components' failure, given it has both electrical and mechanical failure modes. Introducing this additional local level of redundancy is therefore deemed mandatory to mitigate individual pump malfunction while still retaining full use of that portion of the cooling system.

NAVSEA-532 [33] notes that at least two heat exchangers shall be provided in parallel, with one unit in operation and one unit in standby during normal operations. Although this requirement does not technically improve the system's survivability—both units are located in the same space and would be assumed inoperative if that space took significant battle damage—it serves to enhance the system's reliability in case of miscellaneous equipment malfunction. Therefore, in keeping with naval ECWS conventions and standards, two heat exchangers in parallel will be incorporated into each "source of cooling."

The pair of pumps, in conjunction with the dual heat exchangers and other major components constituting a "source of cooling" (*i.e.* expansion tank, demineralizer loop, and associated controls) will be considered a singular, functionally non-redundant instance of cooling to a given portion of the corridor.

The second and third design objectives will broadly be achieved by separating the location of these instances of cooling, but co-locating the required components of each vital instance within the same compartment, as dictated by relevant military standards [33]. This will effectively create multiple cooling source spaces strategically located throughout the ship, arranged to enable the first objective of dual-sourced cooling for any portion of the corridor. It is further assumed that if a cooling source space were to take damage, all the components constituting that source would be

considered lost, and a backup cooling source would be required.

5.1.1 Improved Redundancy

In order to achieve a heightened degree of redundancy and survivability with respect to PEBB arrangement, a more deliberate PEBB allocation assignment strategy was pursued. Previously, the number of PEBBs required for each compartment was just evenly divided amongst the four corridor quadrants within that compartment (Port 2nd/4th Decks, Starboard 2nd/4th Decks). However, this relatively coarse approach increased the possibility of losing a given load's primary and backup PEBB sources simultaneously in the case of battle damage or some other casualty scenario. Instead, a diagonal dual-sourcing strategy was implemented. In this approach, a given load's primary PEBB sources are assigned to the corridor region nearest that load, based on that load's physical location within the notional destroyer. The load's backup PEBBs were then assigned to the cross-diagonal region of the corridor within that same compartment.

For example, the Compartment 3 Air Conditioning Chiller has the following longitudinal, transverse, and vertical coordinates: (34.18 m, -2.78 m, 2.8 m), where a negative transverse coordinate indicates a location port of centerline. Therefore, this chiller's primary PEBBs were assigned to the Port 4th Deck quadrant of the Compartment 3 corridor, and its backup PEBBs were assigned to the Starboard 2nd Deck quadrant of the Compartment 3 corridor. The vertical assignment boundary was chosen to be four (4) meters above the keel, which allowed for an equitable distribution of PEBBs between the decks in order to properly account for those select loads which would *not* have redundant power sources, as detailed below. This assignment policy was otherwise repeated for all the ship's loads.

Non-Redundant Loads

• PMMs. The propulsion motors require such a significant number of PEBBs that it was deemed infeasible to duplicate their requirement. The PMMs are

designed to have dedicated watertight compartments with minimal additional equipment or space and thus are two of the shortest compartments within the notional destroyer. Accommodating just the minimum number of PEBB stacks necessary for PMM operation may require a bespoke arrangement distinct from the rest of the corridor which could not be feasibly duplicated in the cross-diagonal compartment quadrant. Moreover, it is expected that these PEBBs will be installed very close to the PMMs given the compartment restrictions, and thus any significant damage incurred by the PEBBs would be incurred by the motors themselves, rendering backup PEBBs unnecessary.

- Generator Sets. Likewise, each of the generator sets requires a significant number of PEBBs to handle all the conversion and transformation processes to provide power to the MVDC bus. And like the PMM arrangement, it is proposed that the generators' PEBBs would be very closely located to the equipment itself. Therefore, duplication of these PEBBs was deemed both infeasible and unnecessary.
- Conversion Stations. The proposed electrical distribution system was designed to have five MVDC-LVDC conversion stations each on the port side and starboard side. The 12 PEBBs required for these stations do not need to be duplicated to the cross-diagonal quadrant, as they are already interconnected via the distribution bus to provide backup to one another.

5.2 Zonal Strategy and Arrangement

5.2.1 First Design: One System Per Corridor

The initial rendering of the NiPEC cooling system architecture proposed individual cooling systems for each of the four corridors. Cross-connect piping would enable dual-source cooling, likely from the other cooling skid on that side of the ship. However, this approach introduced certain undesirable features which worsened system susceptibility and reliability. If an individual cooling system were to service an en-

the longest run of piping, which would reduce system headloss, and in turn, reduce pump sizing and cost. This would result in the cooling skids on one side of the ship being closely located to one another and failing to achieve the second system performance objective of separating redundant instances of vital functions. Battle damage taken near midships could more easily impair both sets of cooling piping servicing their respective decks, potentially rendering two corridors inoperative and resulting in unacceptable load loss.

5.2.2 Second Design: Forward and Aft Quadrants

Instead, a more zonal approach was proposed as an alternative solution, whereby a cooling zone (quadrant) is provided separately for the forward and aft portions of both corridors on each side of the ship. In other words, the "Forward Port" cooling quadrant provides cooling to the forward portions of the 2nd Deck and 4th Deck port corridors. Riser piping from the heat exchanger splits to distribute or receive coolant, either to the main supply header or from the main return header, located on each deck. The NPS 5 main supply and return headers run in parallel with a slight vertical offset within the cooling conduit, located underneath the power corridor base. Two-inch branch piping at the side of each stack taps off of these headers to supply coolant to, and receive heated coolant from, each individual cold plate via one-inch inlet piping.

In this arrangement, there are still four normal cooling zones provided, but each one only services approximately half of each corridor on that side of the ship. This will reduce the total dynamic head requirements of the system's pumps, which will no longer be required to pump coolant through piping spanning the entire corridor length. This design decision also better facilitates cooling skid separation. Two cooling skids will be located forward on opposite sides of the ship, two cooling skids will be located aft on opposite ends of the ship, and the backup cooling skids will be approximately centrally located, in order to more easily facilitate alignment to either the forward or aft quadrant in the event of a casualty. Each skid will be separated

by at least one watertight bulkhead, as detailed in Table 5.2.

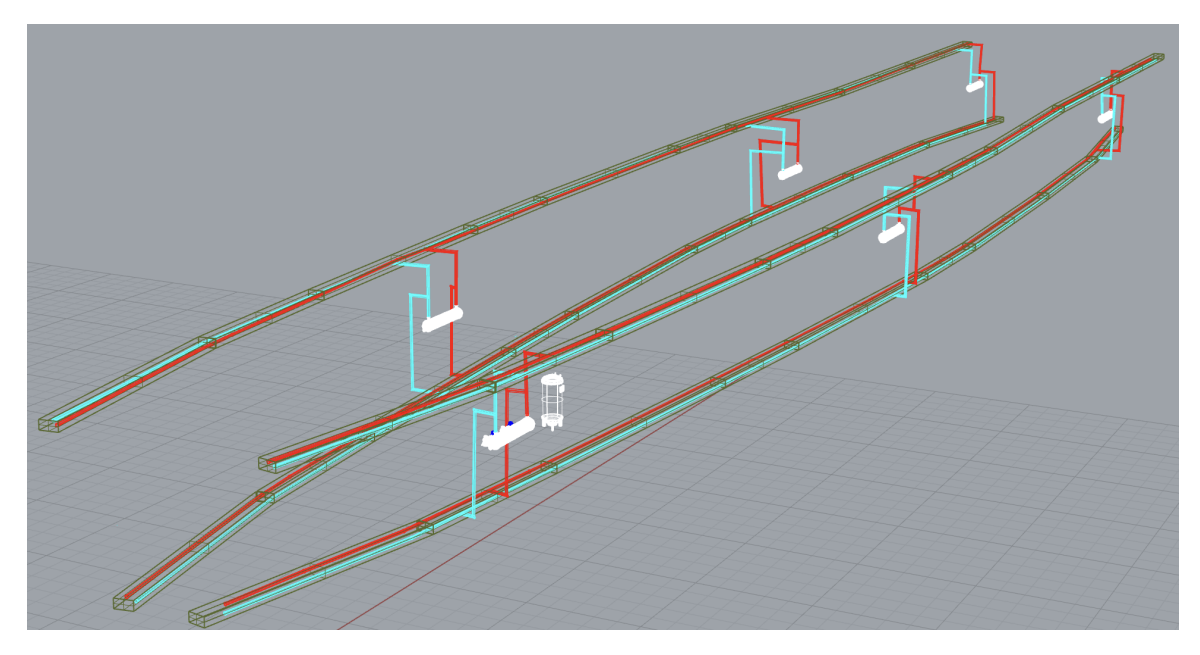


Figure 5-1: Main header piping of NiPEC cooling system. The basic architecture is adaptable to a variety of cooling zone strategies and layouts.

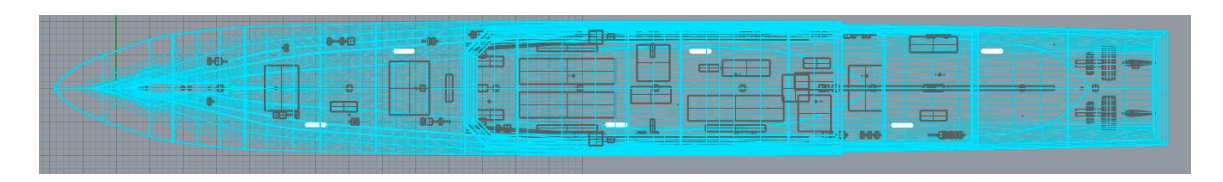


Figure 5-2: Topdown view of cooling skid locations. The white heat exchanger figures are representative of a singular cooling skid, *i.e.* a non-redundant source of cooling.

This modified approach required that none of the four quadrant heat loads exceeded that which was previously assumed of an entire corridor (1515.8 kW). To accomplish this objective, PEBB allocation was optimized for equitable distribution, and none of the expected quadrant heat loads exceeded the design basis assumption. Full details of PEBB allocation and expected quadrant head load are provided in Table 5.1.

Table 5.1: Quadrant Cooling PEBB Allocation and Heat Load

Quadrant	iPEBBs	PEBB 6000s	Total PEBBs	Total Assumed Heat Load (kW)
Forward Port	88	42	130	1292.6
Aft Port	60	78	138	1449.0
Forward Starboard	80	48	128	1288.0
Aft Starboard	68	60	128	1315.6

5.2.3 Inadequate Mass Flow Rate at Cold Plates

In order to mitigate the excessive pressure drops incurred at the heat exchanger, the system mass flow rate was reduced below the recommended value given by MIL-STD-1399 [31], as described in Chapter 4. The heat exchanger itself was designed in light of this concession, by increasing its diameter and accommodating more tubes than would otherwise be required. Additional system modeling was performed to analyze the extent to which the quadrant cooling system flow rate—which is seen at each heat exchanger before being split between the two main headers—would be divided amongst the PEBB stacks in its zone. This analysis determined that the actual mass flow rate would be inadequate to provide the necessary heat transfer locally at each cold plate. There were too many stacks and cold plates allocated to each cooling quadrant, forcing the overall system flow to be divided amongst too many individual supply paths. Thus, assigning roughly a quarter of the entire system heat load to each cooling skid proved too taxing, particularly in light of the competing system performance requirements.

5.3 Final Design: Six Cooling Zones

In order to distribute the system heat load to more sources of cooling, a six-cooling zone design was pursued. Many of the existing system architecture decisions were retained. The principal change was to reassign the centrally located cooling skids as primary cooling sources for the "middle" portion of the NiPEC. In turn, this created

three cooling zones on each side of the ship, each with primary duties during normal operations and the capacity to handle additional heat load during casualty situations.

Table 5.2: Cooling Skid Locations (all are located on 3rd Deck)

Cooling Skid Identifier	Compartment	Longitudinal Location (Aft	Transverse
Cooling Skid Identifier	Compartment	of FP, m)	Location (m)
Forward Port	3	33.1	-5.50
Forward Starboard	4	46.2	5.50
Mid Port	6	73.2	-5.50
Mid Starboard	8	87.7	5.50
Aft Port	10	118.0	-5.50
Aft Starboard	11	128.0	5.50

5.3.1 Heat Loss Dependency on Operational Load

Although previous PEBB allocation estimates had been based on operational load vice connected load (*i.e.* assigning load factors as detailed in Chapter 3), the design basis heat load estimates had still conservatively assumed that every PEBB was operating at 100% capacity, *i.e.* 250 kW for the Navy iPEBB and 1000 kW for the PEBB 6000, such that every PEBB dissipated its maximum heat loss (*i.e.* 8 kW and 10 kW, respectively).

This approach was deemed to be overly conservative. For example, a relatively small LVAC component with an operating load of $60 \ kW$ must be allocated three Navy iPEBBs to effect the necessary DC-AC conversion. In the previous assessment scheme, this correlated to three Navy iPEBBs operating at full capacity, each contributing $8 \ kW$ of heat loss for a total of $24 \ kW$. Although this was addressed to some extent by assigning multiple same-type loads to a singular PEBB until it reached capacity, this mitigation was not robust enough to prevent excessive heat load estimates across all load types and compartments.

Heat load values were recalculated by applying the PEBB efficiencies to the actual operational load values, not the maximum PEBB capacities. Thus, instead of predicting a 24 kW heat loss contribution from the aforementioned 60 kW LVAC load, the new model more accurately predicted just a 1.92 kW heat loss term.

5.3.2 Heat Loss Distribution Across Cooling Zones

Normal Operating Conditions

In order to determine the optimal heat load distribution across the new cooling zones under normal operating conditions, two approaches were considered. In the first method, the heat load would be distributed as equitably as possible in order to avoid one excessively limiting zone. However, actually achieving this goal would have required splitting up the zone assignments between load types, *i.e.* loads which were using Navy iPEBBs versus loads using PEBB 6000s. As a result, different PEBB stacks in a compartment would potentially have different cooling zone assignments. Considering the piping arrangements, valve placements, and overall increased complexity this approach would require, it was deemed infeasible.

Instead, the cooling zones were principally designed to provide coverage for the same compartments across both load types, and then the zones were partitioned to achieve as equitable a heat load distribution as possible. A full breakdown of the resulting cooling zones, compartment assignments, and heat load contributions are provided in Appendix D and summarized in Table 5.3.

Table 5.3: Six-Zone Cooling: Normal Operating Conditions

Cooling Zone	Compartments	Total Assumed Heat Load (kW)
Forward Port	1-6	595.2
Mid Port	7-8	339.9
Aft Port	9-13	477.7
Forward Starboard	1-6	420.9
Mid Starboard	7-8	375.8
Aft Starboard	9-13	144.4

Under normal operating conditions, the Forward Port is the most limiting cooling zone, based on its highest estimated heat load of **595.2** kW.

N-1 Scenario: Loss of Power Corridor

The PEBB allocation redundancy strategy provides a solution to the N-1 corridor condition, where an entire quadrant of the power corridor is assumed lost. If the

entire Starboard 4th deck corridor is lost, there are already backup PEBBs allocated and installed along the Port 2nd deck corridor to assume the loads and the attendant heat loss will be shared and carried by all three cooling zones along the port side. This scenario was carried out for all the cooling zones in order to evaluate the impact this casualty has on each zone's assumed heat load. The Forward Port cooling zone remains the most limiting condition, with an estimated heat load of **644.8** kW.

N-1 Scenario: Loss of Cooling Source

The other primary casualty scenario requiring evaluation is the loss of a cooling source. This scenario entails either battle damage or a general casualty rendering an entire cooling skid inoperative. Per the previously described design requirements, all PEBB stacks and cold plates must have two sources of cooling to meet relevant military standards. Although some of the major loads do not have two sources of power, all sources of power shall still have two sources of cooling.

Each cooling zone is designed such that it can be aligned to the main header and provide cooling to the entire length of the system on that side of the ship. For example, if the Mid Port cooling skid were lost, the Forward and Aft Port cooling skids would be aligned through the main header in order to share the emergent heat load while still carrying their own zone's term. This type of scenario was analyzed across all the cooling zones, in order to determine the most limiting operational scenario. In this casualty, the Forward Port remains the limiting cooling zone and incurs an estimated heat load of 834.1 kW. An additional 20 percent cooling margin was added to this term, as is typical during the early stages of system design and to accommodate anticipated increased loads in the future. Therefore, the most limiting heat loss estimate was updated to 1000.92 kW.

5.3.3 Final System Design Decisions

Temperature Rise

Adopting this improved method of heat loss estimation meant that the system heat exchanger model was retroactively imbued with considerable cooling margin. This excess capacity was leveraged to modify other system parameters that would have otherwise required redesigning the heat exchanger.

Even in light of the benefits incurred by the lower assumed heat load, remaining strictly tethered to the 2°C water temperature rise limit delineated in MIL-STD-1399 [31] would still require an overall system flow rate of 1635 gpm. Although this value is also significantly lower than the previous 2990 gpm value first determined in Chapter 3, it would still flagrantly exceed pressure drop limits, and would also violate the safe piping velocity limits adopted from NSTM-505 [34]. The riser piping from the heat exchanger is assumed to have a hydraulic diameter of 5.5", which has a corresponding velocity limit of 11.5 fps, whereas the suggested flow rate would result in a pipe velocity of 26.7 fps. Although larger diameter piping would increase the velocity limit and decrease the actual pipe velocity, this was deemed spatially infeasible to incorporate into the overall NiPEC system architecture when all the other non-cooling system components were considered.

Therefore, it was deemed necessary to deviate from the 2°C limit. The Naval Sea Service Command (NAVSEA) In-Service Engineering Agents (ISEA) holding technical cognizance over this requirement confirmed that justifiable deviations are permissible and would be approved. In fact, no current ECWS in the U.S. naval fleet currently operates at that low of a temperature rise; most naval systems operate at about 5-6°C. Table 5.4 illustrates the beneficial predicted effects on system flow rates and velocities incurred by increasing the allowable temperature rise. The pipe velocities listed reference the riser piping discussed above.

In light of the subject matter expert guidance and in consideration of the flow rates and velocities listed in Table 5.4, the objective ΔT was increased to 6°C, which resulted in a maximum predicted system flow rate of 545 gpm, and a maximum

Table 5.4: ΔT Effect on Predicted Flow Rates and Velocities

ΔT (°C)	Predicted System Flow Rate (gpm)	Pipe Velocity (fps)
2	1635	26.7
3	1090	17.8
4	817	13.4
5	654	10.7
6	545	8.9
7	467	7.6
8	409	6.7
9	363	5.9
10	327	5.3

predicted riser pipe velocity of $8.9 \ fps$. These parameter changes offered a valid compromise between limiting the maximum temperature rise of the cooling water while striving to meet all major performance benchmarks.

Temperature Range

The thermal resistance network and 80/20 semiconductor load analysis presented in Chapter 2 had predicted acceptable heat transfer performance and component temperatures at a cold plate inlet temperature ($T_{plate,in}$) of 40°C. However, additional cold plate CFD analysis revealed that for a PEBB operating at full capacity (*i.e.* heat loss of 10 kW total, or 5 kW per cold plate), the 150°C MOSFET temperature limit was exceeded when $T_{plate,in} = 35$ °C. The maximum simulated MOSFET temperature under these conditions was 160.36°C [23].

Therefore, the system design had to be iterated to permit a lower operating temperature range and lower $T_{plate,in}$. To this end, the heat exchanger's reserve cooling capacity was again leveraged to lower the demineralized water's outlet temperature, which is assumed to be equal to $T_{plate,in}$ given the adiabatic piping assumptions at this design stage. This updated value for $T_{plate,in}$ could then be validated through further CFD analysis.

By lowering the demineralized water outlet temperature from 40°C to 22°C, and maintaining the chilled water inlet temperature at 7°C, the LMTD was decreased from 29.8°C to 14.6°C. This significant reduction in LMTD would normally require

increased heat transfer surface area, but the cooling margins provided in the proposed model supported these systematic changes without requiring any sizing modifications to the heat exchanger. In fact, the design still provides over a 20% cooling margin at an improved operating efficiency of nearly 70%, compared to 43% previously. Therefore, $T_{plate,in}$ was set at 22°C.

Cold Plate and System Flow Rate Assessment and Validation

As a first pass, the 545 gpm total cooling zone flow rate derived from Table 5.4 was assumed to be evenly distributed amongst all the cold plates in the N-1 Loss of Cooling scenario, which correlated to a cold plate mass flow rate (\dot{m}_{plate}) of 0.115 kg/s. However, MOSFET temperatures still far exceeded the 150°C limit, reaching a maximum of 188.69°C, as seen in Figure 5-3.

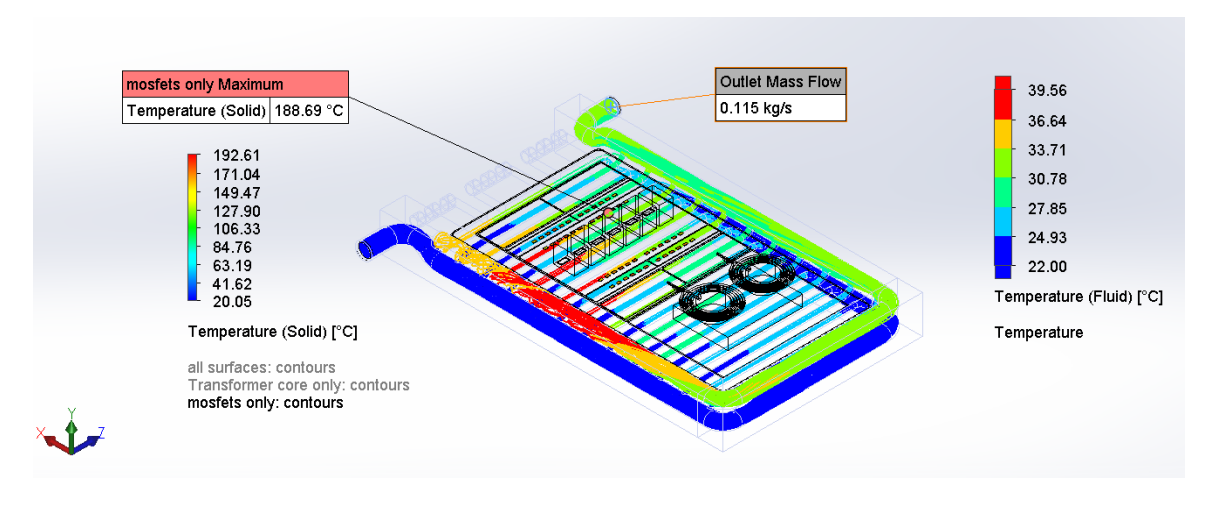


Figure 5-3: Cold plate conditions for a fully loaded PEBB, assuming an inlet temperature of 22°C and \dot{m}_{plate} of 0.115 kg/s. MOSFET temperature limits are exceeded.

A parametric study within Flow Simulation was conducted to determine the lowest \dot{m}_{plate} which maintained MOSFET temperatures less than 150°C. This analysis concluded that the lowest achievable \dot{m}_{plate} was 0.370 kg/s, corresponding to a maximum MOSFET temperature of 149.52°C. Under these conditions, ΔT_{plate} does not reach 6°C; it approaches 4°C. Given the specific topological arrangements of the MOSFETs on the PEBB, a higher mass flow rate than predicted is necessary through certain channels to curtail junction "hot spots" and prevent MOSFET temperature limit

violations.

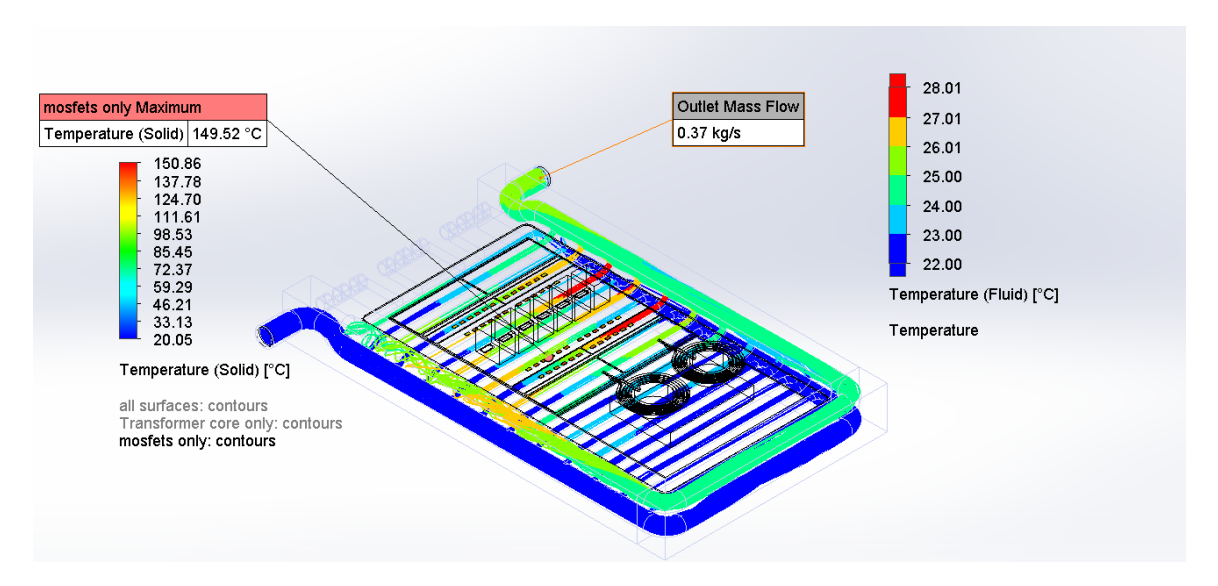


Figure 5-4: Cold plate conditions for a fully loaded PEBB, assuming an inlet temperature of 22°C and \dot{m}_{plate} of 0.370 kg/s.

Since this model reflected a PEBB at full capacity, the number of PEBBs operating at full capacity under the reference N-1 condition was calculated to determine the required flow for these cold plates. Analysis of this loading scenario determined that 54 PEBBs are expected to be at full capacity, so the corresponding 108 cold plates, each receiving 0.370 kg/s of cooling water, require a cumulative flow of 633 gpm.

These fully-loaded PEBBs account for 540 kW of the 834.1 kW heat load, so the remaining 294.1 kW was assumed to be evenly distributed amongst the remaining 95 PEBBs and 190 cold plates. This averages to 1548 kW carried by each cold plate.

Because the fully-loaded PEBBs' cold plates could not achieve the objective ΔT_{plate} , the remaining cold plates had to support a steeper temperature rise to result in a global temperature rise closer to 6°C. This analysis assumed adiabatic piping, such that any temperature losses experienced from the cold plate outlet nozzles to the heat exchanger demineralized water inlet nozzles are considered negligible. Therefore, so long as sufficient fluid mixing occurs within the stacks' return branch piping and the main return headers, a target global temperature rise can theoretically be realized.

The cold plate model was updated to reflect the "low-load" average heat loss

and was simulated across various flow rates to determine resultant temperature rises. Mass flow and temperature balance calculations were then carried out to determine the global temperature rise, considering the contributions from both the fully-loaded PEBBs and the low-loaded PEBBs.

In order to achieve the desired 6°C global temperature rise, the low-load cold plates' mass flow rate had to be set at 0.008 kg/s, which corresponded to a $\Delta T_{plate,lowload}$ of 44.2°C. Although the MOSFET temperatures remain below the 150°C limit in this scenario (see Figure 5-5), the derived temperature rise was too large to be considered as a viable option. A temperature rise that steep over that short a distance would introduce significant thermal stresses which could cause unacceptable piping expansion, potentially instigate component damage, and threaten system reliability.

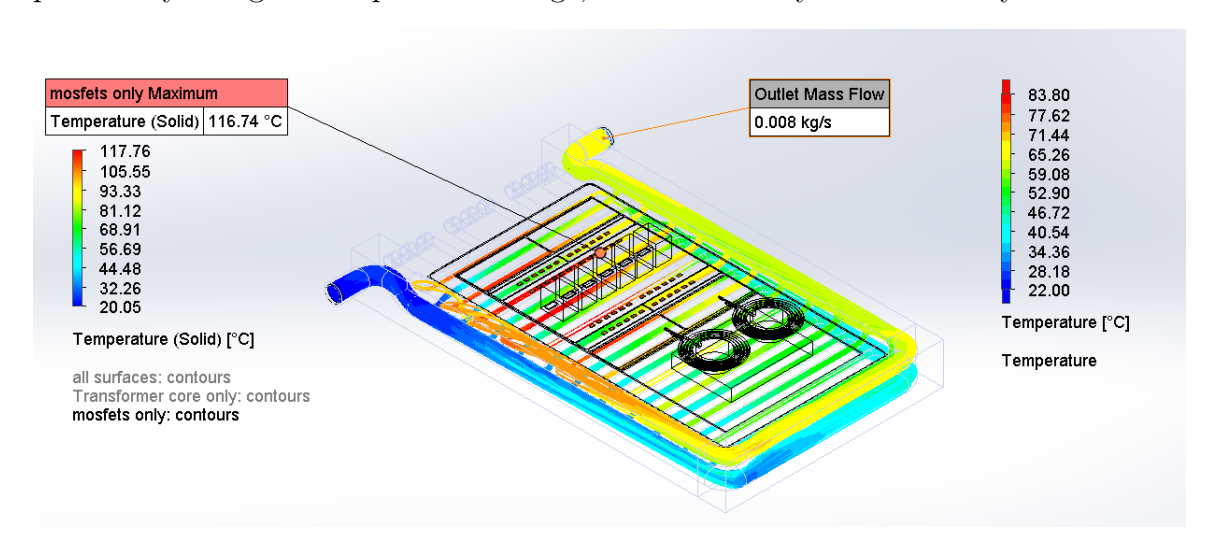


Figure 5-5: Cold plate conditions for a low-loaded PEBB, assuming an inlet temperature of 22°C and \dot{m}_{plate} of 0.008 kg/s.

In light of these results, a more reasonable $\Delta T_{plate,lowload}$ of 12°C was targeted. This required a low-load cold plate mass flow rate of 0.03 kg/s. MOSFET temperatures remain far below the limit, reaching a maximum of 84.86°C. Anticipated thermal stresses from the temperature rise are predicted to be within a much more acceptable range than the previous design. Given this flow rate and the number of remaining cold plates, an additional 90 gpm of flow is required. Thus, the total required cooling zone flow rate is 723 gpm, and for the purposes of follow-on calculations, was assumed to be 725 gpm.

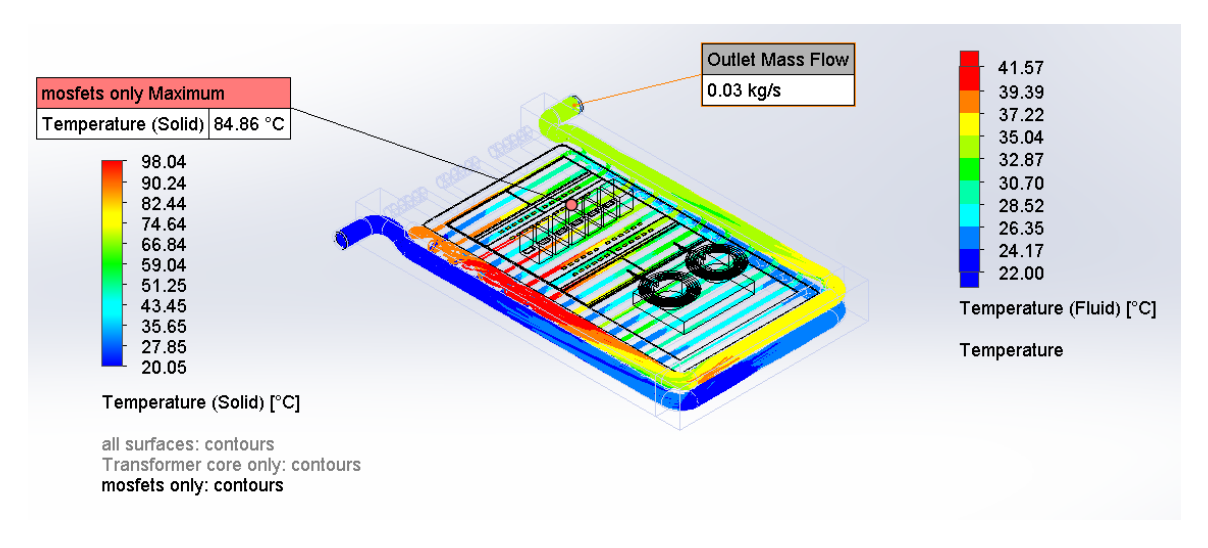


Figure 5-6: Cold plate conditions for a low-loaded PEBB, assuming an inlet temperature of 22°C and \dot{m}_{plate} of 0.030 kg/s.

This total mass flow rate is higher than what was originally predicted by the more general thermodynamic heat balance equation. Still, the maximum velocity experienced by the system—at the heat exchanger inlet, outlet, and riser piping—still falls below the corresponding limit of $11.5 \ fps$, reaching a predicted maximum of $11.3 \ fps$. The velocities experienced elsewhere in the system fall well below their relevant limits despite the smaller pipe sizes due to the division of flow between multiple headers, branches, stacks, and plates. The major enduring concern is that the revised mass flow rates will produce pressure drops in excess of the limits established by MIL-DTL-15730N [30] at the heat exchanger. This remains one of the primary open questions requiring additional investigation and analysis. Specific possible recommendations and future courses of action are provided in Chapter 8.

The calculated global temperature rise was 5.0°C. This value iss less than the objective 6°C, but was back-propagated into the heat exchanger model and, when coupled with the updated demineralized water flow rate value, was determined to still provide the required heat exchanger performance without any additional structural or geometric redesign.

Flow Control

This approach to system operation requires flow regulation at the individual cold plate level. This will require Temperature Control Valves (TCV) to enable reduced or enhanced flow based on PEBB loading. Generally, a TCV senses either inlet or outlet temperature from the heat exchanging component (*i.e* the cold plate). It automatically adjusts its position to adjust the flow to the component in order to maintain the desired calibrated temperature.

The results yielded by the cold plate CFD analyses illustrate the additional complexity of successfully implementing this level of control in the system. The loading condition of the PEBB influences the achievable temperature rise across its cold plates. The maximally loaded PEBBs require a \dot{m}_{plate} which does not correspond to a ΔT_{plate} of 5°C, whereas lower-loaded PEBBs can easily support this temperature rise. Therefore, an additional control mechanism may be necessary which, upon sensing PEBB loading crossing above a certain threshold, sends a signal to the TCV to update its calibrated temperature target, forcing a lower ΔT_{plate} to permit increased flow and ensure PEBB temperature limits are not exceeded.

Alternatively, the cooling system could be sized so that every plate receives the maximum required flow (.37 kg/s) at all times. In this way, the system would be designed in a ready state for any PEBB to operate at full capacity. But this would fashion a largely inefficient design which would require a total cooling zone flow rate of nearly 1750 gpm, much of which would be unnecessary for a large portion of the cold plates under most operating conditions. The current heat exchanger model would be unable to support that amount of flow, which would need to be distributed across multiple additional heat exchangers. This would likely incur significant space and volume increases that would require a dedicated and detailed feasibility analysis.

As such, it is highly recommended to include TCVs at each cold plate. Although this design increases the manufacturing and operational complexity, it is likely a necessary inclusion to ensure proper system response to the dynamic and variable loading conditions of the PEBBs.

5.3.4 System Parameter Summary and Concept of Operations

The heat exchanger model's geometry as detailed in Table 4.2 is retained while supporting the final system operational design parameters provided in Table 5.5. The listed parameters represent the requirements for one of the six cooling zones.

Table 5.5: Final System Operational Parameters

Heat Load	\dot{Q}	kW	1000.92
Cold Plate Inlet Temperature	$T_{plate,in}$	$^{\circ}C$	22
Global Temperature Rise	ΔT	$^{\circ}C$	5
Chilled Water Flow	m_{CW}	gpm	260
Cold Plate Mass Flow: Full Load	$m_{plate,FL}$	kg/s	0.370
Cold Plate Mass Flow: Low Load	$m_{plate,LL}$	kg/s	0.030
Normal System Operating Pressure	P_{sys}	psi	100
Maximum Demineralized Water Flow	m_{DI}	gpm	725

All six cooling zones are in use during normal operating conditions. There is no designated backup cooling skid on each side of the ship, which forfeits some of the flexibility offered in the quadrant cooling strategy, which allowed all the cooling skids to rotate through two-to-three week operational windows. However, system longevity and equitable equipment runtime are provided for by the standby pumps and alternate heat exchangers included in each cooling skid. It is recommended that these components swap operational status on a weekly basis as established by the proposed periodic maintenance schedule for the system.

The loss of cooling source scenario assumes that both remaining cooling zones on the affected side will split the resulting heat load from the lost cooling zone. Therefore, the forward cooling zone would have to provide cooling to the aft cooling zone and vice-versa. This requires that each skid's pumps have the capacity to provide sufficient flow through the entire length of the corridor. Although this aspect of the design is not ideal—and was avoided in the quadrant zonal approach—it is ultimately a necessary concession to make in order to better distribute the heat loss and best enable the six-zone approach.

Chapter 6

Other System Component Evaluation

6.1 Pump

In order to appropriately size the NiPEC cooling system coolant circulating pumps, two key parameters were required: (1) the flow rate of liquid the pump is required to deliver, and (2) the total differential head the pump must generate to deliver the required flow rate.

6.1.1 Flow Rate

The iterative design approach documented in the previous chapters addressed the recommendations and requirements governing electronic cooling water flow for naval systems, evaluated against the second and third-order effects that a change in cooling flow had on the system's heat transfer characteristics. The volumetric flow rate was balanced against the competing influences of limiting the pressure drop across the heat exchanger, providing the adequate mass flow rate to all cold plates under both normal and casualty scenarios, and ensuring safe piping velocities throughout all portions of the system. Ultimately, a cooling zone system flow rate of 725 gpm was determined.

The NiPEC cooling system is envisioned such that the coolant circulating pumps draw suction from the return header, are placed before the heat exchangers, and are located closely to the expansion tank in order to accrue the maximum Net Positive

Suction Head (NPSH) benefits. As such, the pumps will receive the system's demineralized water prior to it being cooled, which under normal operating conditions is assumed to be 27°C. Based on this temperature assumption, the corresponding principal water characteristics were determined for use in subsequent pumping power calculations, and are provided in Table 6.1,

Table 6.1: System Coolant Properties

Volumetric Flow	\dot{V}	m^3/s	0.0457
Coolant Temperature	T	$^{\circ}C$	27
Density	ρ	kg/m^3	996.53
Dynamic Viscosity	μ	$N - s/m^2$	0.000850
Vapor Pressure	P_{vap}	kPa	3.569

where dynamic viscosity, μ , measures the force required to overcome internal friction in a fluid, and the vapor pressure, P_{vap} , refers to the equilibrium pressure of a vapor above its liquid in a closed system.

6.1.2 Total Differential Head

The Total Differential Head (TDH) that a system must generate is dictated by the system flow rate, and the system through which the liquid flows [26]. This, in turn, is primarily dictated by two components: the system static head difference and system frictional losses. The static head difference across a pump is the difference in head between the discharge static head and the suction static head. However, in a closed loop system such as this, the static head difference will be zero since the fluid on one side of the system pushes up the fluid on the other side of the system, and so the pump does not need to overcome any elevation differences.

System frictional losses account for all the pressure losses experienced by the system fluid as it flows through the system piping, fittings, and equipment which the system pumping will ultimately have to overcome. Each category was individually assessed and evaluated in terms of suction or discharge losses in order to determine the final TDH. The calculations in the ensuing sections follow the process outlined in Menon [29].

6.1.3 Piping Frictional Pressure Losses

First, the piping frictional losses were calculated using the Darcy-Weisbach equation,

$$\Delta p = f_D \frac{L}{D_{ID}} \frac{\rho}{2} (v)^2 \tag{6.1}$$

where f_D is the Darcy friction factor, L is the length of the pipe (m), D_{ID} is the internal diameter of the pipe (m), ρ is the density of the fluid (kg/m^3) and v is the mean flow velocity (m/s).

The Darcy Friction Factor, f_D , is calculated using the Petukhov approximation for smooth pipes and Reynolds values between $10^4 \le Re \le 5e10^6$:

$$f_D = (0.79 \ln(Re) - 1.64)^{-2} \tag{6.2}$$

where Re is the Reynolds number, which categorizes the ratio of inertial forces to viscous forces for a system fluid. The Reynolds is given by the following equation,

$$Re = \frac{\rho v D_{ID}}{\mu} \tag{6.3}$$

where ρ is the density of the fluid (kg/m^3) , v is the mean flow velocity (m/s), D_{ID} is the internal diameter of the pipe (m) and μ is the dynamic viscosity.

The suction piping is assumed to have an internal diameter of 5.3 in (Schedule 40 pipe wall thickness); the discharge piping is assumed to have an internal diameter of 5.1 in (Schedule 80 pipe wall thickness). The suction piping is sized slightly larger than the discharge piping in order to reduce the friction losses realized prior to the pump and ensure it remains above the fluid vapor pressure to avoid cavitation and subsequent pump damage.

The longest anticipated runs of suction and discharge piping were assumed for these calculations since this approach yields the most conservative (i.e. largest) friction loss estimates. In the limiting N-1 Loss of Cooling scenario described in Chapter 5, a forward or aft cooling zone is lost, and the remaining two cooling zones on that side of the ship are realigned to provide continued cooling to the affected power corri-

dor sections. Therefore, a forward cooling zone pump must be able to pump coolant to the aft-most PEBB stack on that side of the ship, or vice-versa. This pipe length was determined using the 3D CAD model of the NiPEC cooling system created in Rhino3D.

Suction and discharge velocity values were calculated based on the assumed system volumetric flow rate, the internal pipe diameters, and the application of the continuity of mass equation. The key parameters and resulting piping frictional losses are provided in Table 6.2.

Table 6.2: Suction & Discharge Piping Frictional Losses

			Suction	Discharge
Volumetric Flow Rate	V	m^3/s	0.0457	0.0457
Pipe Internal Diameter	D_{ID}	in	5.3	5.1
Pipe Length	L	m	99.74	104.16
Fluid Velocity	v	m/s	3.21	3.47
Piping Pressure Loss	P_{Pipe}	psi	7.21	9.07

6.1.4 Equipment Frictional Pressure Losses

For a given closed circuit within the overall cooling system, the main sources of equipment pressure losses are the heat exchanger, an individual PEBB stack, and the mechanical Y-type strainer located on the suction side of the pump. The heat exchanger and stack pressure drops were conservatively assumed to be at their highest permissible values, 6 psid and 10 psid respectively, in accordance with MIL-DTL-15730N [30] and MIL-STD-1399 [31]. Pressure drop correlations based on strainer size and system flow rate were used to determine an appropriate pressure drop estimate of 5 psid for the main installed strainer [12].

6.1.5 Fitting Frictional Pressure Losses

Fittings—which include valves, pipe bends, tees, reducers, and other functional components—often induce the most significant pressure losses in a system [11]. There are a variety

of methods available to calculate these pressure losses depending on the complexity of the system under analysis, the granularity of system detail available, and the desired level of pressure loss accuracy. For the purposes of this analysis, the "K-Value" or "Resistance Coefficient" method was employed. The K-value of a fitting indicates the number of velocity heads that will be lost by the fluid passing through that fitting [11]. The headloss is given by,

$$h_L = K \frac{v^2}{2q} \tag{6.4}$$

where K is the fitting resistance coefficient, v is the mean flow velocity (m/s), and g is the gravitational acceleration constant. Through this method, the headloss incurred by a single fitting is calculated and then multiplied by the number of same-type fittings in the overall system. All fitting contribution losses are then summed to determine the overall fitting frictional losses.

The expected fitting arrangements and allocations within the cooling skids spaces are expected to largely mirror the system schematic as seen in Figure 1-5, which was used as the basis for the initial fitting determination. The 3D cooling system model was then referenced to determine additional fitting placements and pipe arrangements primarily along the risers and main headers. The distributed shipwide piping introduces 90°bends due to the riser piping from the heat exchanger branching to the 2nd and 4th deck main headers, and additional tee junctions to account for coolant flow splitting to both the forward and aft directions for a given main header.

Four major isolation gate valves are included in each main header to isolate each of the three cooling zones per side during normal operations and allow their alignment in a loss of cooling zone casualty scenario.

An automatic TCV was included at each PEBB cold plate inlet, following the analysis and recommendations set forth in Chapter 5. Although this design decision increases the manufacturing and operational complexity of the PEBB stacks, it was deemed necessary in order to account for the potential dynamic loading profiles of each PEBB and the attendant need to appropriately adjust flow at the cold plate.

The inclusion of this globe valve is disadvantageous from a pumping perspective, as this type of valve induces relatively significant pressure losses, but was a necessary concession to make.

Once all major fittings were accounted for, the cumulative suction and discharge fitting headloss values were determined.

6.1.6 Total Losses and Pumping Power Determination

The aforementioned pressure loss contributions are summarized in Table 6.3. The discharge losses are added to the system pressure requirement (100 psi), while the suction losses are subtracted from the system pressure requirement, which effectively calculates the TDH to ensure the required system pressure is seen at the load (i.e. cold plates).

Table 6.3: System Pressure Losses

			Suction	Discharge
Equipment Pressure Loss	P_{Equip}	psi	5	16
Piping Pressure Loss	P_{Pipe}	psi	7.22	9.07
Fitting Pressure Loss	$P_{Fitting}$	psi	25.95	42.77
Total Pressure Loss	P_{Tot}	psi	61.83	167.83
Total Dynamic Head	TDH	psi	106.0	

The TDH was then used to determine pump sizing by using the pump power equation,

$$P_{pump} = \frac{\dot{V}\rho g(TDH)}{\eta} \tag{6.5}$$

where P_{pump} is the pump power (kW), \dot{V} is the volumetric flow rate (m^3/s) , TDH is the total differential head (m), and η is the pump efficiency. Large-size industrial centrifugal pumps typically operate at approximately 70% efficiency, and this was the value assumed for η [14]. As such, the required pump power was determined to be $47.66 \ kW$, or $63.92 \ HP$.

6.2 Expansion Tank

A closed-loop pressurized water system like the NiPEC cooling system requires an appropriately sized expansion tank to serve the following functions: (1) to accommodate thermal expansion of the system coolant, (2) to maintain positive pressure at points in the system at all times and under all conditions, and (3) to maintain adequate NPSH to the system's cooling pumps [24]. The most common type of expansion tank is a closed tank fitted with a bladder or diaphragm, which serves to separate the air and water within the tank to minimize oxygen entrainment within the coolant and avoid associated corrosion and cavitation concerns. This was assumed as the expansion tank type and served as the basis for the enusing sizing calculations, which follow the process outlined by Kauwale [24].

6.2.1 Volume and Pressure Requirements

The minimum required expansion tank volume is given by the following equation,

$$V_T = V_s \frac{\left[\left(\frac{v_2}{v_1}\right) - 1\right] - 3\alpha\Delta T}{\left(\frac{P_{pre}}{P_1}\right) - \left(\frac{P_{pre}}{P_2}\right)} \tag{6.6}$$

where V_T (gal) is the minimum required expansion tank volume, V_S (gal) is the total cooling system volume, v_1 (m^3/kg) is the specific volume at the lowest assumed coolant temperature, v_2 (m^3/kg) is the specific volume at the highest assumed coolant temperature, α (1/°C) is the linear coefficient of thermal expansion for the piping material, P_{pre} (psia) is the pre-charged pressure of the expansion tank, P_1 (psia) is the minimum allowed tank pressure, and P_2 (psia) is the maximum pressure which can occur at the expansion tank to avoid pressure relief valve operation or system equipment failure. The pre-charged pressure is conservatively set to P_1 , which allows Equation 6.6 to be recast in the form provided by Equation 6.7.

$$V_T = V_s \frac{\left[\left(\frac{v_2}{v_1} \right) - 1 \right] - 3\alpha \Delta T}{1 - \left(\frac{P_1}{P_2} \right)} \tag{6.7}$$

The total system volume was obtained through volumetric analysis of the 3D

CAD model, which included the various runs of major piping, the inlet and outlet piping associated with all the PEBB stacks in the most PEBB-heavy corridor, the cold plate piping for these PEBB stacks, two heat exchangers, and two cooling pumps. Additional volume contributions were included to account for recirculation piping and other equipment not directly included in the model at the time of analysis. The total system volume was determined to be 1100 gallons.

In the extreme scenario where all the PEBBs in a corridor are turned off and the demineralized water conveys no heat load, the demineralized water temperature will decrease as it loses heat to the chilled water at the heat exchanger. This heat transfer process will continue until the temperatures equalize. The chilled water servicing the demineralized water at the system heat exchanger is assumed to operate at an inlet temperature of 7°C. Therefore, the estimated lower bound demineralized water temperature is 7°C.

In a complete loss of cooling flow scenario, the demineralized water will be unable to convey the heat produced by the PEBBs to the system heat exchanger and will begin to heat up and expand. Reyes [39] determined that based on the worst-case semiconductor load conditions, the assumed total thermal network resistance for a PEBB semiconductor switch, and the upper bound semiconductor temperature limit of 180°C to avoid catastrophic equipment damage, the highest demineralized water temperature realized is 79°C. Specific volume and vapor pressure values associated with these water temperatures were retrieved using standard look-up tables.

The minimum system pressure must be no less than $10 \ psi$ in accordance with MIL-STD-1399 [31]. This pressure threshold must be achieved at the highest point in the system, *i.e.* the upper-most rung of inlet and outlet piping on a given PEBB stack located on the 2nd deck. Assuming the system fill line is located at the same elevation as the top of the expansion tank, then the expansion tank must overcome approximately 13.6 feet of head $(5.89 \ psi)$. Thus, the minimum expansion tank pressure was set at $15.89 \ psig$.

The limiting maximum pressure scenario assumes that the cooling pump is online and that the demineralized water is at its highest temperature [24]. The upper design pressure of 110 psi given by MIL-STD-1399 [31] is assumed as the system's Maximum Allowable Working Pressure (MAWP). The expansion tank relief valve setpoint should be at least 10% or 15 psig above the MAWP, whichever is greater [22]. Therefore, the relief valve setpoint is assumed to be 125 psi. If this pressure is assumed present at the cold plates, and given the pump provides 100 psi, the pump suction will be at 25 psig. The piping losses between the expansion tank and pump suction are estimated to be 3.5 psig, which results in an expansion tank high-pressure condition of 28.5 psig.

The $3\alpha\Delta T$ term represents the volumetric expansion of the system piping, which in turn is able to accommodate a portion of the coolant expansion and thus reduce the required expansion tank volume. In keeping with the material selection decisions proposed by Reyes [39], the piping is assumed to be CuNi 90-10 alloy, which has a linear thermal expansion coefficient of $16.2 \times 10^{-6} \, 1/^{\circ}$ C.

Using these values in Equation 6.7 yielded a minimum required expansion tank volume of 93.4 gallons. In order to provide sufficient margin for both low tank and high tank level conditions where operator action may be required, an additional 20% volume margin was included. Therefore, the required expansion tank volume is 115 gallons.

Chapter 7

Dynamic Modeling

Many of the NiPEC cooling system design decisions were predicated on assumptions of component sizing and spacing that have yet to be finalized. Therefore, concurrent work was performed to develop a dynamic PEPDS/NiPEC model which is responsive to a host of design parameters subject to future variation. This includes the principal dimensions of both the Navy iPEBB and the PEBB 6000, their corresponding stack dimensions, the associated power density of each configuration (*i.e.* how many PEBBs can fit within one stack), the necessary spacing required between each stack to accommodate cooling piping, cooling piping dimensions, and space within each compartment allocated for personnel walkthrough access.

Electrical load pre-processing calculations were carried out to determine the number of each type of PEBB stack required in each portion of each compartment of each corridor. These values are then fed into the modeler using the parametric modeling tool Grasshopper, which offers dynamic programming capability as a plug-in for Rhino3D. Using the interface shown in Figure 7-1, the inputs generate PEBB stack array layouts, which are influenced by all the design parameters as described above.

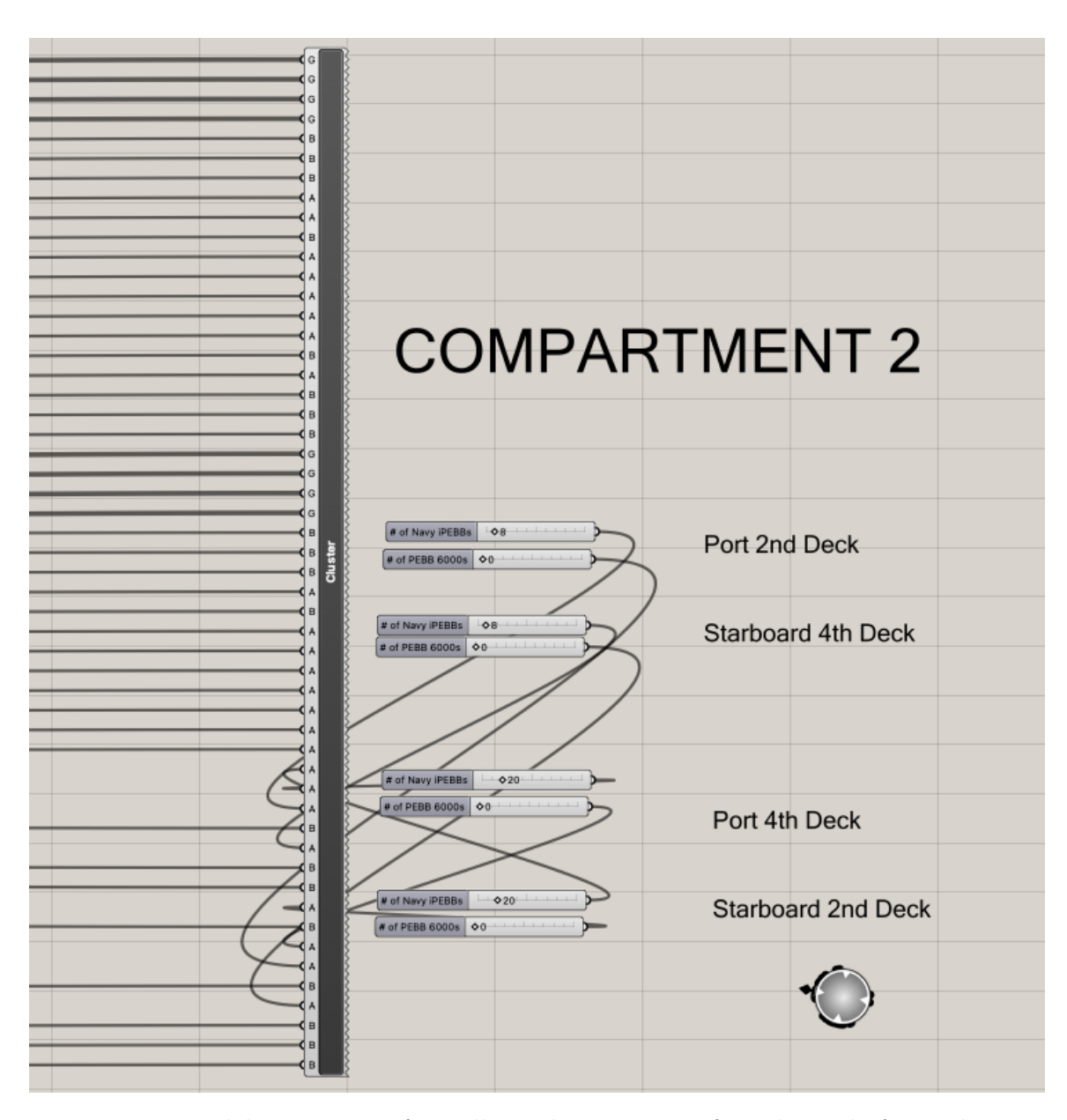


Figure 7-1: Modeler user interface allows direct input of stack needs for each compartment, which are then automatically generated.

7.1 Use Cases

7.1.1 Nominal Destroyer Corridor Arrangement

The dynamic modeler was first employed to render a full PEBB stack layout of the nominal destroyer, shown in Figure 7-2. Of particular concern were the potential stacklength issues in the compartments housing the generators and PMMs, each of which requires many PEBB 6000s to enable proper power conversion and distribution. Based on the first set of design choices—which assumed 12" of horizontal inlet and outlet piping on each side of a PEBB stack (wingspan), and an additional 12" of spacing between two adjacent stacks—stacklength limitations occurred in each portion of a corridor servicing either a generator or PMM. This illustrated that the initial assumptions made about the piping wingspan would have to be reassessed. In conjunction with efforts to reduce the overall system's construction and operational complexity, this insight led to the determination that each PEBB plate did not require its own set of isolation valves. Without the need to incorporate isolation valves within the inlet and outlet piping, the piping wingspan could be reduced considerably.

Within this redefined design space, the dynamic modeler was used to adjust the piping wingspan to 6", by reducing the inlet and outlet piping span to 4" and maintaining the branch piping diameter at 2". The PEBB stack spacing was also decreased to 6", which shortened the overall stack footprint while ensuring that the minimum 3" valve clearance requirements dictated by MIL-STD-1472 [32] were still met to permit the operation and maintenance of the TCV) for each cold plate. These combined spacing reduction efforts relieved the stacklength issues in the generator compartments, improving the overall design's feasibility. The modeler permitted rapid rendering of a potential NiPEC layout solution and provided immediate feedback as to whether certain design choices were viable or not. Of note, these specific described changes did not fully resolve the stacklength issue in the PMM compartments, which remains an open problem.

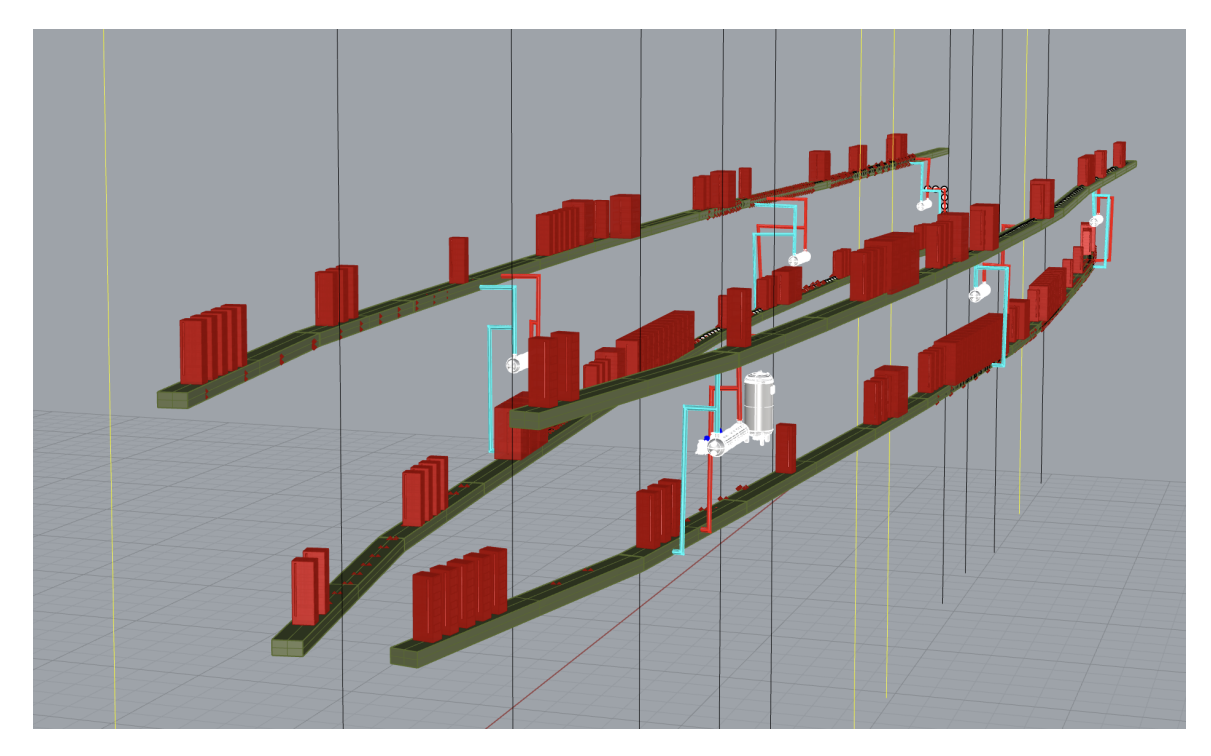


Figure 7-2: Model of six-zone NiPEC cooling system with PEBB arrangements specified by compartment, corridor, and deck.

7.1.2 Single Power Train Arrangements

There are ongoing efforts at the University of Wisconsin-Milwaukee's Center for Sustainable Electrical Energy Systems (UWM-CSEES) to develop a power converter sizing tool that estimates the dimensions of a PEBB drawer based on various inputs, such as voltage, frequency, coolant mass flow rate, and coolant inlet temperature. This work was leveraged to provide an example application of the modeler, and its ability to interface with parallel NiPEC research efforts to evaluate the shipboard arrangement impact of potential power converter solutions.

The ship's primary power train is from one of the onboard generators to the main distribution bus, *i.e.* the conversion of AC power generated at 6900 kVac to distributed DC power at 12 kVdc. Main bus power is then conveyed to an in-zone load via the LVDC 1 kVdc distribution bus. Based on UWM-CSEES' proposed converter architecture, the first leg of this power conversion process would require 12 power converter drawers which are analogous (but not identical) to the PEBB 6000 converter thus far described in this study. The second leg of conversion retains the

use of 12 Navy iPEBBs.

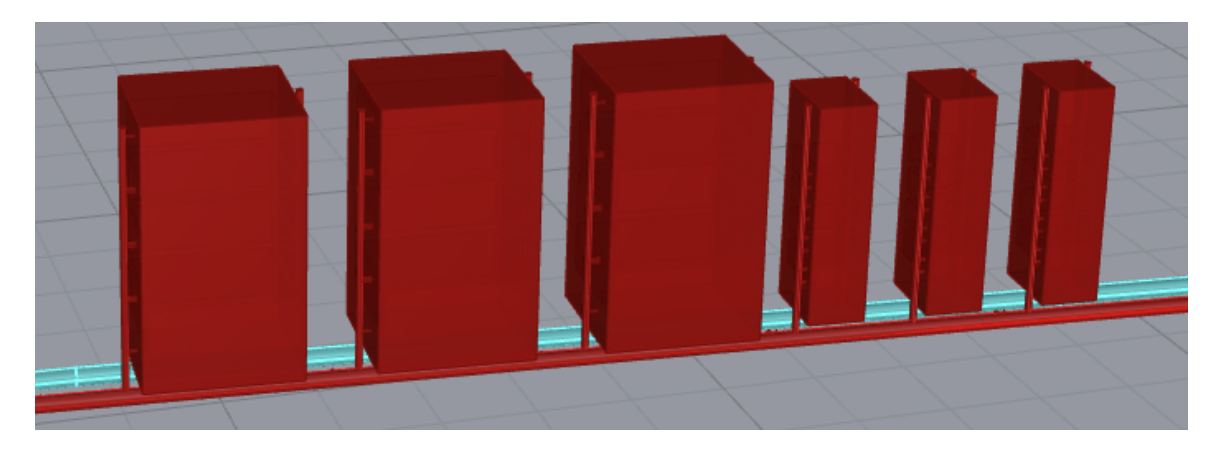


Figure 7-3: NiPEC power train footprint to enable MVAC-MVDC-LVDC conversion.

The sizing tool determined the drawer dimensions as follows: 0.841 m (length) x 0.978 m (width) x 0.328 m (height). These values were directly fed into the modeler, along with the assumption of 2" vertical spacing between PEBB drawers and 2" of padding around each drawer to dictate stack enclosure sizing. Based on these derived drawer dimensions, and the dimensions of the iPEBB and iPEBB stack assumed thus far, this two-step power train process results in a PEBB stack footprint as seen in Figure 7-3. Figure 7-4 shows the internal PEBB arrangements within their respective stacks. The volume of a single PEBB 6000-like stack is 8.67 m^3 ; the volume of a single iPEBB stack is 1.53 m^3 . In this rendering, four of the larger drawers can fit within a single stack, which compares favorably to the previous assumption in which only three PEBB 6000 drawers were allotted per stack based on projected sizing restrictions.

Of note, this particular conversion solution yielded a total useful power output of approximately 3 MW. Given the 29 MW-rated output of the LM2500 generator sets, nine additional instances of the three larger stack groupings would be required to fully convert the generator's power output to the MVDC bus. The total volumetric and spatial footprints are therefore greater than what was previously estimated and would result in stacklength issues in the generator compartments.

Ultimately, the power converter drawers and stack dimensions illustrated here are just one of many potential solutions, dependent on a variety of input parameters, produced by the UWM-CSEES sizing tool. More broadly, this example illustrates the

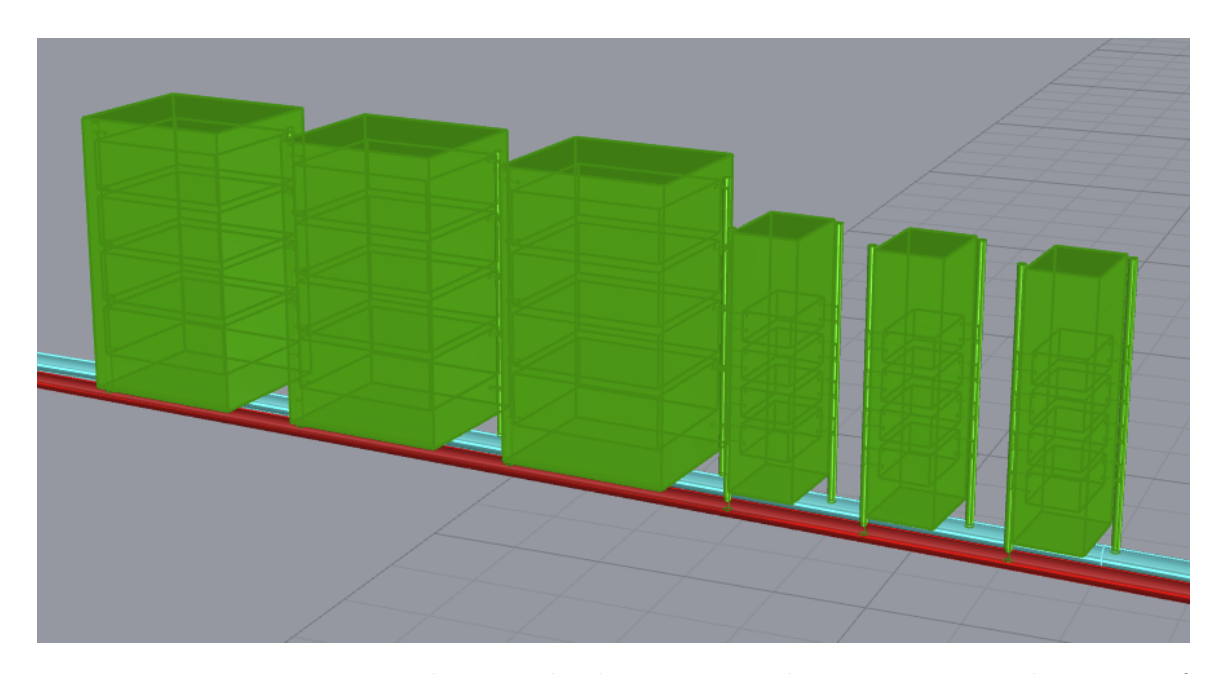


Figure 7-4: Power train stack array displaying internal arrangement and spacing of PEBBs.

modeler's compatibility with other efforts to advance the NiPEC concept. By taking potential power converter solutions and evaluating them in a simulated NiPEC 3D environment, the modeler provides an integrative tool to assess the initial viability of a given PEBB design and the impacts it has on the power corridor arrangement writ large.

Chapter 8

Future Work and Conclusions

This thesis proposed a NiPEC cooling system designed and suitable for shipwide deployment. Building off of previous research in this space, an indirect liquid cooling thermal management strategy was implemented via a closed-loop, pressurized, distributed cooling circuit serviced by the warship's chilled water system. A comprehensive electrical load list developed for this notional all-electric destroyer served as the design basis to assess the total required power, the allocation of PEBBs (tailored to the watertight compartment level) to meet this power demand, and the resultant heat loss from the PEBBs which necessitates the candidate cooling system. Major system components were designed, modeled, and tested against key performance benchmarks and relevant military standards. Various shipwide system architectures were evaluated for feasibility, survivability, and robustness against casualty and operationally limiting scenarios. Initial work was performed to develop a modeler tool that can rapidly evaluate a range of power corridor layout solutions, which either influence or are influenced by design decisions specific to the NiPEC cooling system itself.

8.1 Future Work

Many of the lines of effort summarized above warrant additional research to answer unresolved technical issues, to specify the mechanisms by which to actually build and implement this concept, or to generally improve the overall feasibility and performance of the design.

8.1.1 Detailed Electrical Plant Operational Analysis

This research's treatment of the nominal ship load relied on a relatively simplistic load factor analysis based on the most limiting operating condition as defined and provided in [19]. However, future efforts should employ a more detailed and rigorous stochastic load analysis. This method models loads as a Probability Density Function (PDF) in order to conduct Monte Carlo simulations to generate loading factor expected values and standard deviations across any number of ship operating profiles and ambient conditions [19]. Using PDFs to represent loads accounts for many sources of uncertainty that are otherwise ignored during load analysis and normally just buttressed by service life margin in a later design stage. Specific load-limiting conditions, such as a battle-heavy wartime scenario requiring the continued use of the ship's railgun and VLS weapons systems, could be closely analyzed to confirm whether previous loading assumptions had been valid, or if the design basis must be reassessed, which would have cascading implications on the rest of the cooling system's design.

8.1.2 Heat Exchanger Pressure Drop Mitigation

If the STHE approach is retained, future design analysis should simultaneously seek novel solutions to reduce the pressure drop across the heat exchanger while also exploring the possibility of deviating from MIL-DTL-15730N [30] requirements, as is permissible with valid justification. Possible solution paths to improving this aspect of heat exchanger performance include:

- Increasing the baffle cut. This increases the window flow area, reduces the window velocity, and therefore reduces the pressure drop.
- Using No-Tubes-in-Window (NTIW) baffles. In this design approach, the tubesheet does not contain any tubes within the baffle window. This permits baffle spacing to be increased beyond nominal TEMA limits, which will

decrease the cross-flow velocity and decrease the pressure drop [42]. It can also significantly reduce the pressure drop in the window zones.

• Simultaneous Operation of Parallel Heat Exchangers. The current cooling skid designs could be modified such that two or more heat exchangers are in operation at all times for each cooling zone. Flow from each of the main headers would join at the shared return line within the cooling skid space as currently proposed, but would then be evenly distributed amongst the heat exchangers in order to reduce the mass flow rate at each unit. Once cooled, the demineralized water from each unit would be rejoined at the common supply riser to then be distributed to each of the main headers. As the CFD analysis confirmed, reducing the required mass flow rate is the most direct method to lower the pressure drop. This approach would introduce additional concerns regarding space and volume requirements and would increase construction, maintenance, and operational costs long-term, but could address one of the primary technical shortcomings in the current design.

More broadly, overall heat exchanger performance should be more precisely defined using a multi-objective optimization approach, not only to better tailor the design of future STHE iterations but also to explore the utility and viability of alternative heat exchanger types.

8.1.3 PEBB Arrangement Solution in PMM Compartments

Despite concerted efforts to improve the PEBB stack power density, and reduce the PEBB stack spacing and cooling piping wingspans, stacklength issues persist in the PMM compartments. The PMMs are the largest loads on the nominal destroyer, and under current assumptions require 45 PEBB 6000 drawers to enable their operation at maximum capacity. Absent a significant compartment resizing, a novel approach will have to be pursued to allocate all the necessary PEBBs in these spaces. The stack layout may have to depart from the baseline corridor approach, such as having two rows of power corridors or an even more bespoke arrangement of PEBB stacks

located adjacent to the PMMs. Whatever approach is pursued will affect the current cooling system design, which will have to be modified to reflect the unique piping and fitting arrangements leading into and out of these compartments.

8.1.4 Expansion of Dynamic Modeler Capabilities

Additional functionality should be built into the dynamic modeler to enhance its utility in system design decision-making and evaluation. Areas to focus on include:

- Adjusting the sizing of all the system's piping, to include automatic adjustment of header piping, as necessary, based on changes in heat load assumptions.
- Complete rendering of the cooling skid space arrangements to better specify piping and equipment layout in order to either justify or revise current pumping and expansion tank calculations.
- Automatic calculation of excess corridor space in each compartment to allocate and generate energy storage representations. This work should be merged with concurrent energy storage sizing research to improve the model's accuracy.
- Determine a viable method to export the model to a suitable software domain to conduct in-depth CFD analysis of the overall cooling system.

8.2 Conclusions

This thesis demonstrated both the benefits and challenges associated with addressing the NiPEC's thermal management problem with the proposed indirect liquid cooling strategy.

Electrical load and PEBB allotment calculations indicated the clear benefits accrued by incorporating a joint Navy iPEBB and PEBB 6000 approach. The significant reduction in LRU component requirements in turn provided a more power-dense solution compared to the iPEBB-only approach. The resulting power corridor stacklength requirements proved feasible in all but the PMM compartments, as discussed above.

This joint approach introduces additional complexity to the system design which will have to be addressed in greater detail. Cold plate, stack, and cooling piping designs specific to the PEBB 6000 will have to be further developed, validated, and incorporated to prove the overall design's feasibility. The findings presented in this study can serve as the initial groundwork for these future efforts.

The six-cooling zone system architecture offers a promising balance between limiting the number of required components for full-ship operation while ensuring that no singular zone's demand is overly taxing. Certain technical issues persist, such as the pressure drop concerns at the heat exchanger detailed above, as well as the mismatch between the amount of redundancy provided for the PEBBs versus the amount of redundancy provided for their cooling. PEBB redundancy is allocated at the watertight compartment level, whereas backup cooling for any given PEBB is provided by two other cooling sources located elsewhere in the ship. Although this satisfies the baseline military requirement, it may not be adequately robust against future organizational and programmatic goals considering the NiPEC's essential role in providing power to all of the ship's loads. Losing NiPEC functionality will not just affect one component, system, or mission area, but has the potential to incapacitate major portions of shipboard operation and warfighting capability. This represents a paradigm shift of sorts in considering how to design a ECWS with first-rate reliability. This may manifest itself in a requirement to provide either primary or backup cooling in a more localized manner, up to and including at the watertight compartment level.

Moreover, ongoing NiPEC and PEPDS research aims to improve the overall system power density, and the cooling system design directly influences this measure. Future development of the NiPEC cooling system must continue to bear in mind this central objective and seek solutions that positively contribute to that goal. The base system design presented in this study can continue to be evaluated and modified to produce better-performing components and zonal strategies which contribute to the goal of improved power density while continuing to meet or exceed all thermal management requirements. This work can also serve as a comparative study against which to benchmark other cooling system proposals which may incorporate different

heat exchanger designs or coolant distribution strategies.

Bibliography

- [1] Bell Delaware method calculation of correction coefficients for shell side heat transfer. URL https://powderprocess.net/Tools_html/Thermodynamics/Shell_Tube_Bell_Delaware_Correction_Coeff.html.
- [2] FIPC Supplies Key Component for New US Navy Chiller System. URL https://fairleadint.com/news-archives/us-navy-hes-c-variable-speed-drive/.
- [3] Heat exchanger guide. URL https://www.csidesigns.com/e-books/guide-to-heat-exchangers/.
- [4] Printed-Circuit Heat Exchanger (PCHE). URL https://ase.mit.edu/projects/printed-circuit-heat-exchanger-pche/.
- [5] Welded spiral heat exchangers. URL https://www.alfalaval.us/products/heat-transfer/plate-heat-exchangers/welded-spiral-heat-exchangers/.
- [6] Engineering-Guide-YZ-Centrifugal-Chiller. URL https://tyco.widen.net/view/pdf/ydgkvomge3/161. 01-EG1-EN-Engineering-Guide-YZ-Centrifugal-Chiller.pdf?t. download=true&u=d73svt.
- [7] 5 reasons to use plate-and-frame heat exchangers instead of shell-and-tube, . URL https://www.alfalaval.us/microsites/gasketed-plate-heat-exchangers/tools/gphe-vs-shell-and-tube//.
- [8] High-Efficiency VSD, Variable Speed Drive, U.S. Navy, HESC Chillers,
 URL https://www.calnetix.com/newsroom/press-release/
 calnetix-technologies-supplies-key-components-new-us-navy-chiller-system.
- [9] Onboard DC Grid™ | ABB Marine & Ports, . URL https://new.abb.com/marine/systems-and-solutions/power-generation-and-distribution/onboard-dc-grid.
- [10] PEPDS Final (Revision 1 July 26 2020).pdf, . URL https://www.dropbox.com/home/NiPEC20References/PEPDS20Proposal?preview=PEPDS+Final+28Revision+1+-+July+26+202029.pdf.

- [11] Pressure Loss from Fittings Excess Head (K) Method | Neutrium, . URL https://neutrium.net/fluid-flow/pressure-loss-from-fittings-excess-head-k-method/.
- [12] Y-Strainer Flow Rate Vs Pressure Drop | Sure Flow Equipment Inc., . URL https://www.sureflowequipment.com/solution/y-strainer-flow-rate-vs-pressure-drop/.
- [13] The Delaware Method. Academic Press, Jan. 2014. ISBN 978-0-12-397195-1. doi: 10.1016/B978-0-12-397195-1.00006-6. URL https://www-sciencedirect-com.libproxy.mit.edu/science/article/pii/B9780123971951000066. Pages: 199-222.
- [14] How to Define & Measure Centrifugal Pump Efficiency: Part 1, Nov. 2020. URL https://www.pumpsandsystems.com/how-define-measure-centrifugal-pump-efficiency-part-1.
- [15] Plate heat exchanger, Jan. 2023. URL https://en.wikipedia.org/w/index.php?title=Plate_heat_exchanger&oldid=1134980654. Page Version ID: 1134980654.
- [16] P. 320. Naval power and energy systems technology development roadmap. *Naval Sea Systems Command*, 2019.
- [17] A. Almasi. Consider Printed Circuit Heat Exchangers, Oct. 2021. URL https://www.chemicalprocessing.com/processing-equipment/heat-exchangers/article/11291324/consider-printed-circuit-heat-exchangers-chemical-processing.
- [18] C. Cooke, C. Chryssostomidis, and J. Chalfant. Modular integrated power corridor. In 2017 IEEE Electric Ship Technologies Symposium (ESTS), pages 91–95. IEEE, 2017.
- [19] DDS-310. Electric plant load analysis for surface ships. Department of Navy Design Data Sheet, September 2012. Revision 1.
- [20] J. del Águila Ferrandis, J. Chalfant, C. M. Cooke, and C. Chryssostomidis. Design of a power corridor distribution network. In 2019 IEEE Electric Ship Technologies Symposium (ESTS), pages 284–292. IEEE, 2019.
- [21] C. DiMarino. Navy integrated power electronics building block (iPEBB). In Office of Naval Research iPEBB Program Review, November 2020.
- [22] G. Farooq. How to size and select your next pressure relief valve, Nov. 2020. URL https://www.controlglobal.com/measure/pressure/article/11294762/how-to-size-and-select-your-next-pressure-relief-valve.

- [23] D. Hernandez. Thermal analysis of indirect liquid cooling for the navy integrated power electronics building block. Master's thesis, Massachusetts Institute of Technology, 2023.
- [24] J. Kauwale. Engineering Pro Guides. URL https://www.engproguides.com/expansion-tank-design-chilled-water.html.
- [25] R. Khatri, K. Wiley, L. Zheng, A. Tecce, O. Solis, H. Galloway, and A. Yuskevich. Enabling technology for the next generation of u.s. navy chillers: Development of an oil-free chiller compressor equipped with active magnetic bearings and driven by a high-speed motor. ASNE, 2023.
- [26] S. Learman. How To Size A Pump, Oct. 2021. URL https://www.blackmonkengineering.com/how-to-size-a-pump.html. Section: blog.
- [27] J. H. Lienhard. A heat transfer textbook. Dover Publications, Inc., Mineola, New York, fifth edition edition, 2019. ISBN 978-0-486-83735-2.
- [28] S. Markle. IPES harnessing total ship energy & power. Sea-Air-Space Exposition, 2018.
- [29] E. S. Menon. Working guide to pumps and pumping stations: calculations and simulations. Gulf Professional Pub., Burlington, Mass, 2010. ISBN 978-1-85617-828-0.
- [30] MIL-DTL-15730N. Coolers, fluid, naval shipboard hydrocarbon base oil and freshwater services. Department of Defense Detail Specification, June 2021. Revision N.
- [31] MIL-STD-1399. Cooling water for support of electronic equipment. Department of Defense Interface Standard, June 2021. Section 532.
- [32] MIL-STD-1472. Human engineering. Department of Defense Design Criteria Standard, September 2020. Revision H.
- [33] NAVSEA-532. Navsea design practices and criteria manual for surface ship freshwater systems. NAVSEA Design Practices and Criteria Manual, June 1988. Chapter 532.
- [34] NSTM-505. Naval ships' technical manual chapter 505 piping systems. Department of Navy Technical Manual, January 2008. Revision 4.
- [35] J. Padilla. Cooling power electronic building blocks aboard navy ships. Bachelor's thesis, Massachusetts Institute of Technology, 2021.
- [36] J. Padilla, J. Chalfant, C. Chryssostomidis, and C. Cooke. Preliminary investigation into liquid-cooled PEBBs. In 2021 IEEE Electric Ship Technologies Symposium (ESTS), August 2021.

- [37] L. Petersen, C. Schegan, T. Ericsen, D. Boroyevich, R. Burgos, N. Hingorani, M. Steurer, J. Chalfant, H. Ginn, C. DiMarino, G. Montanari, F. Peng, C. Chryssostomidis, C. Cooke, and I. Cvetkovic. Power electronic power distribution systems (PEPDS). ESRDC Website, www.esrdc.com, 2022.
- [38] N. Rajagopal, R. Raju, T. Moaz, and C. DiMarino. Design of a High-Frequency Transformer and 1.7 kV Switching-Cells for an Integrated Power Electronics Building Block (iPEBB). In 2021 IEEE Electric Ship Technologies Symposium (ESTS), pages 1–8, Aug. 2021. doi: 10.1109/ESTS49166.2021.9512358.
- [39] I. Reyes. Design and modeling of the navy integrated power and energy corridor cooling system. Master's thesis, Massachusetts Institute of Technology, 2022.
- [40] B. Rosenberg. The roadmap for naval electrification, Nov. 2021. URL https://breakingdefense.sites.breakingmedia.com/2021/11/the-roadmap-for-naval-electrification/.
- [41] R. W. Serth. Process Heat Transfer: Principles and Applications. Academic Press, Burlington, MA, 2007. URL https://mit-library.skillport.com/skillportfe/main.action?assetid=RW\protect\T1\textdollar41366:
 _ss_book:28259#summary/BOOKS/RW\protect\T1\textdollar41366:
 _ss_book:28259.
- [42] D. Stephan. Managing Pressure Drop in the Design of Shell and Tube Heat Exchangers. URL https://www.process-worldwide.com/managing-pressure-drop-in-the-design-of-shell-and-tube-heat-exchangers-a-458491/?p=2.
- [43] TEMA. Standards of the tubular exchanger manufacturers association. TEMA Technical Committee, 2007. 9th Edition.
- [44] L. Xie, D. Zhuang, Z. Li, and G. Ding. Technical Characteristics and Development Trend of Printed Circuit Heat Exchanger Applied in Floating Liquefied Natural Gas. Frontiers in Energy Research, 10, 2022. ISSN 2296-598X. URL https://www.frontiersin.org/articles/10.3389/fenrg.2022.885607.
- [45] S. Yang, J. Chalfant, J. Ordonez, J. Khan, C. Li, I. Cvetkovic, J. Vargas, M. Chagas, Y. Xu, R. Burgos, et al. Shipboard PEBB cooling strategies. In 2019 IEEE Electric Ship Technologies Symposium (ESTS), pages 24–31. IEEE, 2019.

Appendix A

List of Acronyms

AC Alternating Current

AMDR Air and Missile Defense Radar

ASSET Advanced Ship and Submarine Evaluation

CAD Computer Aided Design

CFD Computational Fluid Dynamics

CPES Center for Power Electronics System

CuNi Copper-Nickel

DC Direct Current

DI demineralized water

ECWS Electronic Cooling Water Systems

EPLA Electric Power Load Analysis

ESM Energy Storage Module

EW Electronic Warfare

HES-C High Efficiency Super Capacity

InTop Integrated Topside

iPEBB integrated Power Electronics Building Block

IPES Integrated Power and Energy System

IPS Integrated Power System

ISEA In-Service Engineering Agents

LCS Littoral Combat Ships

LMTD Logarithmic Mean Temperature Difference

LRU Least Replaceable Unit

LVAC Low Voltage Alternating Current

LVDC Low Voltage Direct Current

MAWP Maximum Allowable Working Pressure

MIT Massachusetts Institute of Technology

MOSFET Metal-Oxide-Semiconductor Field-Effect Transistor

MVAC Medium Voltage Alternating Current

MVDC Medium Voltage Direct Current

NAVSEA Naval Sea Service Command

NiPEC Navy integrated Power and Energy Corridor

NPES Naval Power and Energy Systems

NPS Nominal Pipe Size

NPSH Net Positive Suction Head

NSTM Naval Ship's Technical Manual

NTIW No-Tubes-in-Window

ONR Office of Naval Research

PCHE Printed Circuit Heat Exchanger

PCM Power Conversion Module

PDF Probability Density Function

PEBB Power Electronics Building Block

PEPDS Power Electronics Power Distribution System

PHE Plate Heat Exchangers

PMM Permanent Magnet Motors

SiC Silicon-Carbide

SHE Spiral Heat Exchangers

STHE shell-and-tube heat exchangers

SWBS Ship Work Breakdown Structure

 ${f TCV}$ Temperature Control Valves

TDH Total Differential Head

TDR Technology Development Roadmap

TEM Tactical Energy Management

TEMA Tubular Exchangers' Manufacturers Association

TIM Thermal Interface Material

UWM-CSEES University of Wisconsin-Milwaukee's Center for Sustainable Electrical Energy Systems

VLS Vertical Launch System

Appendix B

Load Factor Analysis and Values

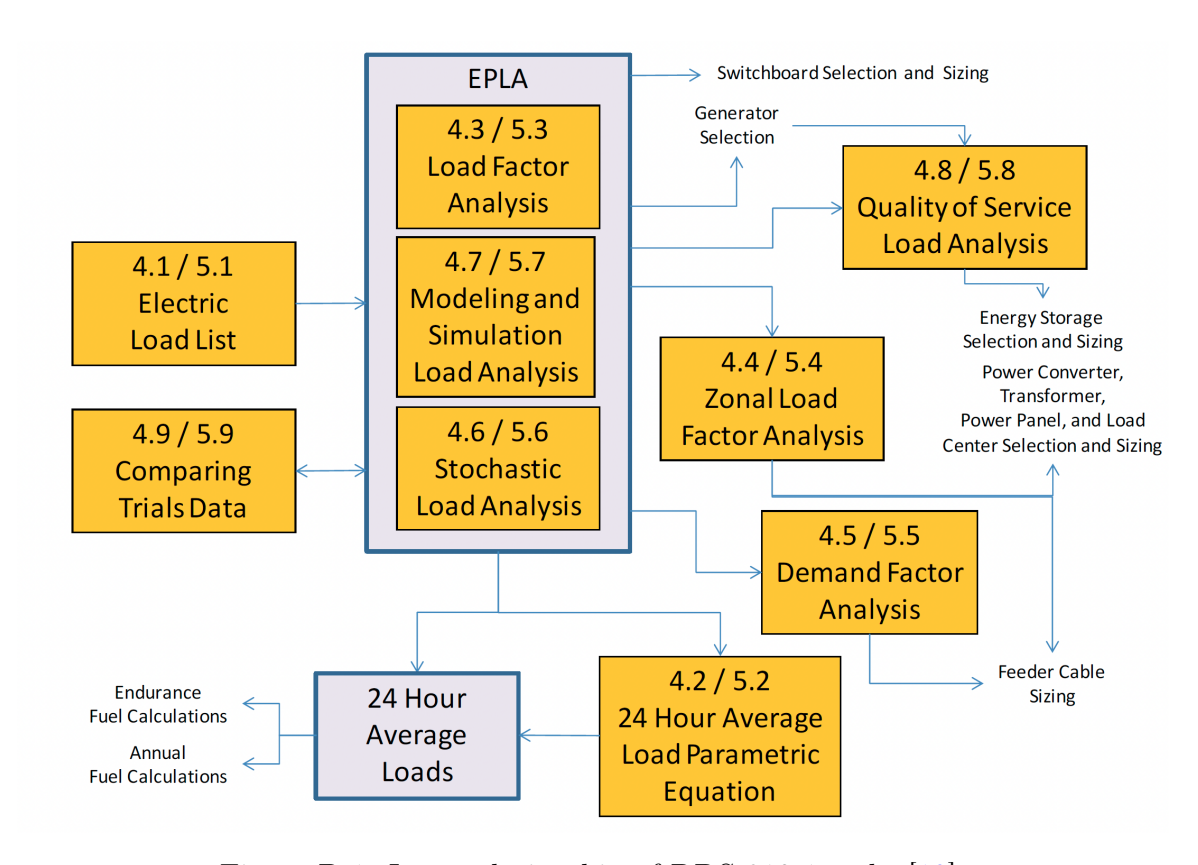


Figure B-1: Inter-relationship of DDS 310-1 tasks [19].

Note: Items with (T) after their title should at a minimum be evaluated for temperature dependency.

SWBS Group 2 - Propulsion Plant General	ANCHOR	SHORE	CRUISING	FUNCTIONAL	EMERGENCY
Auxiliary seawater circulating pump	0.3	0.3	0.6	0.6	0
Blow in door heater, gas turbine	0	0	0.9	0.9	0
Controllable pitch propeller hydraulic oil heater	0.3	0.3	0.3	0.3	0
Controllable pitch propeller hydraulic oil pump	0	0	0.9	0.9	0
Controllable pitch propeller hydraulic oil purifier heater	0.1	0	0.1	0	0
Controllable pitch propeller hydraulic oil purifier	0.3	0	0.3	0.3	0
Electric propulsion equipment space heaters	0.9	0.9	0	0	0
Electric propulsion exciter	0	0	0.9	0.9	0
Emergency feed booster and transfer pump	0	0	0	0	0
Fuel service pump	0.4	0.1	0.9	0.9	0
Inlet louver heater, gas turbine	0	0	0.9	0.9	0
Lighting off forced draft blower	0.1	0	0	0	0
Lube oil purifier	0.3	0	0.3	0.3	0
Main circulating MO valve	0	0	0	0	0
Main circulating pump	0	0	0.9	0.9	0
Main condensate pump	0	0	0.9	0.9	0
Main engine cooling fan, gas turbine	0	0	0.9	0.9	0
Main engine prelube pump	0	0	0	0	0
Main feed booster pump	0.1	0	0.9	0.9	0.5
Main turbine gland exhaust	0	0	0.9	0.9	0
Main vacuum pump	0	0	0.9	0.9	0
Main feed lube pump	0.2	0	0.9	0.9	0
Module equipment, gas turbine	0.4	0.4	0.2	0.2	0
Port fuel oil service pump	0	0.1	0	0	0
Port-use forced draft blower	0.2	0	0	0	0
Propulsion control console	0.5	0.2	0.6	0.8	0
Propulsion motor lubricating oil pump	0	0	0.9	0.9	0
Propulsion motor ventilation fan	0	0	0.9	0.9	0
Reserve feed transfer pump	0.2	0.2	0.2	0	0
Seawater booster pump	0	0	0.3	0.9	0
Shaft turning gear	0.1	0.1	0	0	0.1
Standby reduction gear lubricating oil pump	0	0	0	0	0.2
Standby lubricating oil service pump	0	0	0	0	0.2

Figure B-2: SWBS Group 2 Load Factors [19].

SWBS Group 3 - Electric Plant	ANCHOR	SHORE	CRUISING	FUNCTIONAL	EMERGENCY
General			42		X
Electrical plant control console	0.2	0.2	0.2	0.2	0.2
Emergency gen salt water booster pump	0	0	0	0	0.9
Forklift battery charger	0.2	0.2	0.3	0.3	0
Generator space heaters	0.9	0.9	0	0	0
Gas turbine gen enclosure cooling fan	0.9	0	0.9	0.9	0
Gas turbine salt water pump	0.9	0	0.9	0.9	0
Lighting machinery spaces	0.9	0.9	0.9	0.9	0.9
Lighting outside machinery spaces	0.6	0.4	0.6	0.6	0.4
Ship battery charger	0.2	0.2	0.2	0.2	0
STGEN circulating pump	0.5	0	0.5	0.9	0
STGEN condensate pump	0.5	0	0.5	0.9	0
STGEN start-up lubricating oil pump	0	0	0	0	0.9
STGEN vacuum pump	0.5	0	0.5	0.9	0
Aircraft Carriers					
Aircraft & helicopter start	0.1	0	0.1	0.5	0
Amphibious Ships					
Helicopter starting rectifier	0	0	0.1	0.1	0.1
Auxiliary Ships					
Helicopter starting rectifier	0	0	0	0	0
Cruisers-Destroyers-Frigates					
Helicopter starting rectifier	0	0	0	0	0
SWBS Group 4 - Command and Surveillance	ANCHO	SHORE	CRUISIN	FUNCTION	EMERGEN
General)R		NG	NAL	NCY
Bathythermograph winch	0	0	0	0	0
Combat information center	0.2	0	0.4	0.7	0
Degaussing system	0.8	0	0.8	0.8	0
Electronic countermeasures	0	0	0.4	0.7	0.5
Electronic cooling system	0.4	0.2	0.7	0.7	0.5
Entertainment system	0.1	0.1	0.3	0	0
IC system	0.2	0.2	0.4	0.7	0.4
Lighting, navigation	0.6	0.4	0.6	0.4	0.2
Missile fire control	0.1	0	0.1	0.6	0

Figure B-3: SWBS Group 3 Load Factors [19].

SWBS Group 4 - Command and Surveillance - Continued		SHORE	CRUISING	FUNCTIONAL	EMERGENCY
General - Continued	ANCHOR		G	AL	CY
Radar	0.2	0	0.5	0.7	0.5
Radio	0.2	0.1	0.4	0.7	0.4
Searchlight	0	0	0	0.2	0
Sonar	0	0	0.4	0.4	0
Amphibious Ships					
Fire control	0.2	0.1	0.3	0.4	0.4
Auxiliary Ships					
Fire control	0	0	0	0	0.6
Cruisers-Destroyers-Frigates					
Fire control	0.2	0.1	0.4	0.7	0.4
SWBS Group 5 - Auxiliary Systems	ANCHOR	SHORE	CRUISING	FUNCTIONAL	EMERGENCY
General	~		G	A	СУ
A/C chilled water pump (T)	0.7	0.5	0.7	0.7	0.4
A/C compressor (T)	0.7	0.5	0.7	0.7	0.4
A/C purge recovery unit (T)	0.3	0.3	0.3	0.3	0
A/C seawater circulating pump (T)	0.7	0.5	0.7	0.7	0.4
Anchor windlass	0	0	0	0	0
Bilge & fuel tank stripping	0.1	0.1	0.1	0	0
Bilge pump	0.1	0.1	0.1	0.1	0
Boat winch	0	0	0	0	0
Capstan	0	0	0	0	0
Cargo refrigerator compressor (T)	0.3	0.3	0.3	0.3	0
Cathodic protection	0.9	0.9	0.9	0	0
Class circle W ventilation (T)	0.9	0.9	0.9	0.9	0.4
Class circle Z ventilation (T)	0.7	0.7	0.7	0	0
Class W ventilation (T)	0.9	0.9	0.9	0.9	0.4
Class X and Y ventilation (T)	0.7	0.7	0.7	0	0
Class Z ventilation (T)	0.9	0.9	0.9	0	0
Control air compressor	0.2	0	0.6	0.6	0
Disinfectant agent pump	0.1	0.1	0.1	0.1	0
					1
Distiller plant	0.5	0	0.7	0.7	0
Distiller plant Drinking fountain Duct heater class Z (T)	0.5 0.4 0.9	0 0.4 0.9	0.7 0.4 0.9	0.7 0.4	0

Figure B-4: SWBS Group 4 Load Factors [19].

SWBS Group 5 - Auxiliary Systems - Continued General - Continued	ANCHOR	SHORE	CRUISING	FUNCTIONAL	EMERGENCY
Duct heater class W (T)	0.9	0.9	0.9	0.9	0
Duct heater class circle W (T)	0.9	0.9	0.9	0.9	0
Dumbwaiter	0.1	0.1	0.1	0	0
Fire pump	0.2	0.2	0.2	0.4	0.4
Fuel drain and transfer pump	0.3	0	0.3	0.3	0
Fuel transfer pump	0.1	0.1	0.1	0.1	0
Fuel transfer pump purifier	0.3	0	0.3	0	0
Fuel tank stripping pump	0	0	0	0	0
Flushing system	0	0	0.1	0.1	0
Fresh water drain tank pump	0.3	0.1	0.6	0	0
General service pump	0	0	0.1	0.1	0
Gas turbine wash down pump	0	0	0	0	0
Gas turbine water wash tank heater	0.1	0.1	0.1	0.1	0
High pressure air compressor	0.1	0.1	0.1	0.1	0
Hot water circulating pump	0.3	0.3	0.6	0.6	0
HP air compressor air dryer	0.1	0.1	0.1	0.1	0
LAMPS equipment	0	0	0.1	0.5	0.5
Lubricating oil transfer pump	0.1	0.1	0.1	0	0
Main steering gear pump	0	0	0.3	0.3	0.3
02 N2 plant	0	0	0.9	0.9	0
PRAIRIE/MASKER compressor	0	0	0.9	0.9	0
Potable water booster pump	0.3	0.2	0.3	0.3	0
Potable water priming pump	0	0	0	0	0
Potable water pump	0.3	0.2	0.3	0.3	0
Sewage macerator	0.1	0.1	0.1	0.1	0
Sewage pump	0	0	0.1	0.1	0
Ship service air compressor	0.1	0.1	0.1	0.1	0
Soluble fog foam	0	0	0	0	0
Space heater class W (T)	0.9	0.9	0.9	0.9	0
Space heater class Z (T)	0.9	0.9	0.9	0	0
SS air compressor air dryer	0.1	0.1	0.1	0.1	0
SS refrigerator compressor	0.3	0.3	0.3	0.3	0
Steering auxiliary heater (T)	0.9	0.9	0	0	0
Steering gear control	0	0	0.5	0.5	0.5
Steering gear servo pump	0	0	0.5	0.5	0.1
Standby steering gear pump	0	0	0	0	0
Steering gear fill & drain pump	0	0	0	0	0
Towing machine	0	0	0	0.3	0

Figure B-5: SWBS Group 5 Load Factors [19].

SWBS Group 5 - Auxiliary Systems - Continued General - Continued	ANCHOR	SHORE	CRUISING	FUNCTIONAL	EMERGENCY
Unit coolers (T)	0.2	0.2	0.2	0.2	0
Ventilation, no class (T)	0.9	0.7	0.9	0.9	0.4
Aircraft Carriers					
Aircraft/hydraulic test unit	0	0	0	0.5	0
Aircraft elevator side door	0	0	0	0.1	0
Aircraft component elevator	0	0.1	0.1	0.2	0
Aircraft cooling carts	0	0	0	0.5	0
Aircraft crane	0	0	0	0	0
Aircraft elevator main pump	0	0	0.2	0.2	0
Aircraft elevator sump pump	0	0	0.1	0.1	0
Aircraft positioner	0	0	0.1	0.1	0
Arresting gear system	0	0	0	0.2	0.2
Aviation gasoline pump	0	0	0	0.1	0.9
Barricade standby hydraulic pump package	0	0	0	0.1	0
Catapult system	0	0	0	0.2	0
Decanning boom hoist	0.1	0.1	0.1	0	0
Elevator platform gate valve	0	0	0.2	0.2	0
Hangar division door	0	0	0	0.1	0
Island elevator	0.2	0.2	0.2	0.2	0
Jet blast deflector hydraulic pump	0	0	0	0.2	0
JP-5 defueling pump	0	0	0	0.2	0
JP-5 purifier	0	0	0	0.2	0
JP-5 service pump	0	0	0	0.2	0
JP-5 tank drain pump	0	0	0	0	0
Personnel elevators	0.2	0.1	0.2	0.2	0
Replenishment-at-sea system	0	0	0.2	0	0
Stern hoist, flammable liquid	0.2	0.2	0	0	0
Stores conveyor	0.1	0.1	0.1	0	0
Amphibious Ships					
Aircraft crane	0	0	0	0	0
Aircraft elevator main pump	0	0	0.2	0.2	0
Aircraft elevator sump pump	0	0	0.2	0.2	0
Aircraft engine hoist	0.2	0.2	0.2	0.2	0
Automotive gas defueling pump	0.2	0.2	0	0	0.2
Aviation gasoline pumps	0	0	0.2	0.2	0.2
Automotive gasoline pump	0.2	0.2	0	0.2	0.2

Figure B-6: SWBS Group 5 Load Factors (cont'd) [19].

SWBS Group 5 - Auxiliary Systems - Continued Amphibious Ships - Continued	ANCHOR	SHORE	CRUISING	FUNCTIONAL	EMERGENCY
Avionics outlets	0	0	0	0	0
Cargo elevator	0.2	0.2	0	0.2	0.2
Cargo elevator emergency hoist	0	0	0	0	0
Deck edge door	0	0	0.2	0.2	0
Jib crane hoist	0.2	0.2	0	0	0
JP-5 cargo stripping pump	0	0	0	0	0
JP-5 defueling pump	0	0	0.2	0.2	0
JP-5 purifier	0	0	0.2	0.2	0
JP-5 service pump	0	0	0.2	0.2	0
JP-5 transfer pump	0.2	0.2	0.1	0.1	0
Replenishment-at-sea system	0	0	0.2	0	0
Stores conveyor	0.2	0.2	0.1	0	0
Wire rope hoist	0.2	0.2	0.2	0.2	0.2
Auxiliary Ships					
Cargo crane	0.3	0.3	0.1	0.3	0
Cargo crane heater	0.2	0.2	0.2	0	0
Cargo elevator	0.2	0.2	0	0.3	0
Cargo elevator door	0.1	0.1	0.1	0.1	0
Cargo fuel stripping pump	0	0	0	0	0
Component transfer lift	0	0	0	0.2	0
Highline winch	0	0	0	0.6	0
Helicopter boom	0	0	0	0	0
JP-5 priming pump	0	0	0	0	0
JP-5 purifier	0	0	0.1	0.3	0
JP-5 service pump	0	0	0.1	0.3	0
JP-5 transfer pump	0	0	0	0	0
Outboard and inboard saddle winch	0	0	0	0.3	0
Outhaul and inhaul winch	0	0	0	0.3	0
Package conveyor	0	0.7	0	0.5	0
Power operated hangar door	0	0	0	0	0
Rammer cart	0	0	0	0.2	0
Retrieving line winch	0	0	0	0.3	0
Retrieving line winch heater	0	0	0	0	0
Sliding block power unit	0	0	0	0.3	0
Snaking winch	0	0	0	0.3	0
Span wire winch	0	0	0	0.6	0

Figure B-7: SWBS Group 5 Load Factors (cont'd) [19].

SWBS Group 5 - Auxiliary Systems - Continued	ANCHOR	SHORE	CRUISING	FUNCTIONAL	EMERGENCY
Cruisers-Destroyers-Frigates				F	X
Fast elevator system	0.1	0.1	0.1	0	0
Helicopter winch	0	0	0	0	0
JP-5 purifier	0	0	0.1	0	0
JP-5 service pump	0	0	0.1	0	0
JP-5 transfer pump	0	0	0	0	0
Package conveyor	0	0.3	0.1	0	0
Torpedo hatch cover	0	0	0	0	0
SWBS Group 6 - Outfit and Furnishings	ANCHOR	SHORE	CRUISING	FUNCTIONAL	EMERGENCY
General				F	~
Arc welders AC/DC	0.1	0.1	0.1	0.1	0
Bake oven	0.2	0.2	0.2	0	0
Bakery chilled water	0.3	0.2	0.3	0.1	0
Bread slicer	0.3	0.2	0.3	0.1	0
Cash register	0	0	0	0	0
Centrifuge	0	0	0	0	0
Coffee maker	0.3	0.2	0.3	0.3	0
Coil winder	0.2	0.2	0.2	0	0
Deep fat fryer	0.4	0.4	0.4	0	0
Dishwasher	0.3	0.2	0.3	0.2	0
Drill press	0.1	0.1	0.1	0	0
Dryer	0.2	0.2	0.2	0	0
Finisher	0.2	0.2	0.2	0	0
Flatwork ironer	0.2	0.2	0.2	0	0
Fry kettle	0.4	0.2	0.4	0.4	0
Garbage disposal	0.2	0.2	0.2	0	0
Garbage grinder	0.2	0.2	0.2	0	0
Generator test stand	0.1	0.1	0.1	0.1	0
Griddle	0.3	0.2	0.3	0.3	0
Grinder	0.1	0.1	0.1	0	0
Hand iron	0	0	0	0	0
Heated glass	0	0	0	0	0
Hydraulic test stand	0.1	0.1	0.1	0.1	0
Ice cream equipment	0.3	0.2	0.3	0.2	0
Ice maker	0.3	0.2	0.3	0.3	0
Lathe	0.2	0.2	0.2	0	0

Figure B-8: SWBS Group 5 and 6 Load Factors [19].

SWBS Group 6 - Outfit and Furnishings - Continued		SHORE	CRUISING	FUNCTIONAL	EMERGENCY
General - Continued				F	X
Lube unit	0.1	0.1	0.1	0	0
Meat preparation equipment	0.3	0.2	0.3	0	0
Milling machine	0.1	0.1	0.1	0	0
Mixer	0.2	0.2	0.2	0.2	0
Oven	0.4	0.2	0.4	0.4	0
Photo equipment	0.1	0.1	0.1	0.1	0
Planer and joiner	0.1	0.1	0.1	0	0
Power saw	0.1	0.1	0.1	0	0
Pre-rinse booster pump	0.3	0.2	0.3	0.2	0
Range	0.4	0.2	0.4	0.4	0
Recharge pump	0.2	0.2	0.2	0	0
Refrigerator/freezer combination	0.5	0.5	0.5	0.5	0
Refrigerator - small	0.3	0.3	0.3	0.3	0
Sewing machine	0.2	0.2	0.2	0	0
Shearing machine	0.2	0.2	0.2	0	0
Shirt folding machine	0.2	0.2	0.2	0	0
Shop hoist	0.1	0.1	0.1	0	0
Sterilizer - dressing	0	0	0.1	0.7	0.1
Sterilizer - instrument	0.1	0.1	0.1	0.7	0.1
Stitcher	0.2	0.2	0.2	0	0
Test switchboard	0.1	0.1	0.1	0.1	0
Toaster	0.3	0.2	0.3	0	0
Trash burner fan	0.1	0	0.1	0	0
Ultrasonic cleaner	0.1	0.1	0.1	0	0
Valve replacer	0.2	0.2	0.2	0	0
Vegetable cutter	0.2	0.1	0.2	0	0
Vegetable peeler	0.2	0.1	0.2	0	0
Vertical sleever	0.2	0.2	0.2	0	0
Waffle iron	0.1	0.1	0.1	0	0
Washer extractor	0.2	0.2	0.2	0	0
Water heater	0.1	0.1	0.5	0.5	0.1
Window wipers	0	0	0	0	0
X-ray machine	0.1	0.1	0.1	0.2	0.2
Aircraft Carriers					
Accommodation ladder	0	0	0	0	0
Photo equipment	0.4	0	0.4	0.4	0

Figure B-9: SWBS Group 6 Load Factors (cont'd) [19].

SWBS Group 7 - Armament		SHORE	CRUISING	FUNCTIONA	EMERGENCY
General	ANCHOR		G	AL	CY
Gun mounts	0	0	0	0.6	0.6
Magazine bridge crane	0.2	0.2	0.1	0.1	0
Missile launcher	0.2	0	0.2	0	0
Weapons elevator	0.2	0.2	0	0.7	0
Weapons handling hoist	0.2	0.2	0	0.7	0

Figure B-10: SWBS Group 7 Load Factors [19].

Appendix C

PEBB Allocation Breakdown

Table C.1: iPEBB-only: Breakdown Per Compartment (Port)

Comportment	LVDC-LVAC	MVAC-	LVAC-LVDC	MVDC-	MVDC-	Compartment
Compartment	LVDC-LVAC	MVDC	LVAC-LVDC	MVDC	LVDC	Total
1	3	0	1	0	0	4
2	3	0	1	0	0	4
3	3	0	1	0	12	16
4	6	0	2	0	0	8
5	3	0	2	27	0	32
6	9	0	3	10	12	36
7	3	144	2	15	0	164
8	3	0	4	3	0	12
9	3	144	2	5	0	156
10	6	0	2	135	0	144
11	3	0	2	1	12	20
12	3	0	1	0	0	4
13	6	0	2	0	12	20
14	3	0	1	0	0	4
Type Total	57	288	26	196	48	624

Table C.2: iPEBB-only: Breakdown Per Compartment (Starboard)

Compartment	LVDC-LVAC	MVAC-	LVAC-LVDC	MVDC-	MVDC-	Compartment
Compartment	LVDC-LVAC	MVDC	LVAC-LVDC	MVDC	LVDC	Total
1	3	0	1	0	0	4
2	3	0	1	0	12	16
3	3	0	1	0	0	4
4	6	0	2	0	0	8
5	3	0	2	0	12	20
6	9	0	3	10	0	24
7	3	144	2	15	0	164
8	3	0	4	138	0	148
9	3	36	2	5	12	60
10	6	0	2	0	0	8
11	3	0	2	1	0	8
12	3	0	1	0	12	16
13	6	36	2	0	0	44
14	3	0	1	0	0	4
Type Total	57	216	26	169	48	524

Table C.3: Joint Deployment: Breakdown Per Compartment (Port)

Compartment	iPEBB Stacks	PEBB 6000 Stacks	Compartment PEBB Total
0	1	0	4
1	1	0	4
2	4	0	16
3	2	0	8
4	2	4	20
5	9	0	36
6	5	10	50
7	3	0	12
8	3	12	48
9	2	20	68
10	5	0	20
11	1	0	4
12	5	0	20
13	1	0	4
Type Total	43	46	172/138/310 (total)

Table C.4: Joint Deployment: Breakdown Per Compartment (Starboard)

Compartment	iPEBB Stacks	PEBB 6000 Stacks	Compartment PEBB Total
0	1	0	4
1	4	0	16
2	1	0	4
3	2	0	8
4	5	0	20
5	6	0	24
6	5	10	50
7	3	20	72
8	6	4	36
9	2	0	8
10	2	0	8
11	4	0	16
12	2	4	20
13	1	0	4
Type Total	44	38	176/114/290 (total)

Appendix D

Cooling Zone Heat Load Breakdown

Table D.1: Six-Zone Cooling: Compartment Assignments and Heat Loads By Type

Cooling Zone	Compartments	Navy iPEBB Heat Loss (kW)	PEBB 6000 Heat Loss (kW)	Total (kW)
Forward Port	1-6	210.9	384.3	595.2
Mid Port	7-8	49.3	290.6	339.9
Aft Port	9-13	140.2	337.5	477.7
Forward Starboard	1-6	119.0	301.9	420.9
Mid Starboard	7-8	0.67	375.1	375.8
Aft Starboard	9-13	93.5	50.9	144.4

Table D.2: Six-Zone Cooling: Heat Loads Following Loss of Corridor

Cooling Zone	Before N-1 (kW)	Loss of Port $2nd (kW)$	Loss of Port 4 th (kW)	Loss of Starboard $2nd (kW)$	Loss of Starboard 4th (kW)
Forward Port	595.2			617.0	644.8
Mid Port	339.9			340.8	339.9
Aft Port	477.7			493.5	491.7
Forward Starboard	420.9	529.1	512.4		
Mid Starboard	375.8	376.4	400.4		
Aft Starboard	144.4	205.5	153.3	_	_

Table D.3: Six Zone Cooling: Heat Loads Following Loss of Cooling Zone (Port)

Cooling Zone	Before N-1 (kW)	Loss of Forward Port	Loss of Mid	Loss of Aft
	Bolole IV I (NVV)	(kW)	Port (kW)	Port (kW)
Forward Port	595.2	_	765.2	834.1
Mid Port	339.9	637.5		578.7
Aft Port	477.7	775.3	647.6	

Table D.4: Six Zone Cooling: Heat Loads Following Loss of Cooling Zone (Starboard)

Cooling Zone	Before N-1 (kW)	Loss of Forward Starboard (kW)	Loss of Mid Starboard (kW)	Loss of Aft Starboard (kW)
Forward Starboard	420.9	_	608.8	493.1
Mid Starboard	375.8	586.2		448.0
Aft Starboard	144.4	354.9	332.3	

Appendix E

Air Conditioning Plant and Chilled Water System Impacts

Although the primary focus of this research effort is on the design and development of the NiPEC cooling system, its proposed reliance on, and large demands of, the ship's chilled water system warrants closer analysis.

U.S. Navy Flight III destroyers (DDGs) will upgrade the current platform Air Conditioning plant from a 5 x 200-ton refrigerant (RT) chiller lineup to a 5 x 350 RT chiller lineup using the HES-C water chiller (see E-1). This cutting-edge system, developed by York, Johnson Controls Navy Systems, and Calnetix in conjunction with NAVSEA, offers a significantly higher cooling capacity within the same space as the legacy cooling system through improved cooling density and operating efficiency [8] [25]. Although exact dimension and weight specifications for the HES-C system were not publicly available, comparable commercial chiller data published by York was used to approximate these values. The assumed footprint for each HES-C chiller is 3.7' x 2.1' x 2.5', resulting in a unit volume of 19.4 m^3 , and a unit weight of 9.23 MT. For the five units, this yields a total space requirement of 97 m^3 and a total weight addition of 46.15 MT.

However, even this markedly improved and advanced HES-C plant configuration does not provide the capacity required for the notional all-electric destroyer. For reference, one RT corresponds to 3.516 kW, which means that each chiller has a heat



Figure E-1: The higher capacity HES-C units are slated to replace the 200-ton units for Flight III DDGs and other future U.S. Navy platforms [2].

load capacity of 1230.6 kW. Therefore, the future fleet plant will have a capacity of 6153 kW.

The notional destroyer, assumed to be outfitted with a payload and equipment suite which mirrors the electrical load list presented in this study, was synthesized for convergence using the Advanced Ship and Submarine Evaluation (ASSET) analysis tool. The model's initial estimated Air Conditioning plant load was 23803.9 kW, which included a 20% service life cooling margin but which did not account for the additional heat load imposed on the chilled water system by the NiPEC heat losses. The NiPEC cooling zone heat loads under normal operating conditions (provided in Appendix D) cumulatively add 2013.9 kW to the plant load, raising the total assumed AC plant load to 25817.8 kW. This, in turn, would require a 21-unit HES-C plant, which likely represents an infeasible solution based primarily on space constraints.

In order for the proposed ship design to actually converge, a revised Air Conditioning plant configuration was implemented. A valid solution–strictly from a capacity perspective—was achieved by designing an 8-unit plant each with a capacity of 1100 RT (3868.7 kW), with the expectation that seven units would be required for normal operations. Based on the ASSET data provided, each of these units has the

principal dimensions of 5.64' x 2.84' x 2.29', resulting in a unit volume of 36.68 m^3 and a weight of 38.4 metric tons (MT). For the 8 units, this yields a total space requirement of 293.44 m^3 and a total weight addition of 310.4 MT. This results in a threefold increase in space requirements and a nearly sevenfold increase in weight addition compared to the anticipated 5-unit HES-C AC plant footprint.



Figure E-2: York YZ Magnetic Bearing Centrifugal Chiller, Style A [6].

Alternatively, in order to retain the five-chiller plant design with some amount of redundancy requires the implementation of 1840 RT-capacity (6469.4 kW) units, wherein four units would be required for normal operations. A unit with this large a capacity was not an available option within the ASSET module, but there exist many commercial options which do offer this type of capacity. This includes the York YZ Magnetic Bearing Centrifugal Chiller (see Figure E-2) which, like the Navy HES-C, was developed in partnership with Johnson Controls, and has models available to handle up to 7104 kW [6]. The chiller's official engineering brochure was referenced

to determine the following principal dimensions and weight of an approximately 1840 RT chiller: 3.9' x 3.5' x 5.5' and a maximum shipping weight of 33.3 MT [6]. This yields a total space requirement of 375.38 m^3 and a total weight addition of 167.5 MT, which represent a nearly fourfold increase in both space requirements and weight addition compared to the 5-unit HES-C plant footprint.

These initial capacity estimates illustrate the gaps which exist between current shipboard Air Conditioning plant capability, planned upgrades to address the immediate future needs of the Navy, and a yet undetermined solution to address the much greater needs for the future all-electric warship. The predicted increases in space and weight requirements could have significant implications for engineering space design, intact stability, and hydrostatic performance, and could prove to be a principal driver in overall ship design. Although the Air Conditioning plant burden could be alleviated if the NiPEC cooling system did not use chilled water as its cooling medium, cold plate simulation and testing conducted thus far indicate that seawater will not be a viable cooling medium given the required system temperatures.